Frequency Characterization and Control for Future Low Inertia Systems

Nguyen, Ha Thi

Publication date:
2018

Document Version
Publisher's PDF, also known as Version of record

Technical University of Denmark

Ha Thi Nguyen

Frequency Characterization and Control for Future Low Inertia Systems

PhD thesis, August 2018
Lyngby, Denmark

Center for Electric Power and Energy
Department of Electrical Engineering

DANMARKS TEKNISKE UNIVERSITET
Center for Electric Power and Energy (CEE)
DTU Electrical Engineering

Frequency Characterization and Control for Future Low Inertia Systems

Styring og Karakterisering af Frekvens i Fremtidens Lav Inerti Systemer

PhD thesis, by Ha Thi Nguyen

Supervisors:
Associate Professor Guangya Yang, Technical University of Denmark
Associate Professor Arne Hejde Nielsen, Technical University of Denmark
Senior Engineer Peter Højgaard Jensen, Siemens A/S, Denmark

DTU - Technical University of Denmark, Lyngby - August 2018

Frequency Characterization and Control for Future Low Inertia Systems

This thesis was prepared by:
Ha Thi Nguyen

Supervisors:
Associate Professor Guangya Yang, Technical University of Denmark
Associate Professor Arne Hejde Nielsen, Technical University of Denmark
Senior Engineer Peter Højgaard Jensen, Siemens A/S, Denmark

Dissertation Examination Committee:

Professor Poul Ejnar Sørensen (Chairman)
Department of Wind Energy, Technical University of Denmark, Denmark

Professor Bikash Pal
Department of Electrical and Electronic Engineering, Imperial College London, United Kingdom

Professor Vladimir Terzija
School of Electrical and Electronic Engineering, University of Manchester, United Kingdom

Center for Electric Power and Energy (CEE)
DTU Electrical Engineering
Elektrovej, Building 325
DK-2800 Kgs. Lyngby
Denmark

Tel: (+45) 4525 3500
Fax: (+45) 4588 6111
E-mail: cee@elektro.dtu.dk

Release date: August 2018

Edition: First

Class: Internal

Field: Electrical Engineering

Remarks: The PhD thesis is presented to the Department of Electrical Engineering of the Technical University of Denmark in partial fulfillment of the requirements for the degree of Doctor of Philosophy.

ISBN: 000-00-00000-00-0

Preface

This thesis is prepared at the Department of Electrical Engineering of the Technical University of Denmark in partial fulfillment of the requirements for acquiring the degree of Doctor of Philosophy in Engineering. The Ph.D. project was funded by the project Synchronous Condenser Application (SCAPP) (grant: 12196).

This dissertation is composed of 6 chapters which summarizes the work carried out by the author during her Ph.D. project. It started on 15th August 2015, and it was completed on 14th August 2018. During this period, she was hired by the Technical University of Denmark as a Ph.D. student at the Center for Electric Power and Energy (CEE).

Ha Thi Nguyen
14th August, 2018

Acknowledgements

Firstly, I would like to express my sincere gratitude and appreciation to my main supervisor, Assoc. Prof. Guangya Yang, for his guidance, patience, and encouragement. I find myself very fortunate for being able to work with a considerate and encouraging supervisor like him. I benefited greatly from many fruitful discussions with him. His positive outlook in my research inspired me and gave me confidence and motivation. His careful editing contributed enormously to the production of this work. Without his incredible support and encouragement, I would not be able to finish my study.

I am deeply grateful to my supervisors; to my supervisor, Assoc. Prof. Arne Hejde Nielsen, for his support and encouragement, his door was always open for me to ask support; to my industrial supervisor, Peter Højgaard Jensen, for his guidance and support with his senior experience and knowledge. I cannot forget the valuable help and discussion from him.

A special acknowledgment to the Center for Electric Power and Energy at the Technical University of Denmark, for providing excellent material, research facilities, and working conditions; to Siemens A/S, Denmark for the support and the opportunity for me to work in this great area.

I would like to thank my friends and my colleagues at the Center for Electric Power and Energy, especially my office mates (Theis, Jundi, Christina, Jakob and Can) for their companionship and for providing a friendly working atmosphere. I am truly thankful for their help and sharing in my ups and downs whenever I needed.

I gratefully acknowledge the financial support for my research project (SCAPP) of Danish transmission system operator (Energinet) under the Electrical Energy Research Program (ForskEL, grant number 12196); for my external stay and conference of the Otto Mønsteds Fond.

A big thank is dedicated to the transmission system operators; Energinet and San Diego Gas and Electric company (SDG&E) for providing data in this study.

I would also like to give special thanks to all the members of the reference group for their valuable knowledge, questions, and feedback; to Prof. Carlos FM Coimbra and the University of California San Diego, for giving me a great opportunity to do my external stay there.

Finally, I gratefully thank my family, especially my parents for their unconditional support, encouragement, and love. I believe that they are the happiest and the proudest when seeing their daughter gets this far.

Ha Thi Nguyen

Lyngby, Denmark, 2018

Table of Contents

List of Figures

List of Tables

Abstract

The rapid penetration of renewable energy sources (RESs) into power systems has introduced many challenges in securing a stable network operation and has forced power systems to operate in low inertia conditions. Low short-circuit power and intrinsic inertial response from converter-interfaced RES may cause poor dynamic performance of systems and render the system frequency more vulnerable than conventional grids. Instability issues from low-frequency oscillations due to low inertia operating conditions and weak interconnections among power systems are more significant.

The objective of this work is to investigate the impact of converter-interfaced generation on system frequency characteristics during disturbances. The combination of synchronous condensers (SCs) and synthetic inertia (SI) of wind power plants (WPPs) for the inertial response is examined. Afterwards, effort is given to optimize the design and parameter setting of power oscillation damping (POD), which incorporates SCs to provide enhanced frequency stability during transient and emergency situations.

A review of relevant theoretical concepts in power system frequency characteristics and control in renewable-based systems is analyzed. The analyzed system develops from the current Danish power system, which uses a part of fossil fuel sources toward a future scenario with 100% renewable sources in 2035. The system is modeled and validated based on the measurement data provided by the local operator (Energinet) using a real-time digital simulator (RTDS) in PowerlabDK.

The benefit of SCs to frequency stability in terms of inertia support during disturbances is examined to indicate the important role of SCs in modern power systems. Hardware-in-the-loop (HiL) testing of an automatic voltage regulator (AVR) and limiters of SCs in steady-state and dynamic conditions for verifying the control algorithms and tuning the parameters are implemented. HiL testing overcomes the high cost and inefficiency of the tests in real systems. Additionally, software-in-the-loop (SiL) simulation, which is employed for parameter optimization of AVR simulation to achieve similar characteristics as the AVR hardware, is performed.

The capacity of WPPs for providing an inertial response referred to as SI during disturbances is investigated. A mathematical model of SI for WPPs is developed and verified in the future Danish power system, which shows that WPPs are able to supply valuable inertial response during disturbances. This study also examines how the combination of SC and SI provides better performance, which enhances the frequency deviation and rate of change of frequency while enabling the low inertia systems to become more synchronized during disturbances.

POD that incorporates SCs using a local frequency and a tie line power measurement, which adapts to modern system characteristics, is proposed to damp the power oscillation and improve frequency stability during disturbances. An optimal parameter set of the POD is determined using an SiL simulation based on the damping ratio maximization objective of the dominant oscillation mode. The simulation results show that POD based on the optimization algorithm can perform a significant enhancement to the oscillation damping and frequency stability and help control designers save time compared with the empirical tuning method.

Resumé

En kraftige stigning i andelen af vedvarende energikilder (VE) i el-systemet har introduceret adskillige udfordringer mod at opretholde en sikker drift og har herunder tvunget el-systemet til at operere under lave inerti forhold. Sammenlignet med det konventionelle el-system, vil den lavere kortslutnings effekt og indre inerti regulering fra konverter-baseret VE medvirke til dårligere dynamik og gøre systemfrekvensen mere sårbar. De lave inerti forhold samt svage forbindelser mellem el-systemer, gør stabilitetsproblemer fra lavfrekvente svingninger mere markante.

Målet for dette arbejde er først at undersøge konverter-baseret genererings indvirkning på systemfrekvensen i forbindelse med transienter. Efterfølgende analyseres inerti regulering fra en kombination af synkronkondensatorer og syntetisk inerti fra vindfarme. Derudover indeholder dette arbejde en proces til optimal design og bestemmelse af parametre for synkronkondensatorers dæmpning af effektsvingninger. Med dæmpning af effektsvingninger kan synkronkondensatorer forbedre frekvensstabilitet, under transiente og kritiske forhold, og derved bidrage med essentielle netværksservice i moderne el-systemer.

Relevante teoretiske koncepter indenfor frekvenskarakterisering og -kontrol i el-systemer er analyseret ud fra et VE-baseret el-system. Det betragtede system er baseret på det nuværende danske el-system hvor den nuværende andel af VE er forhøjet til 2035-målet om 100% VE i el-systemet. Systemet er modelleret i en digital real tids simulator og valideret vha. måledata fra Energinet.

Fordelen ved synkronkondensatorers bidrag til inerti regulering under forstyrrelser er undersøgt fra et frekvensstabilitets perspektiv, hvilket beviser vigtigheden af synkronkondensatorer i moderne el-systemer. Gennem hardware-in-the-loop (HiL) test af en synkronkondensators automatisk spændingsregulartor (AVR), under statiske og dynamiske forhold, er dens kontrol algoritme verificeret og parametriseret. Derved undgås høje udgifter og ineffektivitet ved AVR test af synkronkondensatorer efter implementering i el-systemet. Derudover er der foretaget software-in-the-loop (SiL) simuleringer, med det formål at få AVR simulering til at efterligne AVR hardware karakteristika gennem parametrisering ad simuleringsmodellen.

Vindfarmes evne til at bidrage med inerti regulering gennem syntetisk inerti under forstyrrelser er undersøgt. En matematisk model af syntetisk inerti fra en samling af vindfarme er udviklet og verificeret for det fremtidige danske el-system under betragtning. Resultaterne viser at vindfarme er i stand til at bidrage med værdifuld inerti regulering under forstyrrelser. Undersøgelsen indeholder derudover en evaluering af en kombination af inerti regulering fra synkronkondensatorer og syntetisk inerti fra vindfarme. Denne viser en mere markant forbedring på frekvensstabiliteten ved at mindske frekvensafvigelsen og frekvensændringsraten. Samtidig hjælper denne kombination med til at forbedre synkroniseringen af lav-inerti-systemet under forstyrrelser.

Brugen af lokal frekvensmåling og effektmåling på forbindelsen til el-systemet er foreslået til dæmpning af effektsvingninger gennem synkronkondensatorer, hvilket forbedre effektsvingningerne

og frekvensstabiliteten under forstyrrelser. Den optimale parametriseringen af effektsvingningsdæmperen er gjort gennem SiL simulering baseret på en maksimering af dampningsforholdet for den dominerende normalsvingning. Simulerings resultaterne viser at optimeringsalgoritmen betydeligt forbedre dæmpningen af effektsvingninger samt frekvensstabiliteten. Derudover hjælper optimeringen med til at reguleringsteknikere sparer tid ved at undgå empirisk parametrisering.

CHAPTER 1

Introduction

1.1 Background and motivation

Many countries have been switching from fossil fuel and nuclear generation to a low-carbon emission and sustainable development that is based on renewable energy sources to achieve climate change goals. Over the last decade, the popularity of renewable energy sources has been increasing. Renewable energy generated 22% of the total global energy consumption in 2013 and has become considerably more prominent in the world's energy generation. By 2020, the amount of global electricity generation from renewable energy will be over 26% higher than the combined electricity demand of China, India, and Brazil. Deployment continues to shift toward energy-hungry emerging markets and some countries, such as China and India [1]. The European Union (EU) has made an ambitious agreement to obtain at least 27% of the whole energy consumption in the EU from renewable energy sources by 2030 [2].

However, high-level power electronic-based generation penetration renders the system operation more challenging due to a lack of short-circuit power and inertia support. Frequency stability and control are expected to be inevitable issues for modern power systems due to the major energy transition from synchronous-machine-based systems to renewable-based systems. Traditional power plants are vast synchronous generators that are capable of providing ancillary services for balancing and transient characteristics. Conversely, the majority of the renewable energy generators are interfaced to the grid via power electronic converters, which have different characteristics and are often controlled in such a way that they are independent of the system frequency. In addition, high importing HVDC interconnections are also expected to replace the traditional generation. These factors have introduced many challenges to secure operation and forced power systems to operate in low inertia conditions. Low short-circuit power and intrinsic inertial response from converter-interfaced generation may cause poor dynamic performance and render the system frequency more vulnerable than conventional grids. Comprehensive reviews of the renewable energy impact on the power system operation in the United States are presented in [3, 4]. In Australia, renewable capacity has been achieved 20% in the National Electricity market [5]. On September 28, 2016, the Australian power system had undergone a frequency collapse due to the presence of a high penetration of renewable energy (majority from wind power) and insufficient reserve to secure against disturbances [6]. With a combination of increasing renewable source integration and decommissioning of conventional power plants, maintaining sufficient inertia in the system to guarantee operational security is the main challenge of the Nordic power system [7]. Recently, a 1200-MW solar photovoltaic (PV) resource in the southern California system was disconnected due to a perceived system frequency below the threshold [8]. European transmission system operators are required to study the frequency characteristic for the European system due to low inertia conditions [9]. The frequency characterization of the interconnection system remains acceptable with reduced system inertia. However, a case of isolated operation after disturbances, the resulting power imbalances and low inertia conditions can cause a system blackout.

The Danish power system has set a long-term target of reaching 100% independence of fossil fuels by 2050 [10]. In the future Danish power system, conventional generators will be phased out in favor of renewable generation units with lower marginal costs. These renewable energy generators are generally connected through partial or full power electronic converters, which leads to the link between the rotational speed of the plants and the grid frequency is removed. As a result, these generators do not naturally contribute to the system inertia and the rotational energy available in conventional generators to counteract frequency changes is missing. In addition, it is expected that more and more HVDC links to neighboring countries and wind farms will be installed, such as COBRA cable to the Netherlands, Viking link to England, and offshore wind farm HR3 400 MW, as shown in Fig. 1.1 [11]. Denmark becomes an important corridor to transport huge amounts of renewable energy from the rich renewable-based countries like Norway and Germany to countries with high consumption or high electricity prices, such as England, the Netherlands, and Sweden. As these HVDC links to Sweden, the Netherlands, and Norway electrically decouple, the Danish system inertia is not directly accessible to the other countries and much more depends on the German interconnection. However, the German grid is expected to integrate more renewable energy sources in the coming years, which weakens the inertia support. Consequently, in order to completely phase out fossil fuel generators in 2050, the system inertia will be decreased significantly, which may introduce many challenges for power system operation and frequency stability and control of the future Danish power system.

In consideration of this potential future scenario, the SCAPP project [12] is conceived to quantify the impact of converter-based generation on system frequency and voltage characteristics during transients. The SCAPP project looks at system inertia, short-circuit power, optimal design and parameter setting of synchronous condenser (SC) to provide essential grid services in renewable-based systems, and to set the system controls during transient and emergency situations, thereby enhancing the system security.

This work is a part of the SCAPP project that evaluates the effect of a converter-based platform on the system frequency and proposes solutions to deal with the modern system challenges in terms of frequency stability and power oscillation. This research is achieved by using SCs and optimal design and parameters of its incorporating controller to improve the system frequency for low inertia systems. The capability of wind power plants (WPPs) for providing an inertial response for frequency control is investigated. Hardware-in-the-Loop (HiL) testing for an automatic voltage regulator (AVR) and limiters of SC is implemented to verify control functions in steady-state and dynamic conditions before commissioning into actual field demonstration.

1.2 Overview of the thesis

This thesis studies the frequency characterization and control for low inertia systems. Like other issues, why and how questions are addressed for this work as follows:

1.2.1 Why?

Frequency stability is one of three important indicators of power system stability [13]. To guarantee a secure system operation, the system frequency must be within an allowable range. Hence, the frequency stability not only ensures that a system operates in a stable and reliable mode but also improves the system quality.

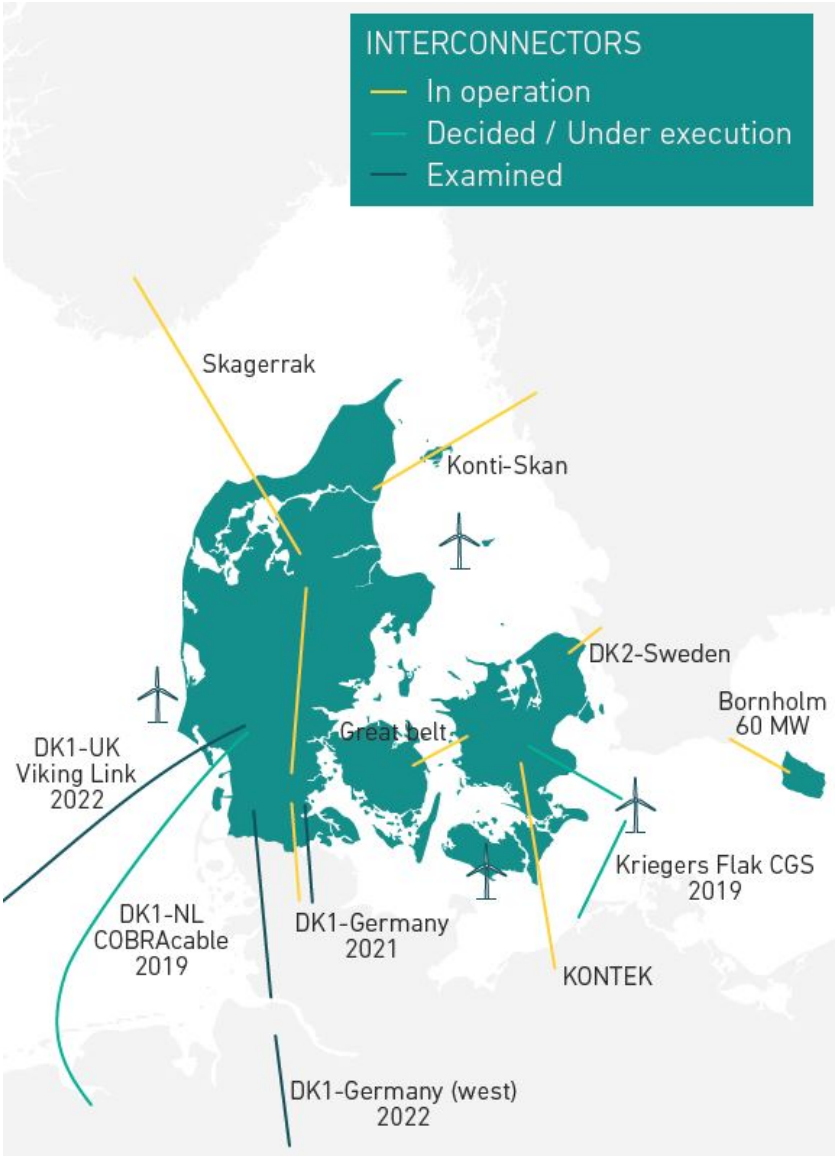

Figure 1.1: International connections in the future Danish power system.

The system frequency change during power imbalances is decided by the system inertia, which is obtained from synchronously connected rotating machines. With the dominance of converter-based generation in modern power systems, where the significant inherent rotational inertia property of conventional power plants is replaced by a small or nonexistent rotational inertia of converter-interfaced generators. Consequently, high-level power electronic-based generation penetration substantially reduces the system inertia and produces a system frequency that is more vulnerable and probable frequency instability under disturbances. Research on frequency characteristic and control for low inertia systems is urgently needed.

1.2.2 How?

To evaluate the frequency response of a power system during a frequency drop event, four important indicators should be considered as follows:

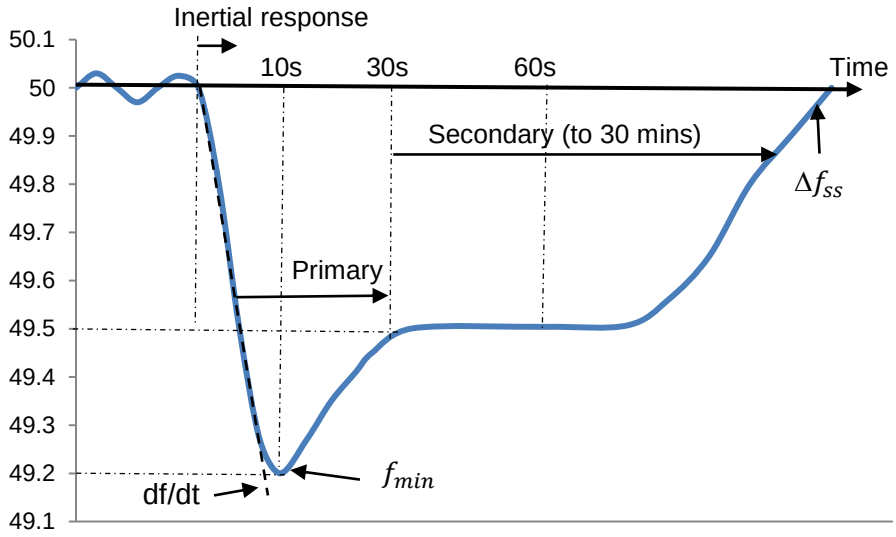

Figure 1.2: Time frames of system frequency response.

1. Rate of change of frequency (ROCOF or df/dt): how fast the frequency changes during disturbances, which is typically observed by ROCOF-based relays.

2. Minimum frequency or frequency nadir (f_{min}): how far the frequency reaches during disturbances, which is usually monitored by underfrequency relays.

3. Steady-state frequency deviation or error (Δf_{ss}): how the frequency deviates from its nominal value after the system achieves a new equilibrium.

4. Settling time: how fast the frequency can recover a new equilibrium after disturbances. In this study, focus on the short time and do not take into account secondary control; therefore, the settling time is considered after the primary control response.

These important indicators are depicted in Fig. 1.2. The goal of frequency control is to maintain the power balance to keep the frequency inside the specific boundaries. To deal with the low inertia system challenges on the frequency control, several works are investigated in this thesis as follows:

Synchronous condenser

An SC is a rotating machine that can supply an inherently inertial response due to the electromagnetic coupling with the grid. The kinetic energy stored in its rotating mass can naturally support an inertial response during frequency excursions. Therefore, SCs significantly improve ROCOF of low inertia systems during disturbances.

Synthetic inertia from WPPs

Wind generators are rotating machines; however, they do not naturally provide an inertial response due to a decoupling connection by converters. Therefore, a proper controller is designed to extract the inertia of the wind generators for frequency control support. This design is achieved by designing a control method for aggregate WPPs to support inertia for power systems during frequency excursions. The control approach also considers activation schemes and the preconditions

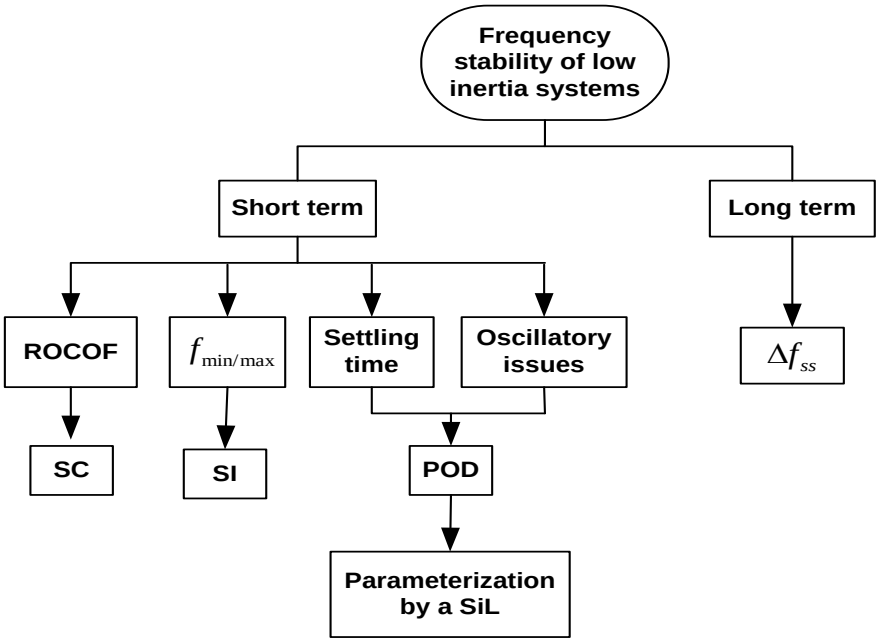

Figure 1.3: The overview of the work.

of wind turbines to properly activate the controller. However, the response occurs via a controller, which is not natural and immediate as in synchronous machines. The control reaction requires time and is not sufficiently fast for the ROCOF improvement but significantly enhances the frequency nadir. Consequently, a combination of SCs and SI of WPPs, which may pronounce an inertial response and fast frequency control of a synchronous generator during frequency excursions, is the best approach for frequency stability enhancement in terms of the ROCOF and frequency nadir.

Power oscillation damping controller

However, operating in low inertia conditions and weak interconnections among power systems may freely suffer from oscillatory stability issues due to a poor frequency response. To deal with this issue, a power oscillation damping (POD) controller that embodies SCs is proposed to adapt to modern system characteristics. This controller is designed and optimized to achieve satisfactory performance for oscillation damping and frequency stability in terms of frequency deviation and settling time.

Parameter optimization based on an SiL simulation

To optimize the parameter set of controllers, an software-in-the-loop (SiL) simulation using Matlab and a real-time digital simulator (RTDS) interface via object linking and embedding for process control (OPC) is implemented. This approach is applied for parameter optimization of a POD controller and an AVR simulation model to satisfy the optimization purposes. This model reduces the time required by control engineers and can solve similar issues of power systems.

The significant changes in the system dynamic characteristics due to a rapid increase of converter-based generation also require more verification and testing of the reliability, optimization, and functionality of power system elements and controllers to ensure a secure system operation. HiL testing is

recognized as an effective approach for testing devices prior to deployment, which can solve the issue of physical controller tests with lower cost, higher efficiency, and more flexibility. HiL enables a user to efficiently implement and safely modify complicated control algorithms and system conditions.

An overview of the work is presented in Fig. 1.3. The future Western Danish power system, which is supplied by 100% converter-based generation, is a typical low inertia system in this study. The results are based on the real-time simulations using the RTDS platform in PowerlabDK. Furthermore, the experimental results for the HiL testing of AVR are also conducted.

1.3 State-of-the-art

The frequency of a power system is one of the most important indicators of the system stability, security, and quality. The frequency of a system depends on the active power balance between generation and demand. When the balance is not achieved, the system frequency experiences an oscillation, which depends on the initial power mismatch and the system inertia.

With the replacement of conventional generation by power electronic-based generation (wind power plants, PV plants, and importing HVDC links), the significant inherent rotational inertia property of traditional power plants is displaced by a smaller or non-rotational inertia of converter-interfaced generation. Therefore, the system inertia significantly decreases, which renders the system frequency more vulnerable and may cause frequency instability under severe disturbances. Additionally, new stability issues and requirements for the controls are introduced due to the different physical characteristics and interactions with the grid of converter-interfaced components.

A substantial amount of research considers the impact of low inertia conditions on power system stability and operation due to the high renewable energy penetration level [14–16]. In [17], the research related to system inertia that analyzes the challenges in system operation due to the inertia reduction is reviewed. The research proposes storage devices or inertia implementation from converter-interfaced generation as a solution for low inertia systems. The low inertia effect on power system operation and stability with a high converter-connected wind turbine and PV penetration level is analyzed in [18]. The study demonstrates that system inertia becomes heterogeneous and frequency dynamics are faster in power systems with low inertia. Foundations and challenges of low-inertia systems in power system stability, operation, and control are reviewed in [19]. Consequently, the low inertia issue has been generally recognized.

1.3.1 Synchronous condenser application

SCs have had an important role for reactive power compensation and maintaining voltage stability in power systems for more than 50 years [20–22]. The generation or consumption of reactive power is achieved by regulating the excitation current to control the voltage in a system or to maintain the system power factor at a specified level. Another important benefit of SCs is short-circuit power support in a network, which can improve the system stability with weak interconnections and facilitate system protection [23].

SCs have been successfully applied to many grids for dynamic voltage regulation and short-circuit current support. Seven SCs were installed at five LCC-HVDC terminals for reactive power compensation in the Danish power system [24]. Nine SCs were equipped with the Hydro Quebec system for fast voltage stability enhancement [25, 26]. To maintain a proper short circuit ratio

at the converter station in the Jeju Island, two new 13.2 kV, +50/-25 Mvar SCs were installed for HVDC control stability [27, 28]. Four SCs with +25/-12.5 Mvar were installed in Vermont due to a low voltage ride-through issue [29, 30]. To improve the dynamic voltage regulation and support short-circuit power, one +560/-310 Mvar SC converted from a coal power plant was implemented in the Midwest Metropolitan Area, while SC application has been proposed for short-circuit current support of WPPs connected to weak AC systems [31].

Recently, to address the impact of renewable resources on grid performance due to poor short-circuit power and low inertia support from converter-interfaced sources, SCs have been proposed as a potential solution for low inertia systems to support system dynamic performance [32]. The benefit of SCs in terms of the inertial response support for frequency stability in renewable-based systems was also investigated in [33]. In [34], the use of SCs is proposed to decrease under frequency load shedding and improve the system frequency response with a different number of synchronous machine scenarios.

Awareness of the importance of inertia and short-circuit power support of future California renewable-based systems, San Diego Gas and Electric (SDG&E) has been installing seven synchronous condensers commissioned by Siemens in the California system for voltage regulation and inertia and short-circuit power support. Currently, six units are in operation; the seventh unit is under commission and is expected to operate in August 2018.

SCs have been successfully applied for dynamic voltage and short-circuit power support in traditional systems, and similar demands of SCs may be observed in converter-based systems in the near future. Based on the benefits of SC, the need for a synchronous condenser and its incorporating controller in modern systems to dynamically adjust the operating conditions for inertia and short-circuit power support, as well as voltage regulation, are distinctly foreseeable, and further research is required.

In this thesis, first, an SC is employed to support the inertial response for frequency stability of low inertia systems. Second, a combination of SC and SI of WPPs is proposed to coordinate the inertial response and fast primary control, respectively, for frequency control during disturbances. Last, a power oscillation damping controller that incorporates SC is proposed to regulate reactive power, which will affect the active power flow to improve the power oscillation of low inertia systems.

1.3.2 Synthetic inertia from wind power plants

To maintain system frequency stability in a grid with a high-level penetration of wind power, WPPs have to perform an increasing number of tasks of conventional power plants related to frequency control. To improve the frequency stability, ENTSO-E (the European Network of Transmission System Operators for Electricity) has issued network codes that apply to all grid-connected generators, i.e., WPPs in continental Europe with rated power above 50 MW, WPPs in the UK with rated power above 10 MW, and WPPs in Ireland with rated power above 5 MW. These WPPs must be equipped with supplementary control services for frequency response [35, 36].

Recent literature proposed strategies for implementing inertial support of WPPs. The majority of WPPs propose a supplementary control that is implemented in an active power loop and is activated during frequency changes. The control can be classified into four main categories. The first category attempts to mimic the inertial response of conventional power plants [37, 38], which uses df/dt as an input signal (df/dt dependent). The second category considers the frequency deviation as

an input signal (Δf dependent) with a fast response time [39, 40]. The authors in [41, 42] apply the combination of the two control strategies to provide inertial response for WPPs, which is referred to as df/dt and Δf dependent. An ancillary control signal proportional to df/dt and frequency deviation is used to increase/decrease the electric power of WPP. In [43], a coordinated frequency control of pitch angle and rotor speed control for a doubly-fed induction generator (DFIG) based wind turbine is proposed for low, medium and high wind speed modes. However, only $\frac{df}{dt}$ dependent control loop is assessed in this study. The active power control of a DFIG is investigated in [44] to satisfy the operator request and maintain frequency stability without losing the stability of operation during different wind speeds. A comparison of different inertia control methods for WPPs is investigated in [45] without providing detail about the control methods. In [46], several operating strategies for DFIGs to support the system frequency are proposed; however, they use the speed deviation of wind generators as the input signal to control the active power command. The four category is referred to as f independent [47, 48]. A torque limit-based inertial control method of a DFIG that calculates the kinetic energy based on the minimum allowable rotor speed to support the system frequency control during a frequency excursion is explored in [47], while a super-capacitor-based synthetic inertia (SI) of DFIG is investigated in [48]. SI control considering the rotor speed is examined in [49, 50]. A coordination of real and reactive power control, namely, GE WindCONTROL is studied in [51], which enables WPPs to regulate the voltage magnitude of the grid, provides governor frequency response, and limits the ramp rate of power. However, this method is mainly applied to overfrequency conditions.

The referenced literature about the SI focused on the control strategies without studying activation schemes. In [52], the author studies the coordination of the inertial response of a WPP and grid event detector to simultaneous satisfy three different conditions. Different activation methods that focus on trigger schemes without coordinated control methods are proposed and analyzed in [53].

From reviewing the above-referenced analysis, a fulfilled control strategy that investigates both the control method and the activation scheme for SI of WPPs has not been completed. This work will analyze and implement an SI control method that is coordinated with an activation scheme for aggregate WPPs of the Western Danish system. A comparison of different control methods for SI controller coordinated with an activation scheme will be analyzed and implemented in the testing system. Furthermore, a combination of SC and SI will be investigated for frequency stability enhancement of low inertia systems.

1.3.3 Hardware-in-the-loop simulation

With a continuously increasing penetration of converter-based generation and the simultaneous reduction in system inertia, system dynamic characteristics are significantly changing. This change requires high reliability and functionality of the equipment and their control systems. Consequently, verification and testing of these elements are becoming more important.

HiL tests represent a bridge between pure simulation and complete system construction by providing an efficient, real-time, and safe environment. HiL tests can focus on the functionality of a controller and verify all dynamic conditions of a system. HiL tests are recognized as an effective approach for testing devices before deployment, which enables testers to solve the issue of a physical controller test with lower cost, higher efficiency, and more flexibility.

In recent years, HiL technology has been applied to develop controls and components with healthy and faulty conditions in power grids, automotive industry, transportation, and other sectors to

overcome the drawback of low accuracy in a pure simulation. In general, HiL testing can be divided into two main categories. The first category of HiL testing is referred to as control HiL (CHiL), which enables a physical control device to be connected in a closed-loop with a power system model. The closed-loop interaction of a CHiL system and a grid model provides insight into both the performance of the control strategy and its effect on the network. The interfaced signals between the CHiL and the simulator are low-power control signals that often fall within the range of $\pm$10 V, 0-100 mA, and commercial digital/analog converters. The second type of HiL testing, power HiL (PHiL), is an extension of CHiL that is capable of exchange current and voltage signals according to the power of external equipment.

In [54], a PV control system is implemented in CHiL testing to evaluate the control method in dynamic conditions. DSPACE real-time simulation is used to verify the field oriented control approach of a permanent magnet synchronous motor in [55]. In [56], a CHiL test for an excitation control system of a synchronous generator using external stabilizing signals to improve oscillation damping is investigated. The CHiL test of a complete control and protection system for a modular multilevel converter-based unified power flow controller coupled with an Opal real-time simulator is studied in [57]. Furthermore, an application of the CHiL test for an AVR of a synchronous generator based on an identification model interfaced with a real-time LAB is implemented in [58]. A maximum power point tracking control based on a polynomial fuzzy model is investigated in [59] to evaluate the performance and efficiency of the control strategy in PV generation. A CHiL simulation of a permanent magnet synchronous motor in healthy and faulty conditions is proposed in [60], which proves that CHiL is a safe and relatively inexpensive environment for developing fault detection and diagnostic algorithms.

A PHiL application for a dynamic electric PV model integrated with a five-layer thermal model is examined to verify the dynamic condition during various load changes in [61]. In addition, a PHiL simulation for a megawatt-scale motor drive is implemented in [62] to validate the device during different disturbances. A PHiL test bench for large-scale power system stability analysis is implemented in [63]. In [64], a PHiL simulation setup has been developed to analyze the effects of real direct load control-enabled variable-speed heat pumps and battery energy storage system units on real-time grid frequency regulation.

In this study, a CHiL is implemented for testing an AVR system and limiters of an SC in steady-state and dynamic conditions. The grid and SC are modeled and run in real-time using RTDS interfaced with an AVR hardware platform to examine and compare how the actual and simulated AVR systems react. Different tests, such as overexcitation, underexcitation, and AVR setpoint loss, are implemented to evaluate the control function of an AVR system that satisfies the requirements that are difficult and complicated to implement in a real system.

1.3.4 Power oscillation damping for low inertia systems

In synchronous-machine-based systems, the oscillatory issues are caused by the power exchange of synchronous generators, in which either a single generator that oscillates against the system, which is referred to as local oscillation, or involves many generators in one area of the system that acts against other generators in other areas of the system, namely, interarea oscillation. To address these oscillatory stability issues, many supplementary controllers, which can be classified into four main categories, have been introduced. First, power system stabilizer (PSS) is implemented in existing power plants [65–67]; it serves as an auxiliary excitation control to damp generator

oscillations for power system oscillatory stability enhancement. Second, POD uses FACTS devices that controls the voltage angle of injection buses to adjust the power transferred on transmission lines [68–70]. Third, converter-based generation damps power oscillation, such as wind generators or HVDC links [71–77]. Finally, coordinating existing PSSs with other components, such as wind power plants [78–81] or FACTS devices [82–84], is also investigated.

Moving forward, with the dominance of renewable generators in modern power systems, new stability issues and requirements for controls are introduced for renewable-based systems. The oscillatory issue stems from a poor inertial response and does not involve any power exchange of synchronous generators, which differs from traditional systems, therefore, PSSs may not work well in renewable-based systems. To achieve a smooth transition to renewable energy systems, a POD control design that adapts to modern system characteristics is extremely necessary. POD for low inertia systems that are free of synchronous generators is quite a novel concept. A new controller that interacts between active power and reactive power channels of SCs to improve primary frequency control is investigated in [85]. This control method is capable of assisting governor response via reactive power modulation to improve the frequency nadir and settling time. However, this method does not adequately deal with the oscillation damping and implementation with proposed multiband frequencies is complicated. In [86], the oscillatory stability issue of a low inertia microgrid is enhanced by designing different converter controllers, which enables frequencies at different substations to quickly damp and synchronize after disturbances.

In this study, a POD controller incorporating SCs is proposed for low inertia systems that uses a local frequency and a tie line power measurement to control the reactive power of SCs during disturbances. By controlling the terminal voltage through the reactive power of SCs, the active powers of transmission lines, HVDC links, and loads are influenced to damp the oscillation and significantly enhance the frequency stability in terms of the frequency nadir and settling time.

1.3.5 Parameter optimization

Note that the efficiency of controllers is primarily dependent on the parameter settings of the controllers. Thus, parameter optimization is very important and the implementation of parameter optimization as an efficient way is always a concern for control engineers. In the literature, several researchers have implemented optimization algorithms for determining the optimal parameter set of controllers using the Matlab program. Reference [87] proposes tuning strategies for a robust pulse width modulated series compensator damping controller based on an augmented Lagrangian particle swarm optimization which satisfies the multiple H_∞ performance criteria for the FACTS controller. A PSS parameter optimization using a trajectory sensitivity approach is examined for a multimachine power system in [88]. However, these strategies are implemented using Matlab computations based on linear system models, which are not feasible in large-scale and complex power systems with thousands of state variables. Parameter optimization based only on Matlab computations differs with real-time simulation and is not sufficient for guaranteeing the required system performance and understanding complex systems. A gradient-based nonlinear parameter optimization of FACTS devices in real time using RTDS is investigated in [89]. However, a limit exists due to a lack of optimization algorithm implementation support in the RTDS.

A genetic algorithm (GA) is a powerful nonlinear optimization tool that has received attention from the research community [90–92]. In [93], a GA optimization is applied for tuning control parameters of the proportional-integral controller subject to the H_∞ constraints in terms of linear

matrix inequalities of the state-space system model of a three-area power system. With GA optimization, the issue of parameterization is transformed into a simple optimization problem by setting specific objectives and constraints, which is completely independent of the complexity of systems.

In this study, a parameter optimization that is based on SiL simulation linking RTDS and Matlab via OPC communication is implemented. The near-optimal or optimal parameter sets of the POD controller and AVR simulation model are determined by the GA based on their objective functions.

1.4 Contributions

The main contributions of this PhD work are listed as follows:

1. Validation of the Western Danish power system in real-time using RTDS platform from the measurement data of events provided by the local transmission operator (Energinet).

2. Proposal of different approaches for frequency stability enhancement of low inertia systems using SC, SI, and their combination.

3. Validation and verification control functions of an AVR and limiters of SC in dynamic and steady-state conditions in hardware.

4. Design of a POD controller that incorporates SC to damp power oscillation and enhance frequency stability for low inertia systems.

5. Proposal of software-in-the-loop simulation for parameter optimization of a POD controller and AVR simulation model of SC, which can apply to other issues of power systems.

1.5 Layout of the thesis

The work is organized as follows:

Chapter 1 presents the background and motivation, literature review, project contributions, organization, and publications.

Chapter 2 describes the relevant theoretical concepts of system frequency characteristics and control as well as the description and validation of the investigated system, which is employed as a typical low-inertia system in this work.

Chapter 3 presents the HiL test of an AVR system in steady-state and dynamic conditions and implements an SiL simulation in real time for parameter optimization of the AVR simulation model to achieve a characteristic that is similar to the AVR hardware.

Chapter 4 proposes different frequency stability enhancement approaches using SC and SI of WPPs for low inertia systems and analyzes the combination of SCs and SI of WPPs for frequency stability enhancement, which not only enhances frequency deviation and ROCOF but also helps the low inertia system become more synchronized during different disturbances.

Chapter 5 develops a POD controller that incorporates SCs to damp power oscillation and enhance frequency stability for low inertia systems. A parameter optimization of the POD controller using a SiL simulation in real time based on a nonlinear optimization is also investigated in this chapter.

Chapter 6 summarizes the work, findings and suggested future work.

1.6 List of publications

There are 9 scientific papers which are the core of this thesis, 6 of which (A, B, C, D, E, and G) have been peer-reviewed and published. The remaining ones are currently under review. They are listed as follows:

[Pub. A] H. T. Nguyen, G. Y. Yang, A. H. Nielsen, and P. H. Jensen, "Frequency stability improvement of low inertia systems using synchronous condensers," *2016 IEEE International Conference on Smart Grid Communications (SmartGridComm)*, Sydney, Australia, 2016, pp. 650-655.

[Pub. B] H. T. Nguyen, G. Y. Yang, A. H. Nielsen, and P. H. Jensen, "Frequency stability enhancement for low inertia systems using synthetic inertia of wind power," *2017 IEEE Power & Energy Society General Meeting*, Chicago, IL, USA, July 2017, pp. 1-5.

[Pub. C] H. T. Nguyen, G. Y. Yang, A. H. Nielsen, and P. H. Jensen, "Hardware-in-the-loop test for automatic voltage regulator of synchronous condenser," in *Proc. 20th International Conference on Power Systems and Energy Conversion*, Tokyo, Japan, Mar. 27-28, 2018, pp. 1-6. (Received "Best Paper Award" at the conference.)

[Pub. D] H. T. Nguyen, G. Y. Yang, A. H. Nielsen, P. H. Jensen, and C. F. M. Coimbra, "Control parameterization for power oscillation damping via software-in-the-loop simulation," in *Proc. 7th International Conference on Renewable Power Generation*, DTU, Lyngby, Denmark, Sep. 26-27, 2018, pp. 1-6.

[Pub. E] H. T. Nguyen, C. Guerriero, G. Y. Yang, C. J. Boltonand, T. Rahman, and P. H. Jensen, "Talega synCon - Power grid support for renewable-based systems," in *Proc. the Western Protective Relay Conference 2018*, Washington, USA, Oct. 15-18, 2018, pp. 1-6.

[Pub. F] H. T. Nguyen, G. Y. Yang, A. H. Nielsen, and P. H. Jensen, "Challenges and research opportunities of frequency control in low inertia systems," submitted to *the 2018 5th International Conference on Systems and Informatics (ICSAI 2018)*, Nanjing, China, Nov. 10-12, 2018.

[Pub. G] H. T. Nguyen, G. Y. Yang, A. H. Nielsen, and P. H. Jensen, "Combination of Synchronous Condenser and Synthetic Inertia for Frequency Stability Enhancement in Low Inertia Systems," *IEEE Transactions on Sustainable Energy*, 2018, doi: 10.1109/TSTE.2018.2856938 (Accepted).

[Pub. H] H. T. Nguyen, G. Y. Yang, A. H. Nielsen, and P. H. Jensen, "Hardware- and Software-in-the-loop Simulation for Parameterizing the Model and Control of Synchronous Condenser," submitted to *IEEE Transactions on Sustainable Energy* (Under review).

[Pub. I] H. T. Nguyen, G. Y. Yang, A. H. Nielsen, and P. H. Jensen, "Damping Frequency Oscillation in a Low Inertia System via the Control of Synchronous Condensers," submitted to *IEEE Transactions on Sustainable Energy* (Under review).

CHAPTER 2

Frequency characteristics and control

In this chapter, first, the relevant theoretical concept of frequency characteristic and control is discussed. Second, a system configuration of the Western Danish (DK1) power system and its future scenarios, which is used as a typical low inertia systems, is presented. Finally, a system validation is investigated in terms of the frequency response based on the data provided by the local operator.

2.1 Frequency regulation

To maintain the power system operational security, the system frequency must be within the acceptable range of grid codes. If the frequency is outside of the predefined range, protection systems start activating to protect machines and electric equipment, which may cause sudden imbalances in generation and demand. This imbalance causes the frequency deviation to rise to an unacceptable level, therefore the disconnection of generation can occur, such as renewable generators or HVDC links, which may lead to a cascading failure or even a system collapse.

The system frequency depends on the balance between mechanical power input (generation) and electrical power output (load). An imbalance between generation and load will immediately cause a change in the rotational speed of synchronous generators and correspondingly to a change in the system frequency, as expressed by the following equation:

$$J\omega_m \frac{\mathrm{d}\omega_m}{\mathrm{d}t} = P_{gen} - P_{load} \tag{2.1}$$

where J is the moment of inertia of the system; ω_m is the mechanical rotational speed of synchronous generators; and P_{gen} and P_{load} are the total generation power and load power, respectively.

The load in the system is always changeable; thus, the system frequency always changes since the mechanical power applied to the generator's shaft is unable to follow the same rhythms of the electrical power change. Maintain a perfect nominal frequency value is difficult to achieve. Allowable ranges of frequency operating values are issued by national transmission system operators (TSOs). Whenever a frequency deviation is detected, a proper mechanical modification is applied to compensate the power imbalance and maintain the system frequency inside the acceptable range.

When a sudden change in load or generation occurs, for example, a load increase as shown in Fig. 1.2, the frequency response can be divided into different stages as follows: the inertial response reacts where the synchronous generators in operation inject the kinetic energy stored in their rotating mass, which endures for approximately a few seconds. This characteristic is a physical and inherent characteristic of synchronous generators. If the frequency deviation surpasses a specific value, the primary frequency controller will be immediately activated, which uses the generator governor to return the frequency to acceptable values within 30 s. After approximately 30 s, a

steady-state frequency error exists, the secondary control will be activated to return the system frequency to its nominal value, which needs several minutes to help the frequency completely recover. If the secondary control reserve is insufficient, a tertiary control will be manually applied to adjust the dispatching and unit commitment to restore the secondary control reserve and manually handle eventual congestion.

2.1.1 Inertia

System inertia is defined as the resistance to changes in the system frequency by storing/injecting kinetic energy from/to the system during power imbalance, which comes from synchronously connected rotating machines [17]. The kinetic energy of a system is calculated as

$$E_{rot} = \sum_{i=1}^{n} \left(\frac{1}{2} J_i \omega_{mi}^2 \right) \tag{2.2}$$

where J_i and ω_{mi} are the moment of inertia in $kg.m^2$ and the rotational speed in rad/s of the i-th rotating machine, respectively; and n is the number of rotating machines.

The system inertia constant is determined by the ratio of total stored kinetic energy in MJ at a synchronous speed to the MVA rating of the base system as:

$$H_{sys} = \frac{E_{rots}}{S_{base}} = \frac{\omega_{sm}^2}{2S_{base}} \sum_{i=1}^{n} (J_i) \tag{2.3}$$

where S_{base} is the MVA base of the system; E_{rots} is the total stored kinetic energy in MJ at the synchronous speed; J_i is the moment of inertia of the i-synchronous generator; and ω_{sm} is the synchronous speed of the synchronous generator in rad/s. The system inertia depends on the number of operating rotating machines and the inertia of each machine.

Table 2.1 summarizes the typical inertia constant of different types of generators, which primarily depends on the weight of the generator and the turbine and the high rotating speed [94, 95]. With wind generators, constant-speed wind turbine generators (types I and II) can provide inertial response, while variable-speed wind turbine generators (types III and IV) do not provide inertial response due to the decouple connection through converters. Variable-speed wind turbine generators can be controlled by a synthetic or virtual inertia controller.

The initial ROCOF that is determined by the size of the power imbalance and the system inertia is expressed by

$$ROCOF = \frac{f_0}{2H_{sys}} \frac{\Delta P}{S_{base}} = \frac{f_0 \Delta P}{2E_{rot}} \tag{2.4}$$

where ΔP is the disturbance size; and f_0 is the nominal system frequency. The initial ROCOF is decided by the system inertia or the total kinetic energy and the disturbance size.

A sudden change in load or generation causes a change in the generation-demand equilibrium. The system inertia constant plays a vital role in the first few seconds; afterward, primary control catches up the frequency deviation by controlling the governor to return the frequency to an acceptable operating value within 30 s. A higher inertia constant produces a lower ROCOF and a smaller frequency deviation as shown in Fig. 2.1, which gives time to the primary control regulating the power output. A higher system inertia renders the system stronger and capable of handling transient changes in system frequency and helps to stabilize the system. A lower system inertia

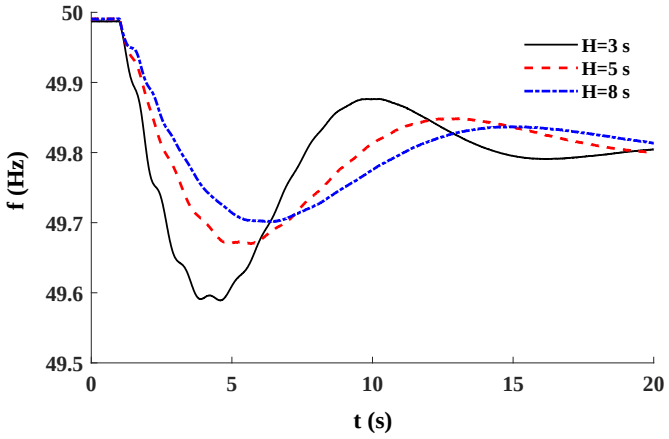

Figure 2.1: System frequency response with different inertia constants.

Table 2.1: Typical inertia constants of different machines.

Type of generation	H **(s)**
Nuclear power generator	5-8
Hydro generator	2-4
Other thermal generator	3-9
wind generator	2.4-6.8

accelerates the system dynamics with a high ROCOF, which may cause a cascading failure or even a system collapse.

Let us define H_1 and $ROCOF_1$ as the system inertia constant and ROCOF of the current system, respectively, and H_2 and $ROCOF_2$ as the system inertia constant and ROCOF of the future system that uses a majority of renewable energy, respectively. Thus, the ROCOFs of these two systems for a given disturbance are described based on (2.4) as follows:

$$ROCOF_1 = \frac{f_0}{2H_1}\frac{\Delta P}{S_{sys}} \tag{2.5}$$

$$ROCOF_2 = \frac{f_0}{2H_2}\frac{\Delta P}{S_{sys}} \tag{2.6}$$

From (2.5) and (2.6):

$$H_2 = H_1\frac{ROCOF_1}{ROCOF_2} \tag{2.7}$$

From (2.7), when the maximum ROCOF ($ROCOF_2$) imposed by TSOs is established, the minimum system inertia of the future system (H_2) for a given disturbance is determined based on the current system (H_1 and $ROCOF_1$). If the system inertia is less than this minimum value, ROCOF of the future system would be greater than the permissible value. The minimum system inertia enables the system to withstand a certain disturbance without exceeding a certain ROCOF is shown in Fig. 2.2. The general evaluation of the minimum inertia will encompass a disturbance size from 5% to 30% of the system load and the maximum ROCOF between 0.5 and 2.5 Hz/s [9]. As can be seen

clearly that there is a reverse correlation between the minimum system inertia and the maximum ROCOF, the higher the maximum ROCOF is allowed, the lower the minimum system inertia is required. Conversely, a positive correlation exists between the minimum system inertia and the disturbance size; a larger disturbance requires a higher system inertia to ensure that the system frequency does not exceed the permissible maximum ROCOF.

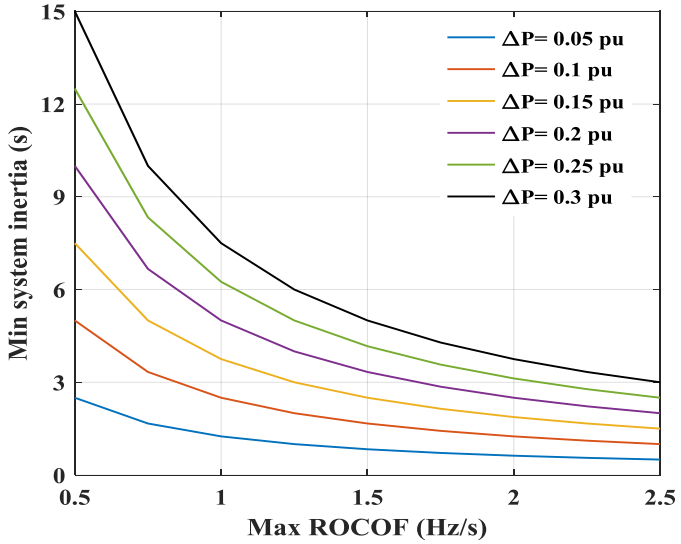

Figure 2.2: The dependence of system inertia on maximum ROCOF and disturbance size.

The frequency deviation is regulated by the available frequency containment reserves. In the DK1 system, the frequency deviation depends on the available primary control headroom of the online synchronous generators (SGs) and the German grid. The Western Danish system is synchronized to the Continental European system where its primary reserve is designed to ensure that the system frequency deviation remains within a certain range for ordinary and severe contingencies [96]. The system primary regulation constant for the entire system in MW/Hz is determined by

$$K_{sys} = \sum_{i=1}^{N} K_i = \sum_{i=1}^{N} \frac{S_{ni}}{R_i f_0} \tag{2.8}$$

where K_i and R_i are the regulation constant and the droop gain, respectively, of i-th synchronous generator. The system primary regulation constant determines how much active power supplies/absorbs against frequency changes. K_{sys} is decided by the primary reserve.

When the system operates with high renewable energy production, high importing HVDC links, and phasing out of conventional power plants, the system inertia significantly decreases, which accelerates the frequency dynamics and renders it more vulnerable. This situation may activate of under-frequency load shedding or ROCOF-operated protection relays for tripping transmission lines. As a result, the system freely splits and becomes more challenging to operate. Cascading failure or even a system blackout can occur.

2.1.2 Inertial response

As shown in Fig. 1.2, in the first few seconds following a disturbance, the system frequency starts to decrease. The initial transient frequency response is controlled by the inertial response of the online

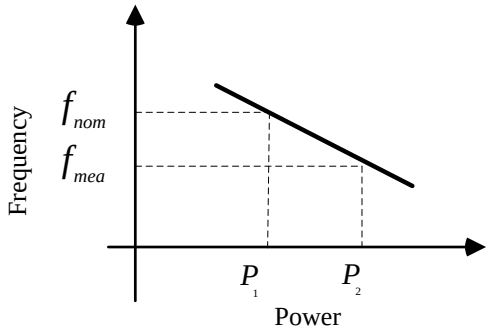

Figure 2.3: Droop characteristics.

rotating machines which is proportional to the ROCOF based on (2.1). The rotating machines release their stored kinetic energy based on (2.2) into the system, which reduces the initial ROCOF and enables the governor to activate and contribute to frequency stability control. The first step is a natural response of rotating machines during a frequency excursion, which usually lasts few seconds after the disturbance.

2.1.3 Primary control

The step following the inertial response is primary control, which is known as the instantaneous proportional increase or decrease in the active power output to respond to the system frequency deviation. This response contradicts any frequency changes and is obtained by governor action to instantly act relative to the frequency deviation.

Primary control usually occurs within seconds to tens of seconds after a change in the system frequency and is achieved by automatic control on prime movers. When the frequency deviates from a nominal value beyond a deadband, the governor will respond to control the prime mover power output, which is proportional to the speed deviation (droop control R_i) as expressed by the following equation:

$$R_i = \frac{1}{K_i} = \frac{\Delta f}{\Delta P} \tag{2.9}$$

where R_i and K_i are the droop constant and governor gain of the i-th synchronous generator, respectively; Δf is the frequency deviation of the system (Hz); and ΔP_i is the active power of the i-th synchronous generator, which contributes to the primary frequency control during the frequency disturbance, as shown in Fig. 2.3. Typical droop gain ranges from 2%-12% [39] for all synchronous generators.

A 6% droop constant indicates that a 6% frequency deviation (3 Hz for 50 Hz nominal frequency) causes a change of 1 pu in power output. A higher R represents lower sensitivity of the generator. The higher is the governor gain K, the higher is the contribution of primary control by the generator. Typically, primary control by governor action may not return the frequency to the nominal value. However, the governors are designed to stabilize at a speed that corresponds to a new equilibrium point, which may differ from the pre-disturbance value. Other control components are used to restore the frequency to the nominal point.

Primary control, which is also commonly known as frequency containment reserves (FCR) according to the ENTSO-E definition, is fast acting capabilities of reserve providers (online power plants,

storage, and demand response) to increase/decrease the power output on a very short term (within 0 to 30 seconds) [97, 98]. FCR are automatically activated by the system frequency deviations by the control equipment to maintain the power balance in the entire synchronously interconnected system. The total FCR volume in the European continental synchronous area is fixed at 3000 MW. Energinet's share is determined by the production of Western Denmark relative to the total production of the continental European system and is fixed once a year. Various FCR properties applied to different synchronous areas are shown in Table 4.10. In the Nordic system, FCR are divided into 2 operational cases; normal operation (FCR-N) and disturbed operation (FCR-D). The FCR-N, is the power reserve to control the system frequency within its standard frequency range ($\pm$100 mHz). The total FCR-N reserve of the Nordic system is 600 MW and is fully available at the nominal frequency value. The FCR-D is the power that is available for frequency regulation within the area of 49.9 - 49.5 Hz. This power must be activated to 50% within 5 seconds and activated to 100% within 30 seconds. The FCR-D volume of the Nordic system is set to 1200 MW [99].

Table 2.2: FCR properties in different synchronous areas.

Properties	**CE**	**GB**	**NE**
FCR activation delay (including deadband)	10 mHz	15 mHz	10 mHz
FCR full activation time	30 s	10 s	30 s
FCR full activation fre. deviation	$\pm$200 mHz	$\pm$500 mHz	$\pm$500 mHz

2.1.4 Secondary control

Secondary control is conducted after primary control to return the frequency to the target value, which is executed by an automatic generation controller and referred to as load frequency control. This control is achieved by a further slow change in the prime mover load reference which is much slower than the primary control, typically a 10-15 minute time frame. In primary control, the amount of power to be shared by generators is determined by the turbine control system settings. In secondary control, the amount of load shared by generating stations or a group of generating stations in an area is determined by the load dispatch center. This control considers the economical operation of the entire system which has several interconnected systems.

Secondary control, which is also known as frequency restoration reserves (FRR) according to the ENTSO-E definition, is the active power reserves that is available to restore system frequency to the nominal frequency [97, 100]. FRR replace FCR if the frequency deviation continues longer than 30 seconds. FRR can be automatically activated, which is referred to as automatic frequency restoration reserves (aFRR), and manually activated, which is referred to as manual frequency restoration reserves (mFRR).

2.1.5 Tertiary control

If the secondary control reserve is not sufficient, a tertiary control will be manually applied to adjust the dispatching and unit commitment to restore the secondary control reserve and manually handle eventual congestion.

The tertiary control, which is known as replacement reserves (RR) according to the ENTSO-E definition, is the active power reserves that is available to restore or support the required level of FRR to be prepared for additional system imbalances, including generation reserves [97, 101]. The activation time ranges from 15 minutes to hours with the Continental European system. Contrary to FCR and FRR, some TSOs in the EU do not implement RR.

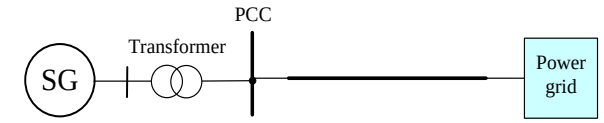

(a) Synchronous generator connected to power grid.

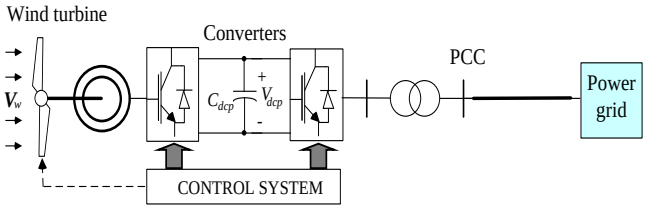

(b) Wind generator connected to power grid.

Figure 2.4: Synchronous generator and wind generator connected to power grids.

2.2 Impact of high-level penetration of converter-based generation on frequency stability

To achieve a smooth energy transition, fossil-fuel-based generators will be decommissioned and replaced by renewable-based power plants. Conventional generators are electromagnetically connected to the system, which can provide rotating energy for inertial response during frequency disturbances and ancillary services for balancing and transient characteristics. Conversely, converter-based generation (wind, solar PV, and HVDC interconnections) is decoupled from the system by converters, as shown in Fig. 2.4, and does not supply inertia for the system during frequency excursions. Furthermore, this replacement reduces the number of generation units provided for frequency control, and increases the requirement for primary control reserves to halt frequency at the same frequency nadir following a sudden increase of load or generator trip.

The significant reduction in system inertia of this replacement renders the system frequency more vulnerable and accelerates the frequency dynamics. Operating at such a low inertia condition may prevent the system frequency from experiencing a power oscillation due to a poor inertial response during disturbances, which may cause asynchronous issues for multi-area systems, and a cascading failure or even a collapse of the whole system.

2.3 Grid codes for frequency requirement

As mentioned above, four important indicators are employed to evaluate the frequency response of a system. The ROCOF and frequency nadir must be kept as small as possible to avoid the relays from being activated. Thus, strict requirements for these parameters must be forced to guarantee a secure system operation, which is referred to as the grid code (GC).

The GC is a technical document issued by the TSO of each transmission system that establishes the requirements governing the operation, maintenance, and development of power systems, which are periodically updated with new rules and are varied from site to site. Countries with high-level penetration of renewable energy have issued a dedicated GC that focuses on power quality, power operation and control, and fault ride-through capability. This work is implemented

based on the Western Danish power system, which is synchronized with the continental central European system operated by ENTSO-E and the local TSO (Energinet). The GC for the frequency requirement applied to the study is listed as Tables 2.3 and 2.4 [102, 103].

Table 2.3: ENTSO-E grid codes for frequency quality defining parameters of the synchronous areas.

-	CE	GB	NE
Standard frequency range	±50 mHz	±200 mHz	±100 mHz
Max. instantaneous frequency deviation	800 mHz	800 mHz	1000 mHz
Max. steady-state frequency deviation	200 mHz	500 mHz	500 mHz
Time to recover frequency	N/A	1 minute	N/A

Table 2.4: Different grid codes applied for different grids.

-	Sweden	Denmark (Energinet)	ENTSO-E (Draft 24 Jan. 2012)
Continuous operating frequency	49-51 Hz	49.9-50.1 Hz	49-51 Hz (for Nordic)
ROCOF	N/A	±2.5 Hz/s	Up to 2 Hz/s

2.4 System configuration and validation

In this section, a system description is presented for the current Western Danish power system and the future Western Danish renewable system scenario, where electricity is supplied by 100% renewable energy. Furthermore, the simulation system is validated in RTDS based on the phasor measurement unit data of a frequency event of the real system provided by the local operator.

2.4.1 System configuration

The Danish electricity system is divided into two non-synchronous areas: the Western Danish power system (DK1) is synchronized with the continental European system, whereas the Eastern Danish power system (DK2) is synchronized with the Nordic power system, which includes Sweden, Norway, and Finland. DK1 and DK2 are linked by an LCC HVDC interconnection, which is known as the Great Belt link with a 400 kV DC connection with a transmission capacity of 600 MW. Currently, the Western Danish power system has three major offshore wind farms; two wind farms are located at Horns Rev 1, 2 (HR 1, 2) and one wind farm is situated at Anholt, as shown in Table 1 [104–106]. Wind turbine generators within a farm are aggregated into a single unit, which is not precise because all wind turbines do not receive similar wind speeds due to wake effects. Each wind turbine experiences losses on its transformer and cables before coming to the point of common coupling. However, this study focuses on the total capacity output of a wind farm which impacts the system frequency stability; thus, an aggregate approach is applied.

For Western Denmark, the interconnection to Sweden occurs through two LCC HVDC links, and the interconnection to Norway consists of three LCC HVDC and one VSC HVDC, according to the

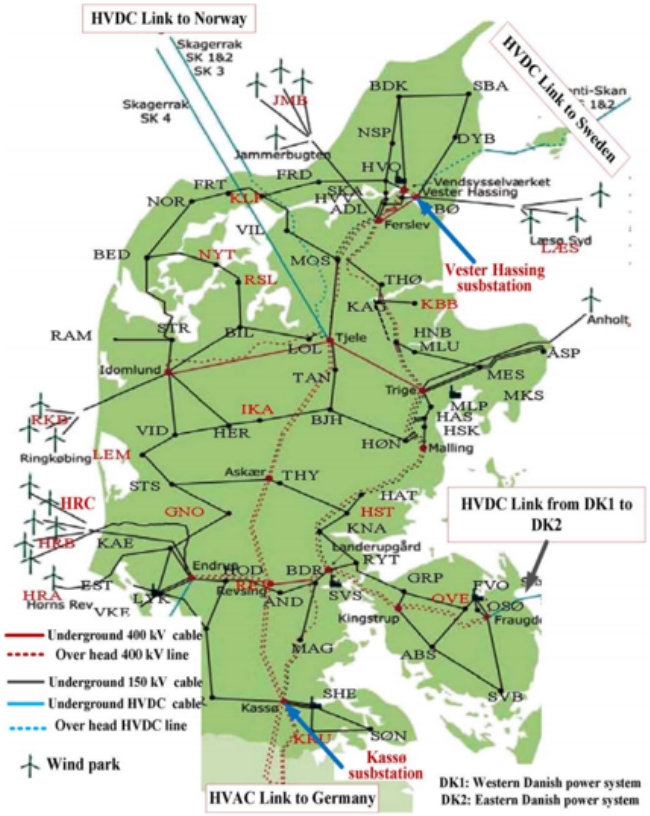

Figure 2.5: Geographical map of the Western Danish power system connected to the neighboring areas.

specification shown in Table 2. The interconnection to Germany comprises four AC connections, two 400 kV connections and two 220 kV connections. Seven synchronous generators and three synchronous condensers are in operation, as shown in Fig. 2.8. The German HVAC interconnection is modeled by a large synchronous generator with an inertia constant of 7.5 s, and its frequency control support is proportionally adjusted to the power exchange based on the data provided by the local operator. The location of the SCs in the Danish system, which is shown in Fig. 2.6, there are 4 SCs located in the DK1 system: three purple SCs are installed in three HVDC terminals to Sweden, Norway, and DK2, which belong to transmission operator (Energinet), and the green SC belongs to a private company, which only operates when necessary.

In the future Western Danish power system, these conventional units will be phased out in favor of renewable generation units with lower marginal costs. Focusing on the system inertia, these renewable-based power plants behave differently from traditional generation facilities and are generally connected through partial or fully power electronic converters, which causes the link between the rotational speed of the plants and the grid frequency to be removed. As a result, these converter-interfaced generators do not naturally contribute to the system inertia during disturbances. In addition, the installation of additional HVDC links and wind farms will be installed in the DK1 power system (COBRA cable to the Netherlands and Viking link to England [107, 108], 400 MW offshore wind farm located at Horns Rev namely HR3 [109, 110]) is expected. Because these converter-based components electrically decouple, the DK1 system inertia is not directly accessible to the others and much more dependent on the German interconnection. To

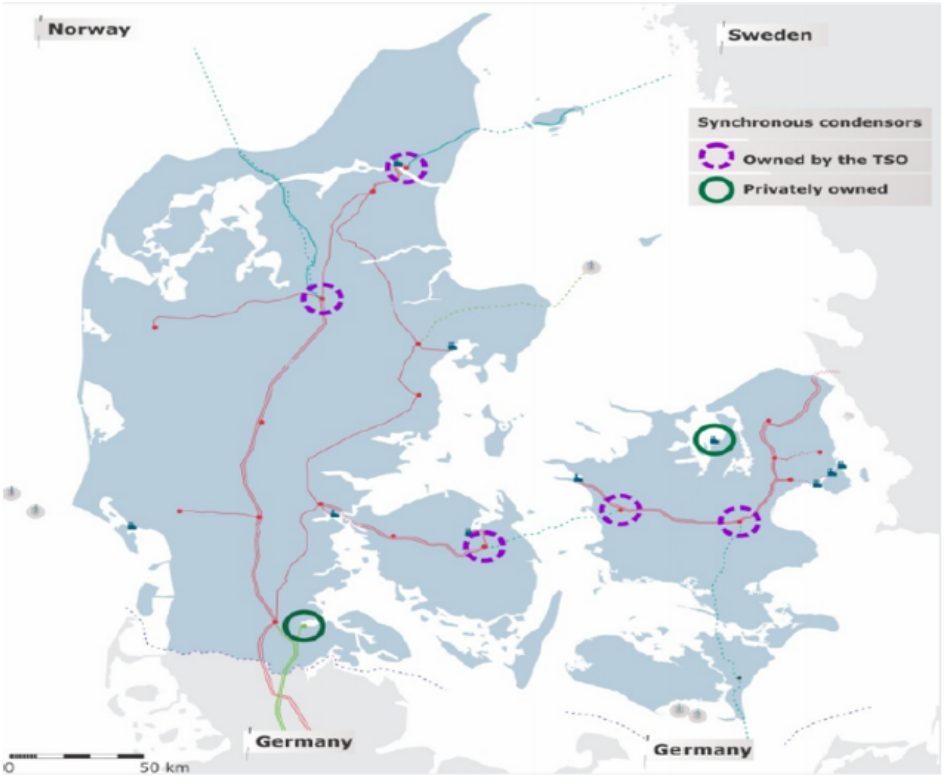

Figure 2.6: Synchronous condenser locations in the current Danish power system.

completely phase out fossil fuel generators in 2050, the system inertia will be significantly reduced, which introduces many challenges for the operation, security, and control of the system. In this study, the future DK1 power system is used as a typical low inertia system of converter-based systems.

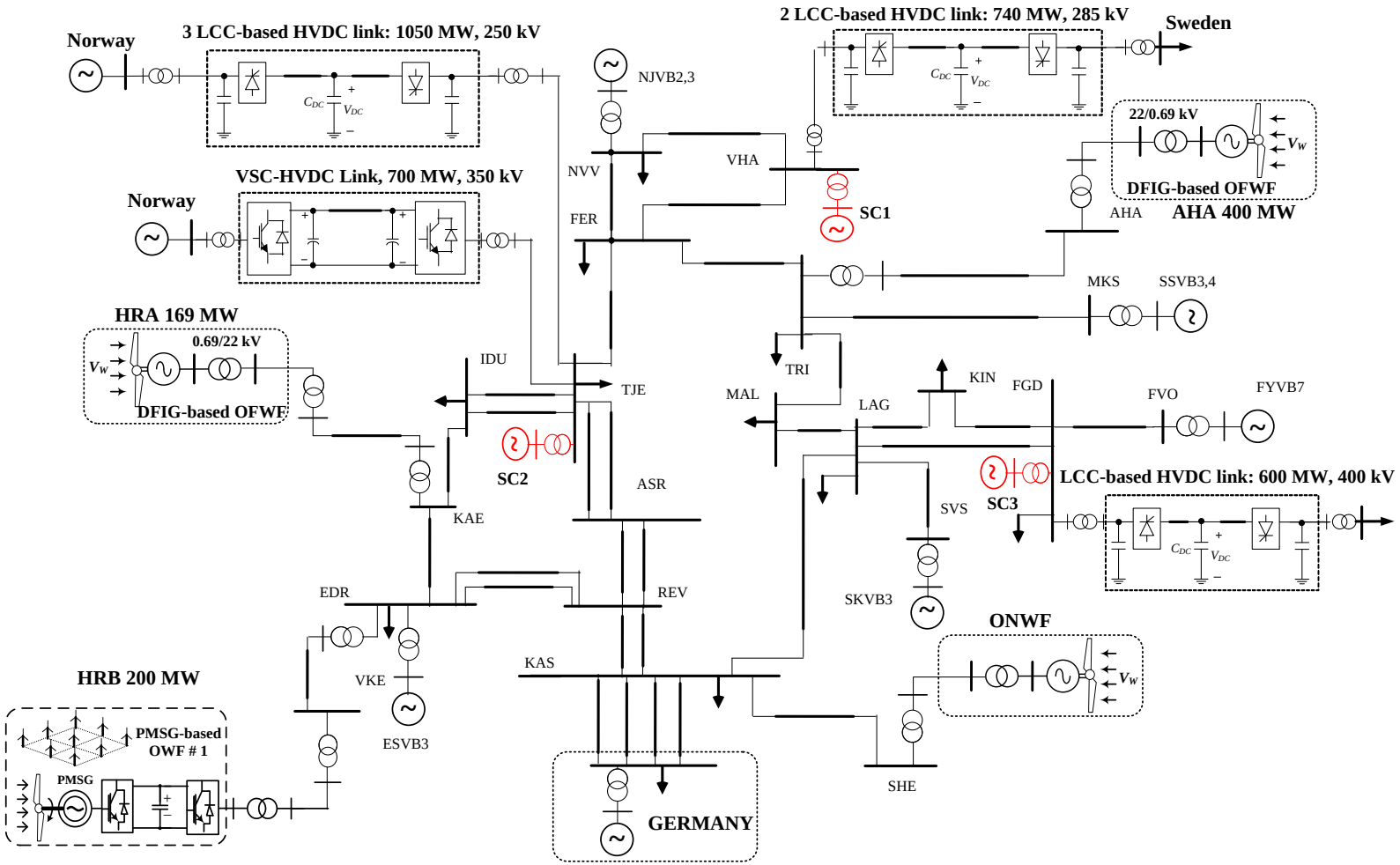

Figure 2.7: Single-line diagram of current 400 kV Western Danish renewable-based system.

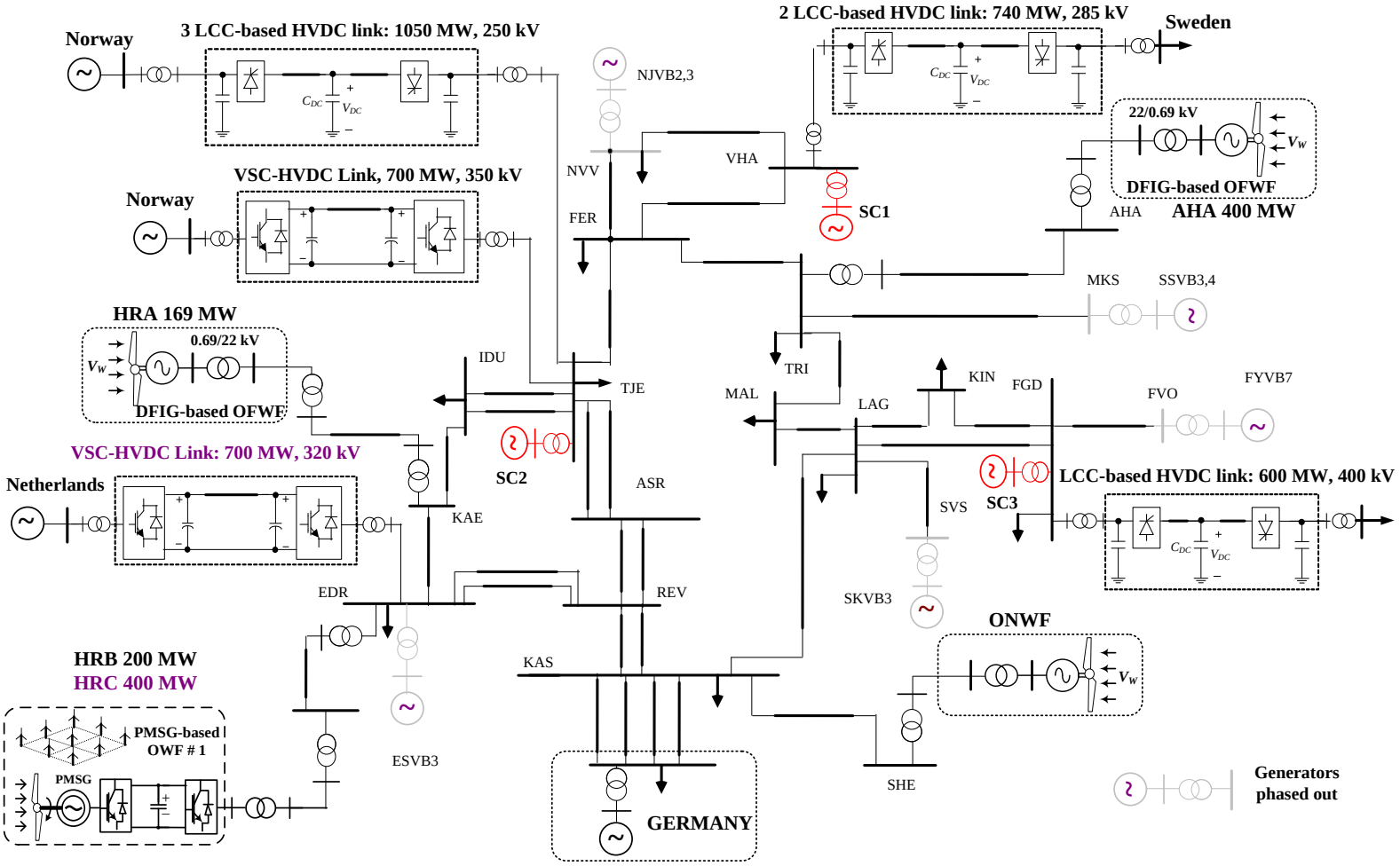

Figure 2.8: Single-line diagram of 400 kV Western Danish renewable-based system in 2020.

The DK1 power system is modeled and run in real time using RTDS platform, which includes different components, such as LCC-HVDC, VSC-HVDC, DFIG, PMSG, synchronous generators, transmission lines, and synchronous condensers. The system specification and different operating scenarios are modeled based on the data provided by the local transmission operator (Energinet).

The single-line 400 kV diagram of the current DK1 system and that of the prospective DK1 system in 2020 are shown in Fig. 2.7 and Fig. 2.8, respectively. Three main differences are observed between the 2 systems as follows: one more HVDC named COBRA cable is connected to the Netherlands, one more OFWF is located at Horns Rev C (HRC) which is aggregated with the HRB and becomes a single unit because they are the same wind generator type (type 4), and all synchronous generators will be decommissioned in 2020.

2.4.2 System validation

In this part, a system validation is investigated based on a generator trip event in France of the continental European system, which had introduced a frequency excursion on the DK1 system. The frequency response at the KAS substation during 932 MW unit (approximately 0.242% of the total generation (385000 MW)) at the Cruas nuclear power plant trip on 29th August 2011 has been retrieved via the Danish PMU system of the central system frequency as shown in the first sub-figure of Fig. 2.9. In the simulation system, this generator is modeled with a scale capacity and connected via a long transmission line. A comparison is made to determine the similarity between the simulation system and the real system in terms of the frequency response as shown in Fig. 2.9. It can be seen that the frequency of the simulation system and the real system are similar in terms of frequency deviation and ROCOF. The frequency drops approximately 0.04 Hz after approximately 10 s.

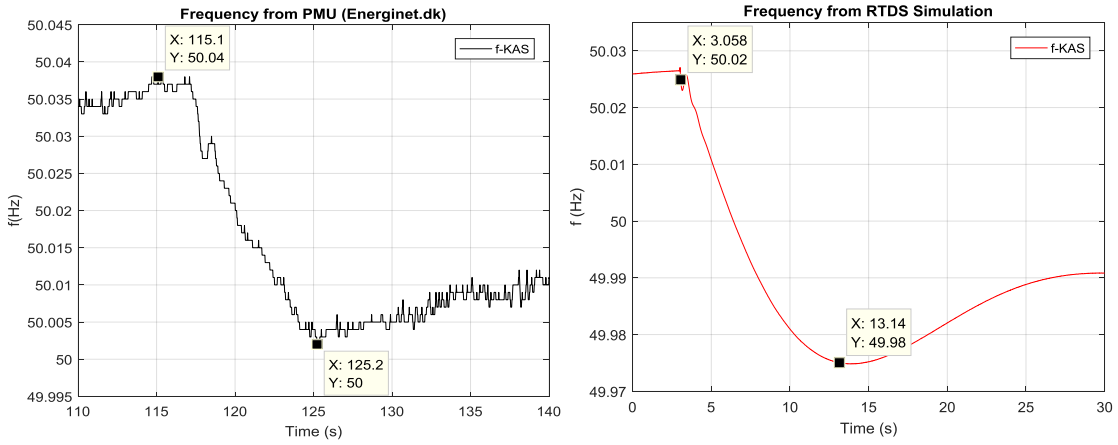

Figure 2.9: Comparison of frequency responses during a generator trip event.

CHAPTER 3

Hardware- and software-in-the-loop simulation for automatic voltage regulator system

In this chapter, first, HiL testing of AVR and limiters of SC is described step by step. Second, software-in-the-loop simulation for parameter optimization of an AVR simulation model, which is based on an IEEE model to achieve a characteristic that is similar to the AVR hardware, is investigated. Finally, a case study following each part is investigated to validate and verify their performance.

3.1 Hardware-in-the-loop test of automatic voltage regulator

An AVR system is considered to be the heart of an SC to fulfill volt/var control in power systems. Maintaining a constant specific voltage level is a challenging task in power systems, especially for renewable-based systems, where components are more sensitive to the voltage. If the voltage is higher than its threshold, it may cause a breakdown of the insulation system. Conversely, a lower voltage than its critical value may cause a disconnection of the voltage-based protection components, which can lead to a cascading failure or even a system blackout. Therefore, a high performance and fast AVR control system are necessary to address these issues.

Testing AVR performance in steady-state and dynamic conditions in real grids is expensive and difficult with low efficiency. To address this issue, a HiL platform is implemented to test the steady-state and dynamic performances of AVR and limiters in different operating conditions with low cost, high efficiency, and flexibility. To validate the AVR hardware control, a startup procedure and voltage setpoint changes are investigated. Overexcited and under-excited conditions, as well as AVR setpoint loss, are tested to compare the performance of an SC with the AVR hardware and that of the simulation.

3.1.1 Synchronous condenser model

A synchronous condenser is a synchronous machine that plays a significant role in power systems for reactive power compensation and voltage control. To analyze the dynamic condition in a synchronous machine, a two-axis model of the synchronous machine is commonly used. Using the 6^{th} order, a synchronous machine is described by [111]:

$$T_{do}^{'}\frac{dE_q^{'}}{dt} = -E_q^{'} - (X_d - X_d^{'})[I_d - \frac{X_d^{'} - X_d^{"}}{(X_d^{'} - X_{ls})^2}(\psi_{1d} + (X_d^{'} - X_{ls})I_d + E_q^{'})] + E_{fd} \tag{3.1}$$

$$T_{do}^{"}\frac{d\psi_{1d}}{dt} = -\psi_{1d} + E_q^{'} - (X_d^{'} - X_{ls})I_d \tag{3.2}$$

$$T_{qo}^{'}\frac{dE_d^{'}}{dt} = -E_d^{'} - (X_q - X_q^{'})[I_q - \frac{X_q^{'} - X_q^{"}}{(X_q^{'} - X_{ls})^2}(\psi_{2q} + (X_q^{'} - X_{ls})I_q + E_d^{'})] \tag{3.3}$$

$$T_{qo}^{"}\frac{d\psi_{2q}}{dt} = -\psi_{2q} + E_d^{'} - (X_q^{'} - X_{ls})I_q \tag{3.4}$$

$$\frac{d\delta}{dt} = \omega - \omega_s \tag{3.5}$$

$$\frac{2H}{\omega_s}\frac{d\omega}{dt} = T_m - T_e - T_D \tag{3.6}$$

with

$$T_e = \frac{X_d^{"} - X_{ls}}{X_d^{'} - X_{ls}}E_q^{'}I_q + \frac{X_d^{'} - X_d^{"}}{X_d^{'} - X_{ls}}\psi_{1d}I_q + \frac{X_q^{"} - X_{ls}}{X_q^{'} - X_{ls}}E_d^{'}I_d - \frac{X_q^{'} - X_q^{"}}{X_q^{'} - X_{ls}}\psi_{2q}I_d + (X_q^{"} - X_d^{"})I_dI_q \tag{3.7}$$

where $E_{q,d}^{'}$ is the transient voltage in q-/d-axis; E_{fd} is the field voltage; H is the inertia constant; $I_{q,d}$ is the current in q-/d-axis; $T_{qo,do}^{'}$ is the transient time constant of q-/d-axis; $T_{qo,do}^{"}$ is the subtransient time constant of q-/d-axis; T_m is the mechanical torque (T_m is zero with SC); T_D is the additional damping torque; $X_{q,d}^{'}$ is the transient reactance in q-/d-axis; $X_{q,d}^{"}$ is the subtransient reactance in q-/d-axis; X_{ls} is the leakage reactance; δ is the rotor angle; ψ_{1d} is the flux linkage d-axis damper winding; ψ_{2q} is the flux linkage q-axis damper winding; ω is the rotor speed; ω_s the synchronous rotor speed.

Equations (3.1)-(3.2) represent the dynamics in the d-axis, equations (3.3)-(3.4) describe the dynamics in the q-axis, and equations (3.5)-(3.6) are the swing equations.

3.1.2 Automatic voltage regulator model

The AVR model implemented in the HiL platform is based on PID control that is modified from the AVR model of the IEEE AC7B excitation system, as shown in Fig. 3.1 [112]. An AVR system is a closed control loop that is used to maintain the terminal voltage of machines at a specific value.

The terminal voltage of the SC is sent through a voltage compensator, is transformed to V_C, which becomes the feedback signal of AVR control, and is then compared with the reference value V_{ref}, as shown in Fig. 3.1. The reference value is the nominal voltage value converted to per unit (1 pu). Any change in the terminal voltage from the reference value is reflected in the error signal (e). The deviation e works as the input for PID control to generate the AVR output V_R:

$$V_R = K_P e + K_I \int_0^t e\mathrm{d}t + K_D \frac{\mathrm{d}e}{\mathrm{d}t} \tag{3.8}$$

where K_P, K_I, and K_D are the proportion, integral, and differential gains, respectively, of the PID control.

Whenever a difference between V_C and V_{ref} is detected, PID control immediately reacts to correct the deviation. The higher is K_P, the faster is the correction. However, a large K_P can cause a

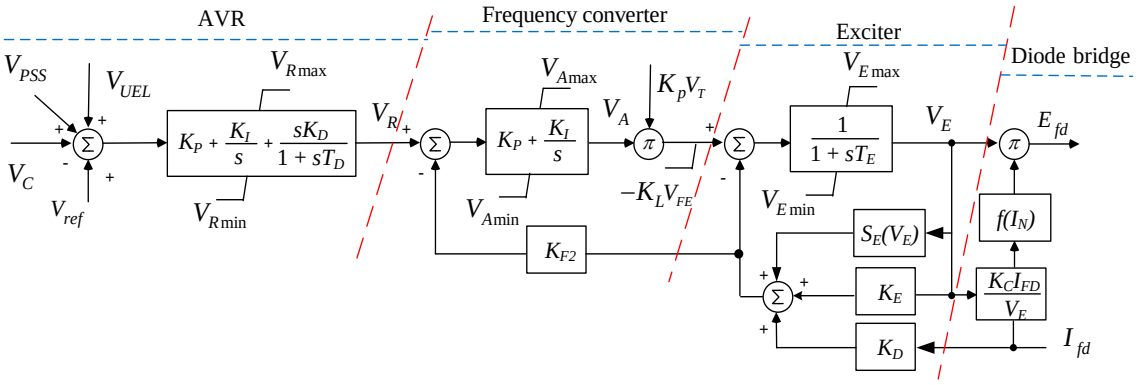

Figure 3.1: IEEE AC7B excitation system.

large oscillation in the output. The static error of the terminal voltage is eliminated by the integral function. The lower is K_I, the smaller is the overshoot obtained by the output; however, the system may experience more oscillations during the dynamic period. The differential function improves the disturbance rejection ability but may carry the noise of the input to the output. A low-pass filter ($\frac{1}{1+sT_D}$) is usually added for the derivative term to reduce the noise.

The value of V_R is converted to a percentage as the AVR setpoint that sends to the frequency converter of the excitation system, as shown in Fig. 3.1. The incorporating limiters of the AVR, such as overexcitation, under-excitation, stator current, and V/Hz limiters, are implemented in HiL. The remaining parts of SC and the grid models are simulated in real-time using RTDS [113].

3.1.3 Automatic voltage regulator hardware implementation

Figure 3.2 presents the configuration diagram of the system interfaced with the hardware-in-the-loop test of the AVR. The entire grid and SC model without the AVR system are simulated in RTDS with the dashed blue boundary, while the AVR system is implemented in the hardware with the dashed red boundary. The RTDS sends the three-phase current and voltage of the generator side, the excitation current and voltage, and the busbar frequency and voltage of the grid side to the hardware platform, whereas the hardware platform transfers the AVR setpoint (AVR SP) and ON GRID signal to the RTDS.

Regarding the RTDS interface, the RTDS can receive and send their analog and digital signals to the HiL platform by Giga Transceiver I/O cards (GTIO), which include Giga Transceiver Analog Input/Output cards (GTAI/GTAO) and Giga Transceiver Digital Input/Output cards (GTDI/GTDO) [114]. One GTAO/GTAI card consists of 12 analog output/input channels with an output/input voltage range of ± 10 V. One GTDO/GTDI card includes 64 optically isolated digital output/input channels, which are arranged into two banks with 32 channels in each bank. Each bank of 32 channels is operated at a voltage level in the range of +5 VDC. If the external device output signal is out of range, a variable resistor must be used to obtain the proper voltage value. Ten analog signals are sent to the hardware platform from the RTDS: three-phase current (I_A, I_B, I_C) and voltage (V_A, V_B, V_C) of the SC, excitation current (I_E) and excitation voltage (V_E), as well as busbar voltage and frequency (V_{Grid}, F_{Grid}), as shown in Fig. 3.3(a). With the terminal voltage and current outputs of the SC, the subsequent measurement of the transformers in RTDS are 115 V and 5 A, which are out of the acceptable range of the GTAO card. Consequently, a scaling ratio

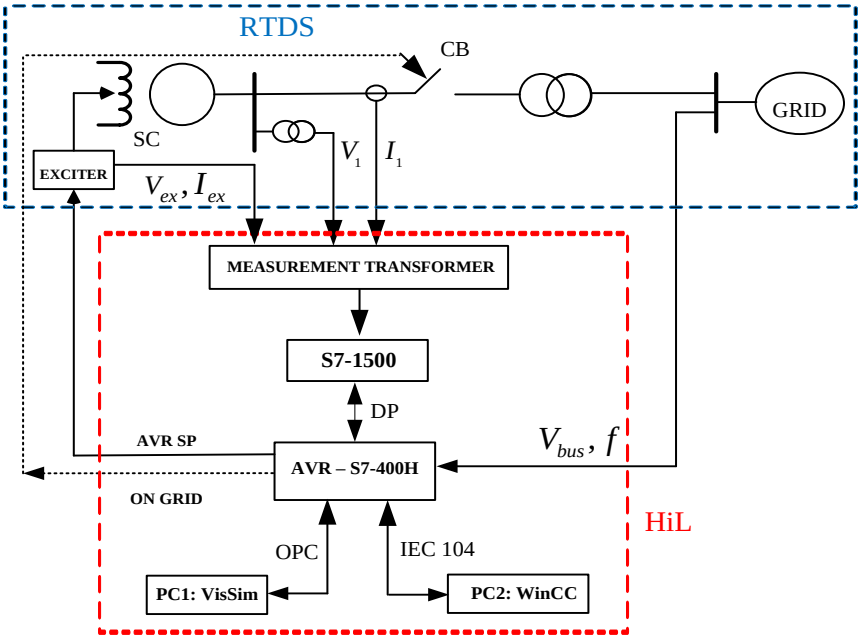

(a) The system interfaced with AVR hardware

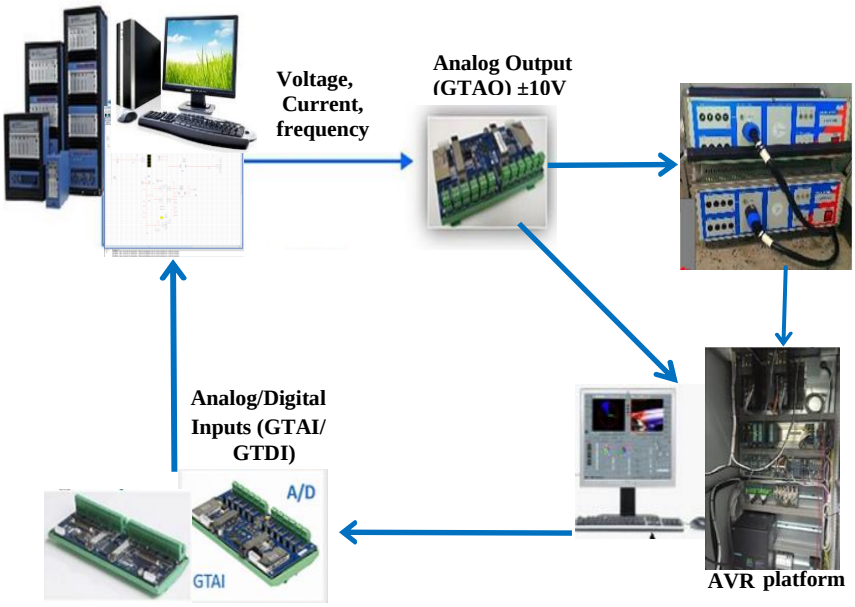

(b) AVR hardware setup

Figure 3.2: The AVR hardware-in-the-loop platform.

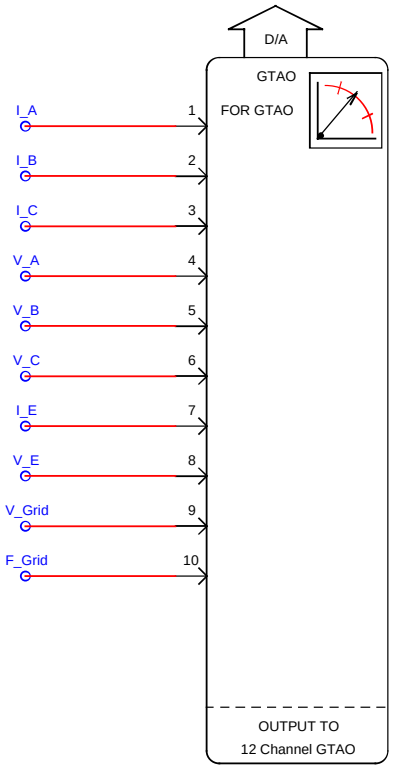

(a) Sending signals to GTAO card

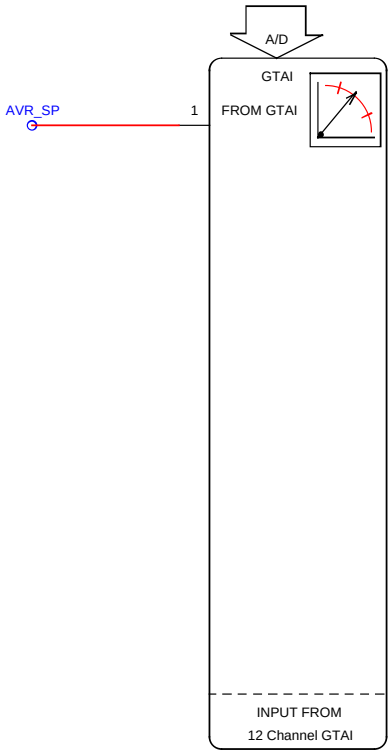

(b) Receiving signals from GTAI card

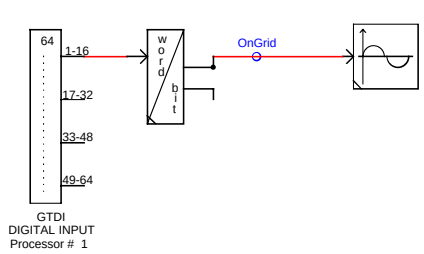

(c) Receiving signals from GTDI card

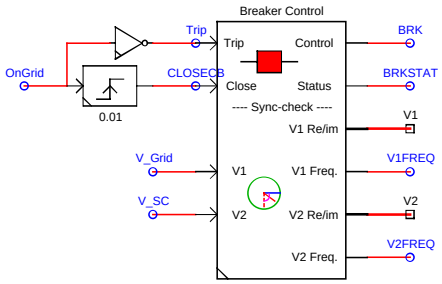

(d) Circuit breaker logic

Figure 3.3: Sending and receiving signal setup for GTAO, GTAI, GTDI, and circuit breaker in RTDS. (a) Sending signals to GTAO card. (b) Receiving signals from GTAI card. (c) Receiving signals from GTDI card. (d) Circuit breaker logic.

is implemented inside of the GTAO card to obtain the proper value is sent through the card, as shown in Fig. 3.3(a). However, the analog input of the external device requires other ranges: 1 A for the current and 100 V for the voltage, which corresponds to their nominal values. A power amplifier is used to satisfy the HiL required values, as shown in Fig. 3.2(b). The excitation current and voltage, as well as the frequency and voltage of the busbar through scaling ratios inside of the GTAO card are sent directly to the hardware.

The ON GRID signal with 24 VDC sent to the RTDS from the hardware is out of the range of the

GTDI card, and a resistor that works as a voltage divider is implemented to obtain a 5 VDC signal for the GTDI card, as shown in Fig. 3.3(c). Furthermore, the AVR setpoint from the hardware operates at a range from 0 to 150%, which corresponds to 0 to 10 VAC, and is sent to RTDS via a GTAI, as shown in Fig. 3.3(b).

A circuit breaker (CB) is responsible for the synchronization check by monitoring the voltage and frequency in terms of the magnitude and phase sequence of the SC side and the grid side as shown in Fig. 3.3(d). When their differences are within a certain tolerance, the CB is closed and the SC model in RTDS is synchronized with the grid. This procedure is described in the case study section.

The entire SC system, including the AVR controller, is programmed in VisSim software in PC1 for the startup procedure of SC, whereas the AVR hardware is programmed in the programmable logic controller (PLC) S7-400 via WinCC, which is located at PC2, as shown in Fig. 3.2(a). The main components of the hardware platform consist of two PLCs S7-1500 and S7-400H and measurement transformers. S7-1500 is responsible for the measurement data and computation of signals from transformers, while S7-400H is in charge of AVR control functions. Three-phase 100 VAC voltage and 1 AAC current outputs from the OMICRON power amplifier are sent directly to the measurement transformers. These voltage and current signals transfer to S7-1500; after storing and processing these signals, they are sent to S7-400H, where the AVR is programmed.

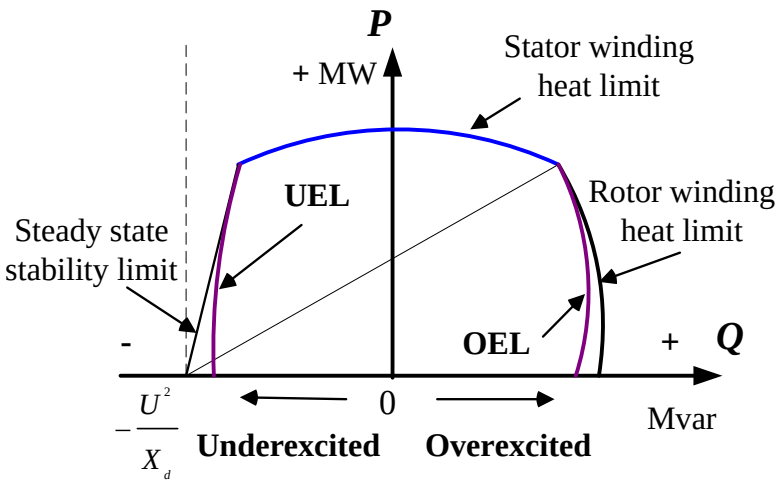

Figure 3.4: The PQ capability diagram of the synchronous generator.

3.1.4 Limiter implementation

Fig. 3.4 shows a PQ capability diagram of the synchronous generator, which is considered to be a thermal diagram of the machine. The stator current limit represents the stator winding isotherm, the field current limit describes the rotor winding isotherm, and the limit in capacitive regime conditions acts for the isotherm of the frontal teeth. Regarding the synchronous condenser, the field current limit, the stator current limit, and the flux limit have a key role to guarantee operation in the steady-state stability margin. These limiters are embedded in the AVR hardware as the thermal protective functions, namely, underexcitation limiter (UEL), overexcitation limiter (OEL), and stator current limiter (SCL). The UEL prevents the synchronous condenser from operating below the

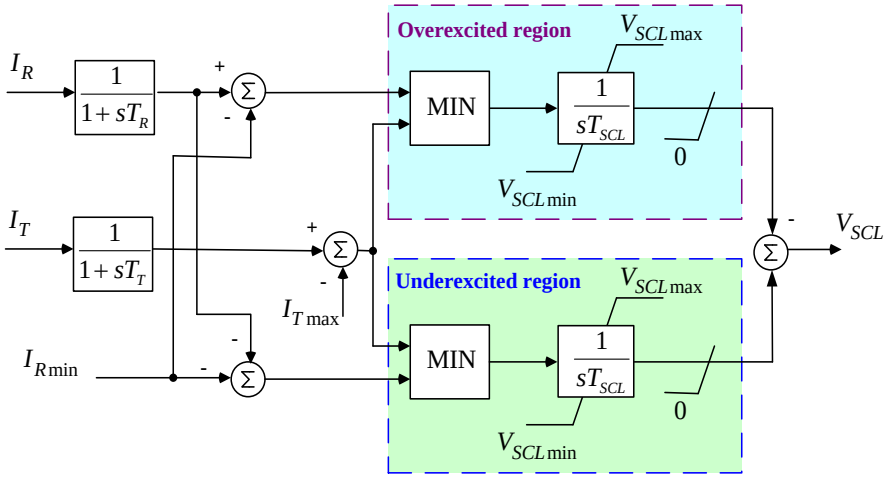

Figure 3.5: SCL limiter

end core limits and the steady-state stability limit; the OEL prevents the synchronous condenser from operating above the rotor winding heat limit; and the SCL protects the stator winding from operating over the heat limit. These limiters enable the SC to operate in the maximum transient to support the power system during disturbances while ensuring that SC operation remains within allowable regions, as indicated in Fig. 3.4.

Stator current limiter implementation

The SCL aims to ensure that the stator is operated within its ratings. Mathematically, the stator current can be decomposed into reactive and active components. This limiter action depends on the operating point, and SCL will control the reactive component to limit the absolute value of the stator current, which limits the losses (or heating I^2R) in the stator winding. In the overexcited region, the limiter needs to reduce the excitation current to reduce the absolute value of the stator current and thus declining the losses in the stator winding. Conversely, in the underexcited region, the excitation current needs to be increased to attain the allowable value which causes a decrease in the stator losses and heating. In the vicinity of a power factor of one, a further change of the terminal voltage will not decrease the stator current and is blocked by the parameter I_{Rmin}.

The limiter is active when the stator current is higher than the pickup value I_{Tmax}. If the difference is positive for more than 10 s, the limiter is activated and worked, as shown in Fig. 3.5. This output is subtracted to the AVR summing point. When the V_{SCL} is equal to 0 for more than 2 s, the limiter is deactivated.

Under-excitation limiter implementation

When the SC becomes underexcited to the point that the negative reactive power may fall below the SC capability limit, the UEL will react by producing a positive error signal that will be supplied to the AVR to require the AVR to increase the output voltage by increasing the voltage setpoint until the SC operating point increases above the UEL limit line characteristics [115]. One important function of the UEL is to prevent SCs from operating beyond their steady-state stability limits,

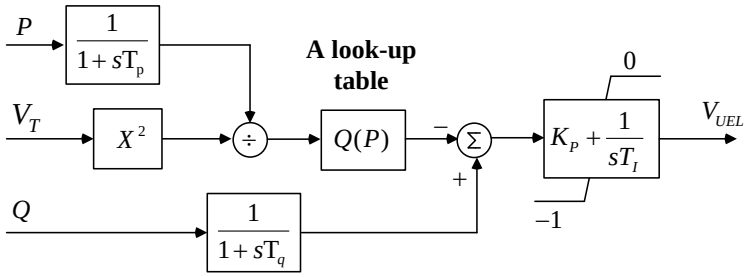

Figure 3.6: UEL limiter

as shown in Fig. 3.4. The underexcited operation is limited to a point, where a small minimum excitation level is required for stability reasons.

Fig. 3.6 shows the UEL limiter that is implemented in the PLC. The function is based on the measured active power, reactive power, and terminal voltage of the SC. The block $Q(P)$ symbolizes a look-up table that converts P values to Q values. Whenever the measured reactive power Q is greater than the output of $Q(P)$, a difference is sent to a PI controller. Additionally, the output of the PI controller can be set to zero using the enable signal.

Overexcitation limiter implementation

The system voltage reduction due to the switching operation or faults produces high reactive power requirements, by increasing the field current to maintain a constant generator voltage. In a remarkable system, the voltage drops, which may cause thermal overloading of the generator rotor winding if the generator voltage setpoint is not reduced within a certain time. In this situation, the OEL is automatically activated to limit the field current.

The purpose of the OEL is to limit the field current value to prevent the generator operating point from exceeding the field current limit and the rotor winding heating limit of Fig. 3.4 [116, 117]. When the field current I_f exceeds the pickup value I_{fN}, which is the nominal value of the field current, a positive signal will be supplied to the integrator, which enables the field current to attain a value of $1.5I_{fN}$ for 5 s. If the grid does not remove the disturbance after 5 s, the OEL will decrease the field current to $1.05I_{fN}$ as the permanent value.

When the field current I_f reduces below the pickup value, a negative signal will reset the integrator, which will provide a null error signal to the AVR summing point. The overexcited capability is limited by the rotor maximum excitation current (thermal limit). The response of OEL differs from that of the ceiling current limiter by the response value and response time.

V/Hz limiter implementation

The V/Hz limiter is activated to prevent the overflux in the machine, which occurs when the permissible ratio of the voltage to the frequency is exceeded by the following cases:

1. The terminal voltage of the generator rises to an impermissible value at a constant frequency.

2. The frequency drops to an impermissible value at a constant generator voltage.

3. The frequency drops and the terminal voltage rises to an impermissible value

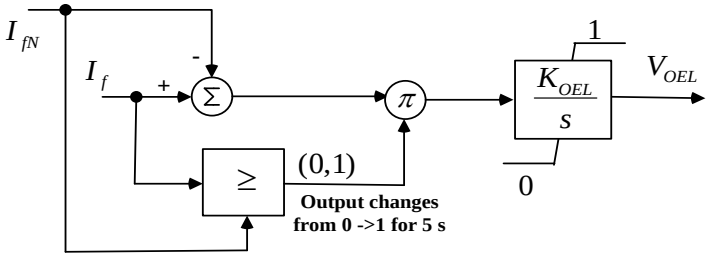

Figure 3.7: OEL limiter.

The input of the V/Hz limiter is the ratio of the per unit machine terminal voltage to the per unit speed. When the ratio exceeds a maximum threshold $(V/f)_{SP}$, shown here as 1.1 pu, the difference is obtained by an interpolation function and is then integrated. The higher is the (V/f) value, the faster the integrator will work. A negative signal V_{Vf} is sent to the AVR summing point. The negative signal reduces the voltage setpoint, and therefore, the SC output voltage decreases until the voltage to frequency ratio falls below the threshold.

When the difference becomes negative via the inequality block, the integrator is reset to zero to obtain null error signal becomes null, as shown in Fig. 3.8. Therefore, a V/Hz will change the SC output voltage but will not have an effect on the machine frequency [118].

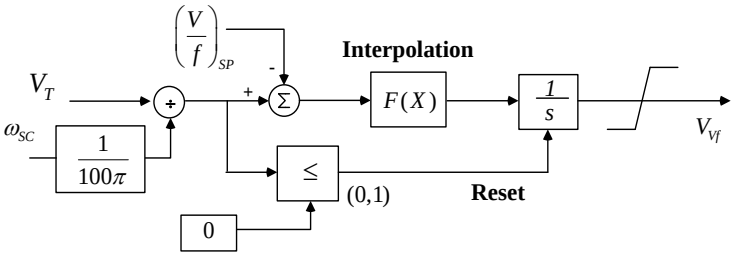

Figure 3.8: V/Hz limiter.

3.1.5 Case study

To evaluate the AVR control functions, different tests are investigated in this section. First, a start-up procedure of the AVR hardware is described step by step. Second, manual voltage setpoint changes are implemented to determine how the terminal voltage tracks its setpoint. Last, comparative results between the AVR in the hardware and the simulation for under-excitation, overexcitation, and AVR SP loss tests are investigated to verify the AVR performance.

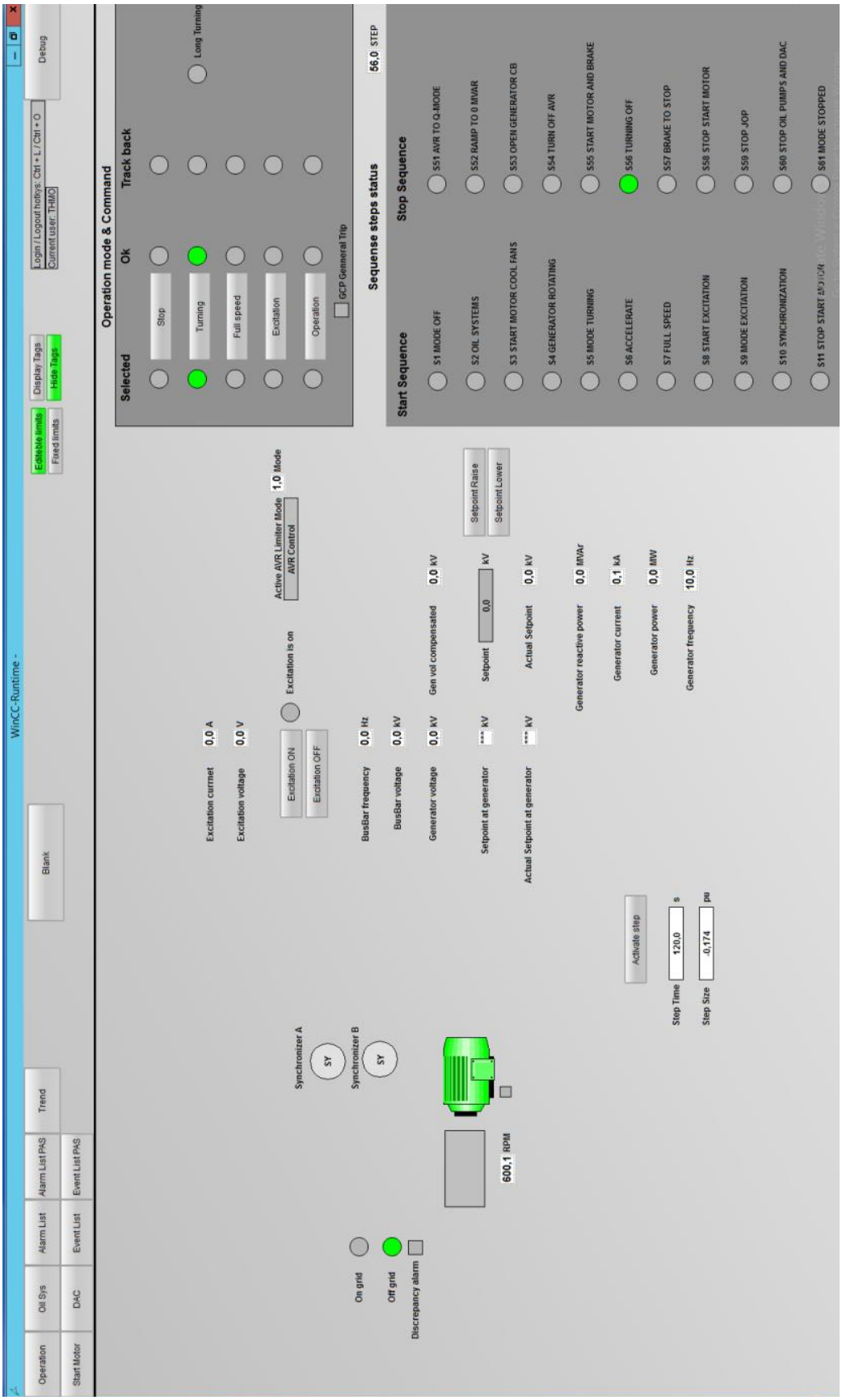

Figure 3.9: SCADA system of AVR hardware.

AVR start-up procedure

Before exchanging power, the SC must be synchronized with the grid. To synchronize with the system, four requirements must be satisfied:

1. SC frequency must equal grid frequency

2. SC voltage must equal grid voltage (at the connection point)

3. SC voltage must be in phase with grid voltage (at connection point)

4. SC phase sequence must match grid phase sequence

To start up the system, first, a real-time simulation is run in the RTDS without the SC connection. Second, the absolute value of voltage and frequency of the busbar at the grid side are sent to the AVR hardware. The start-up process of the SC is modeled in the hardware platform, where a virtual SC is turned and accelerated to its full speed. When the virtual SC reaches the full speed, the excitation is turned on and the AVR SP is sent from the AVR hardware to the RTDS model that is proportional to the corresponding busbar voltage of the grid side. When the terminal voltage of the generator hits the setpoint, an ON GRID digital signal is sent to the CB in the RTDS. The CB is closed when the four requirements regarding the voltage and the frequency of the SC side and grid side are satisfied. The screen of the AVR hardware to monitor the measurement signals and parameter of the SC is shown in Fig. 3.9.

Figure 3.10 shows the busbar voltage (pink), the reactive power (green), the terminal current (blue), the voltage setpoint (red) and the terminal voltage (black) of the SC responses during the startup period. The terminal voltage of the SC gradually increases from 0 to its voltage setpoint (red) within 10 s when the excitation system activates. Due to the synchronization check of the CB, the reactive power and the terminal current experience a small overshoot during the SC synchronization.

Voltage setpoint changes

To verify the response of the AVR hardware, a manual change of the SC voltage setpoint is implemented to determine how the actual terminal voltage tracks its setpoint in dynamic conditions. Figure 3.11 shows the SC responses and busbar voltage during a 0.045 pu step increase and a decrease of the SC voltage setpoint (red). It can be seen clearly that when the setpoint increases/decreases, the terminal voltage tracks quite well to its setpoint with no overshoot during transient periods. Approximately 7 s are required to settle down when the setpoint changes. Furthermore, the reactive power (green), the current (blue) of SC, and the busbar voltage (pink) quickly and very smoothly respond during the setpoint changes.

Under-excitation test

In this test, the voltage of the grid side suddenly increases from 1 pu to 1.1 pu at t = 1.7 s. The SC attempts to absorb the reactive power from the grid side to lower the voltage. The comparative results between the AVR controller of the HiL test and that of the simulation are shown in Fig. 3.12, where the blue curves represent the hardware and the orange curves represent the simulation.

As shown in Fig. 3.12, the reactive power of the AVR simulation has a smoother response and shorter settling time than that of the hardware: approximately 15.3 s and 4 s, respectively. However, with the AVR hardware, the SC can absorb more reactive power, which reaches -142 Mvar instead

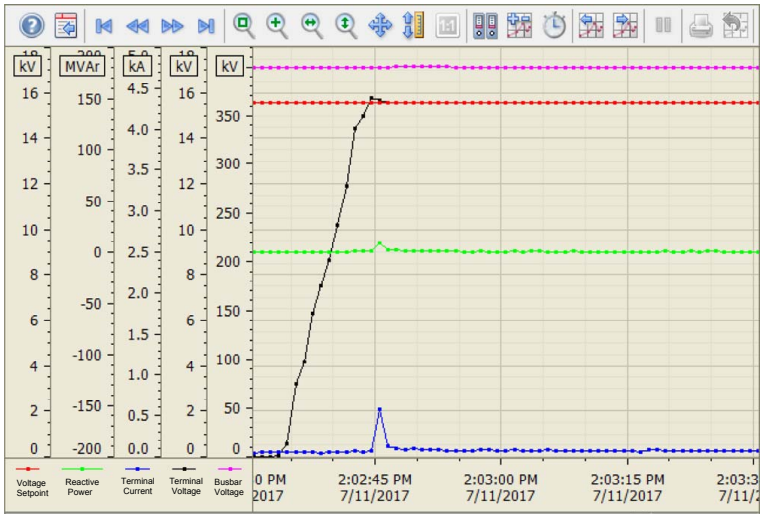

Figure 3.10: SC response with AVR hardware during the startup period.

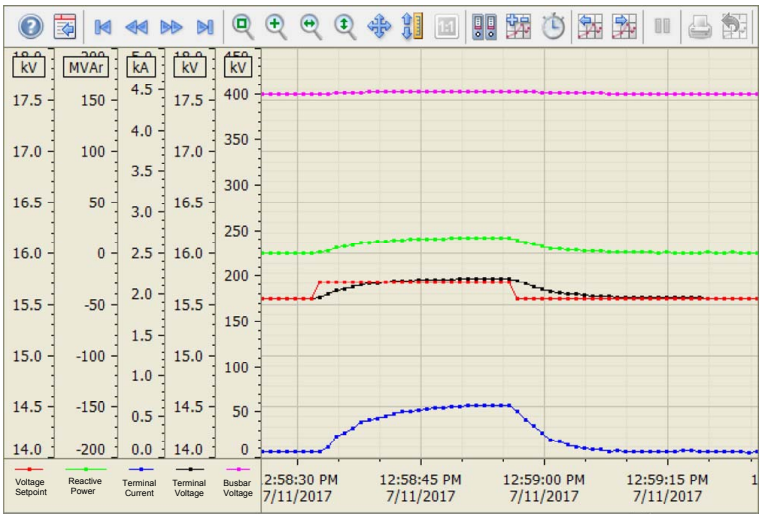

Figure 3.11: SC response with AVR hardware during the voltage setpoint changes.

of -126 Mvar in the simulation with the same under-excitation limit setting. As a result, the voltage of the SC and the grid have a longer recovery time and a higher overshoot but a lower overvoltage value after the incident with the hardware results. It can be explained that with the hardware test, transferring the measurement signals from the RTDS to the hardware platform and the reversed direction requires time, while either the time delay or the sending/receiving time for that of the simulation is minimal.

Note that the active power responses of the AVR hardware and simulation are almost similar because the AVR controller seems insensitive to electric power.

Overexcitation test

A sudden decrease of the grid voltage from 1 pu to 0.9 pu occurs at t = 1.7 s, as shown in Fig. 3.13. From the comparative results between the simulation and hardware of the AVR, the reactive power support of the AVR hardware is slower but higher than that of the simulation, which enables

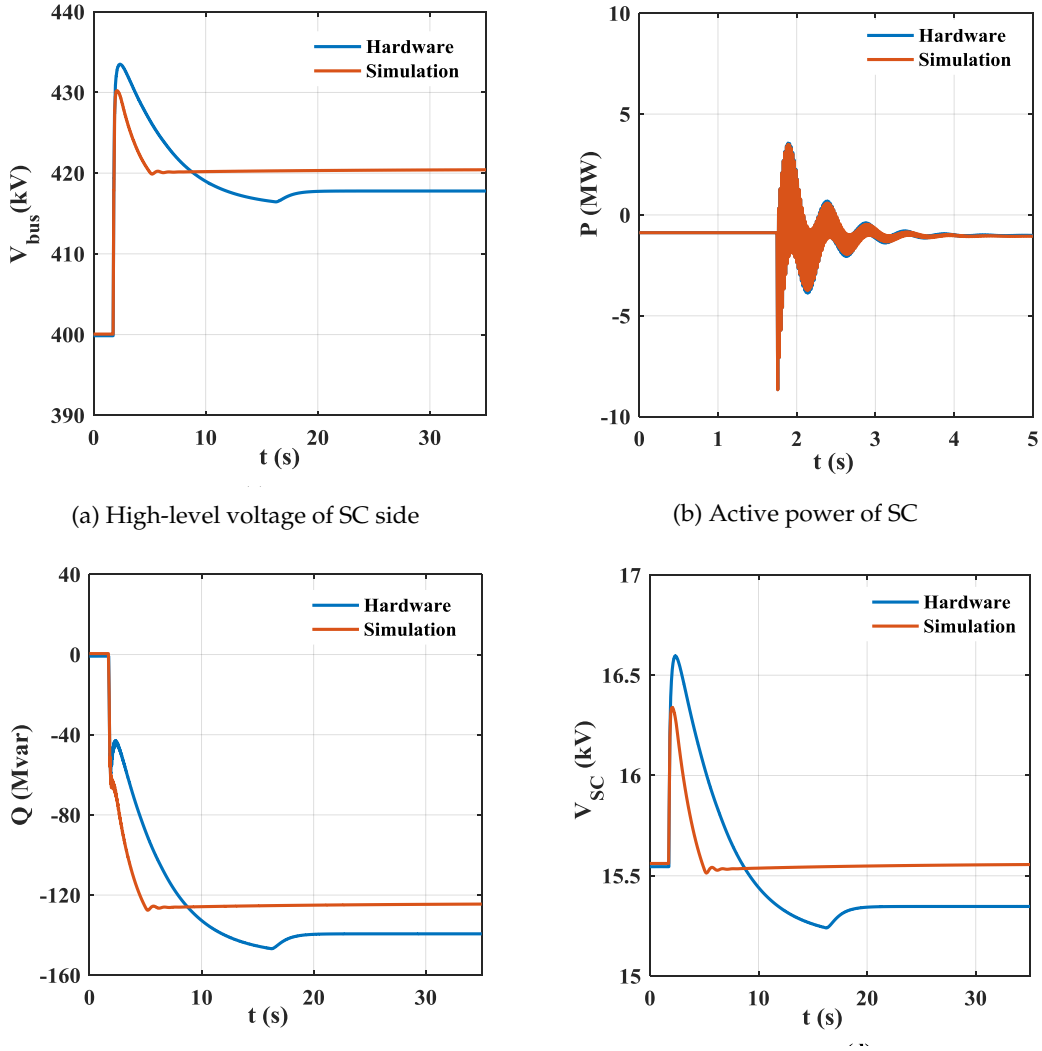

(a) High-level voltage of SC side

(b) Active power of SC

(c) Reactive power of SC

(d) Terminal voltage of SC

Figure 3.12: Under-excitation responses. (a) High-level voltage of SC side. (b) Active power of SC. (c) Reactive power of SC. (d) Terminal voltage of SC.

the SC terminal voltage and the grid voltage to attain lower minimum magnitudes during the transient period but higher recovery values after the incident.

The reactive power of the AVR simulation increases from approximately 2 Mvar at the initial value to nearly 125 Mvar within 1.5 s, whereas that of the hardware with the same interval is within 7 s and increases further to attain approximately 150 Mvar after approximately 18 s. The settling time of the AVR hardware for reactive power and voltage is approximately 18 s longer than that of the AVR simulation, which is nearly 2 s. The active power responses are almost similar in terms of the magnitude and settling time for both approaches.

AVR setpoint loss

An AVR setpoint loss incident occurs at t = 1.7 s, and the SC loses excitation and attempts to draw the reactive power from the grid to operate at the synchronous speed and maintain its terminal

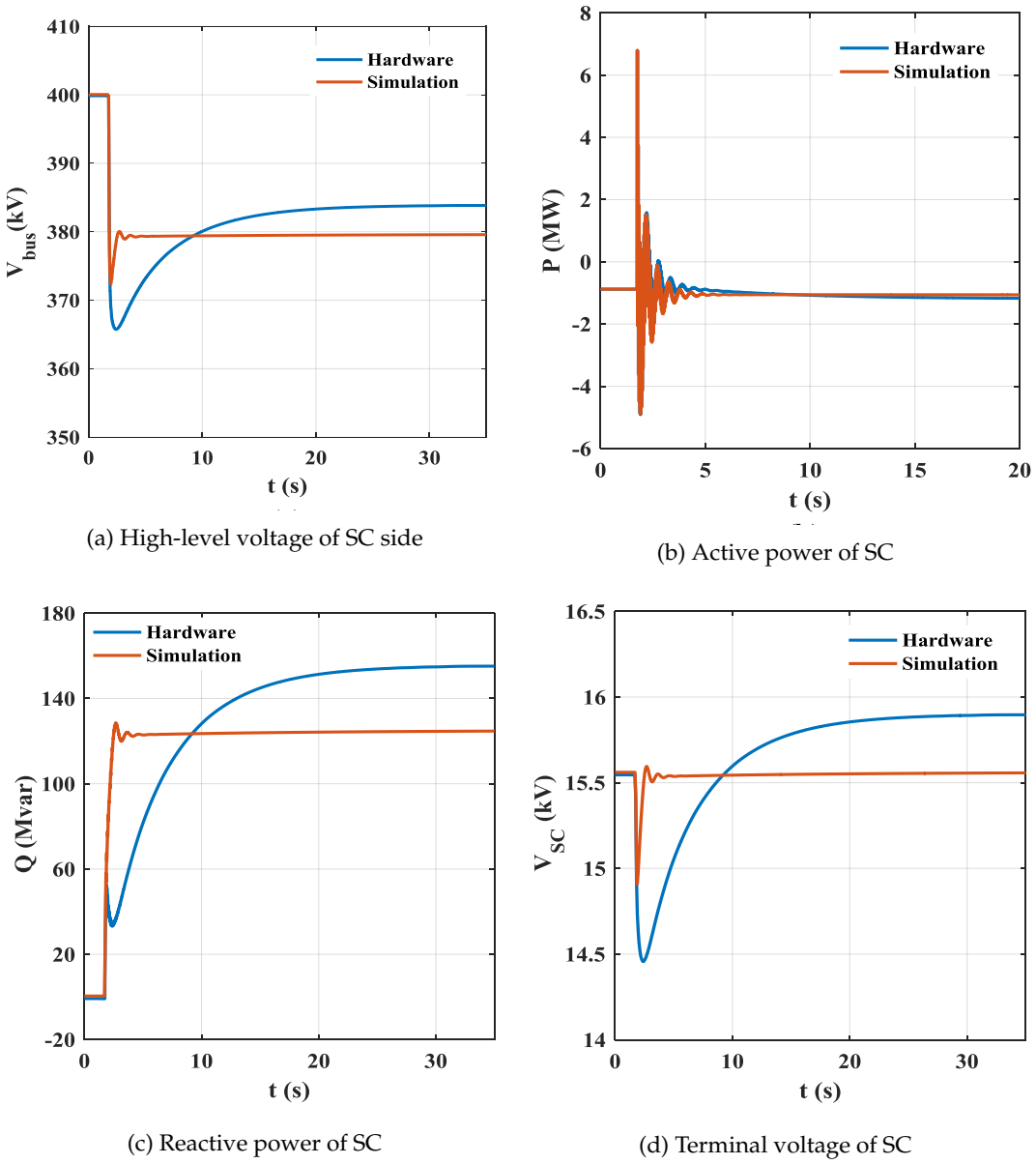

(a) High-level voltage of SC side

(b) Active power of SC

(c) Reactive power of SC

(d) Terminal voltage of SC

Figure 3.13: Overexcitation responses. (a) High-level voltage of SC side. (b) Active power of SC. (c) Reactive power of SC. (d) Terminal voltage of SC.

voltage. Figure 3.14 shows how the HiL test and simulation of the AVR respond during the incident. The voltage and reactive power responses are similar for the AVR hardware and simulation while a difference in the active power response is observed. The reactive powers of both the hardware and the simulation reach -123 Mvar within 10 s. The active power of the AVR hardware undergoes greater oscillation than that of the simulation but settles down at almost the same time during the incident.

Stop sequence

To stop the SC, the SC reactive power first has to ramp to 0 Mvar and then an off-grid signal is sent to RTDS to open the circuit breaker. This sequence will help the circuit breaker is open in low or

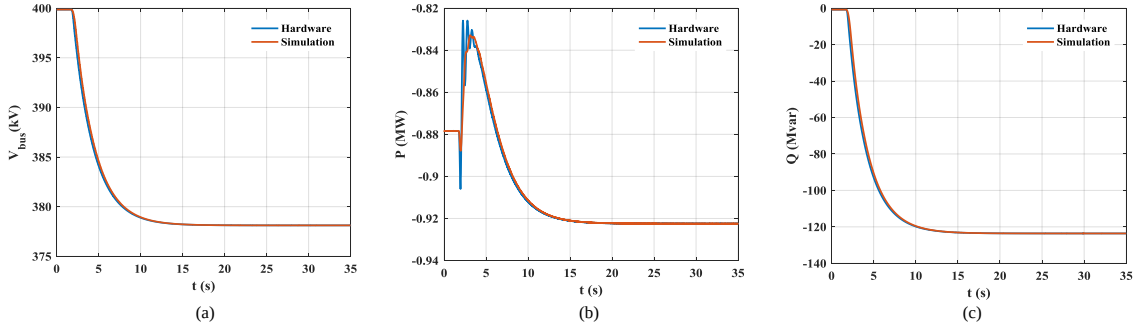

Figure 3.14: Dynamic responses of SC during AVR SP loss. (a) High-level voltage of SC side. (b) Active power of SC. (c) Reactive power of SC.

almost zero current conditions. The time and procedure are implemented as the real system to guarantee that the HiL system is similar to reality. The detailed steps to stop the SC are shown in Fig. 3.9 in the stop sequence column.

3.1.6 Conclusion

This part presents an HiL implementation for the AVR and limiters of the SC, which are the core components of SC for maintaining voltage stability. The startup and stop procedure of the system with AVR hardware and voltage setpoint changes are investigated to evaluate how the AVR hardware responds during the disturbances. Furthermore, under-excitation, overexcitation, and AVR setpoint loss are implemented to compare the different responses of AVR hardware and simulation in terms of the overshoot and settling time. The comparative results demonstrate the possible applications of HiL to validate and adjust the control function of the equipment in steady state and dynamic conditions before final construction implementation with lower cost, higher efficiency, and more flexibility.

3.2 SiL simulation for parameter optimization of AVR simulation

Previous work reveals a difference between the AVR hardware and the simulation responses during disturbances. This part aims to tune the PID parameter set of the AVR simulation model to otain a characteristic that is similar to the AVR hardware based on a software-in-the-loop simulation, which is a closed-loop interface among RTDS, Matlab, and OPC.

The prospective future Western Danish power system run in the RTDS platform is driven by a MatLab script for system startup and disturbance simulations. The data of the system are collected by an OPC server and sent directly to the Matlab workspace. In MatLab, the signal is processed and evaluated by the GA objective. These steps are iterative by a closed loop and run in real time with RTDS, OPC, and Matlab communications, as shown in Figs. 3.15 and 3.16. The loop will continue until the objective function satisfies the constraints to determine the optimal parameters for the AVR simulation model.

3.2.1 RTDS setup

The whole DK1 system is modeled and compiled in RSCAD/Draft, and then run and monitored in RSCAD/Runtime. To run the system by a Matlab script, a communication connection is established between RSCAD/Runtime and Matlab. Once the connection is implemented, RSCAD/Runtime becomes a socket server and Matlab becomes a socket client. RSCAD/Runtime is commanded and run in real-time by a Matlab script via the TCP server [114]. In addition, the new parameter set is updated via this communication.

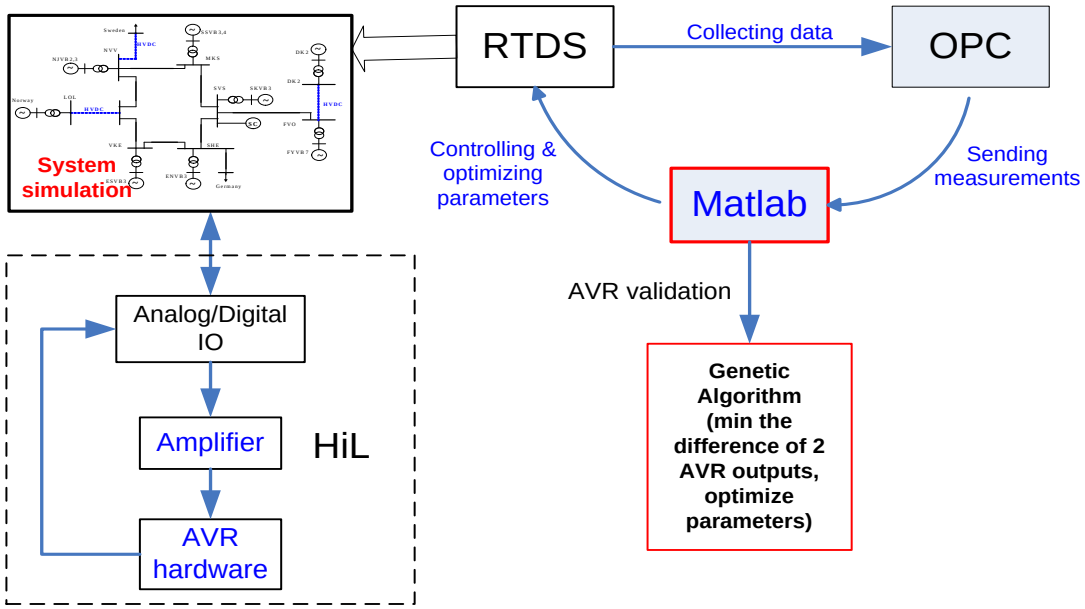

Figure 3.15: System arrangement of HiL and SiL simulations for parameterization of the AVR model.

3.2.2 OPC setup

To collect the data from RTDS, a communication channel between RTDS with MatrikonOPC is setup with 3 steps, including an RTDS network channel, an RTDS network host, and an RTDS DNP3, which are described in [119]. First, the RTDS network channel is setup where the protocol is defined. Second, the RTDS network host is established inside the network channel. In the network host, the IP address of the GTNET card of the RTDS and the port number that have been defined in the GTNET card of the RTDS platform are filled. Last, the RTDS DNP3 is created to view the signals that are collected from the RTDS. After the communication is established, the RTDS and OPC can exchange data with each other. The measurement data are collected in the OPC server and sent to Matlab for the next steps.

3.2.3 Matlab program

A Matlab script commands and runs the system in real-time in RSCAD/Runtime via TCP communication. To acquire the data at the OPC server, a connection is setup in a Matlab script to create a group object with defined properties. After obtaining the data and performing signal processing to convert to the proper format, the data are retrieved in the Matlab workplace for further analysis. When the data are sent to Matlab, OPC cleans up and disconnects to prepare for subsequent data collections.

The parameter set is sent to RSCAD/Runtime by a Matlab command for the next iteration. These steps are continuously repeated until one of the termination parameters is achieved. As a result, a near-optimal or optimal solution of the parameter set is determined. The entire procedure is illustrated in Fig. 3.16.

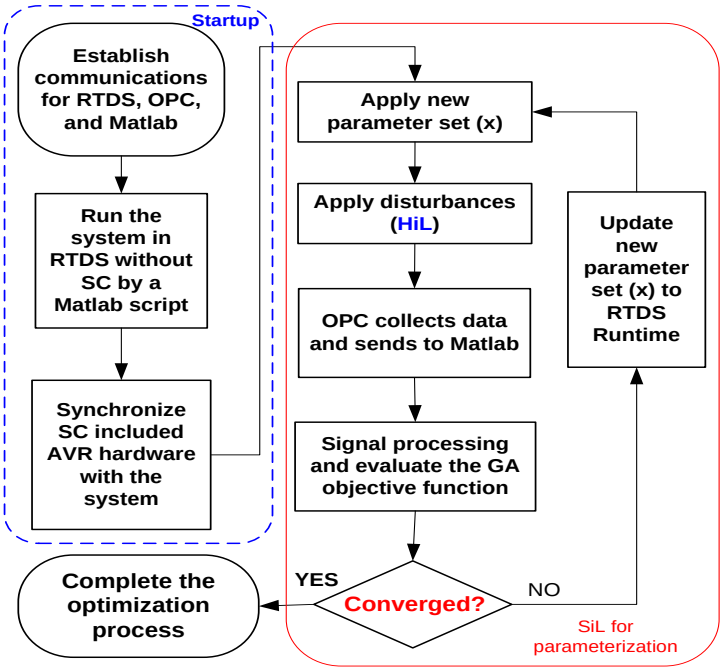

Figure 3.16: The flowchart of optimization process with SiL and HiL simulations.

3.2.4 Genetic algorithm

An optimization approach is a mathematical model where the main objective function is to minimize undesirable things (e.g., costs, errors, and losses) or maximize desirable things (e.g., efficiency, damping ratio, and profit), subject to constraints. Two main approaches exist for the optimization problem: linear and nonlinear methods. The linear approach is based on the linear system model using small-signal analysis, which depends on the initial operation point with several simplifications, e.g., does not consider discrete control behaviors, such as limiters and saturation. As a result, when a control system reaches its limiters during disturbances may be inaccurate. Conversely, the nonlinear method is usually applied to the simulation-based approach, which is less restricted by modeling limitations.

The evaluated system is simulated in real time in RTDS using an electromagnetic transient (EMT) model that employs large-signal analysis and is more accurate than the RMS model using small-signal analysis [120]. Due to this study, which employs the simulation-based approach, a nonlinear optimization tool that is referred to as a genetic algorithm is applied to optimize the controller parameters.

A GA is a global heuristics parameter search technique that is based on genetic operators to find the optimal or near-optimal solutions for a specific problem [121, 122]. Unlike the traditional optimization approaches that require one starting point, a GA uses a set of points (chromosomes) as the initial condition, and the performance of each chromosome is evaluated according to the objective function that characterizes the problem to be solved and defined by the designers. A group of chromosomes is referred to as a population. The process of GA is applied as follows:

1. Initialization: a certain number of individuals, who represent the PID parameters of the AVR model, are randomly created according to the initial population and the upper and lower bound setting.

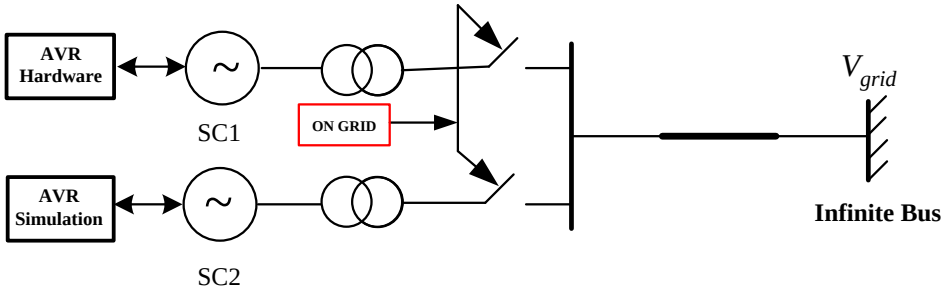

Figure 3.17: Two SCs connected to an infinite bus.

2. Objective evaluation: Using a selection operator, the algorithms select the best result for each individual in accordance with their values defined by the objective function. The main goal of the control system is to minimize the difference between two AVR hardware and simulation outputs, i.e.,

$$f(x) = min\left(\sum(E_{fds} - E_{fdh})^2\right) \tag{3.9}$$

where E_{fds} and E_{fdh} are the output of excitation with the AVR simulation and that of the hardware, respectively.

3. Reproduction: a new set of chromosomes are generated from the selected parameters in step 2 using selection, crossover, and mutation operators. These genetic operators ensure a larger average objective value for the next generation.

4. Termination flagged: these 3 steps are continuously repeated until one of the termination parameters is achieved. The GA may be terminated after a certain number of generations when the objective value does not enhance after a certain generation.

3.2.5 Case study

To verify the parameter optimization for the PID controller of the AVR simulation model based on the GA, different tests, such as under-excitation and overexcitation tests and a load increase scenario, are investigated to compare the responses of the AVR hardware and simulation. The under-excitation and overexcitation conditions are tested in a simple system, where 2 SCs (an SC with the AVR hardware and another with the AVR simulation model) are connected in parallel with an infinite bus through a long transmission line as shown in Fig. 3.17. Another test with load increase disturbance is implemented in the future DK1 power system to guarantee that these two AVR models have the same response in a large-scale and complex power system.

Under-excitation condition test

The voltage of the grid side suddenly increases by 0.1 pu at t = 0.75 s, and the SC immediately absorbs reactive power from the grid side to decrease the voltage. The comparative results between the AVR controller of the HiL test and that of the simulation are shown in Fig. 3.18 with dashed red curves for the hardware and solid black curves for the simulation.

As shown in Fig. 3.18(b), a natural response of the SC is to rapidly absorb reactive power to protect against the voltage increase during the transient period. The AVR control following the response is to absorb more reactive power, which causes the voltage to decrease to the pre-disturbance point.

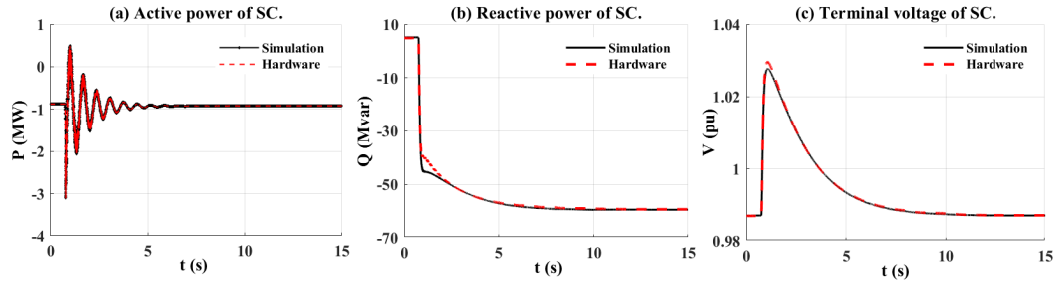

Figure 3.18: Under-excitation responses of SC. (a) Active power of SC. (b) Reactive power of SC. (c) Terminal voltage of SC.

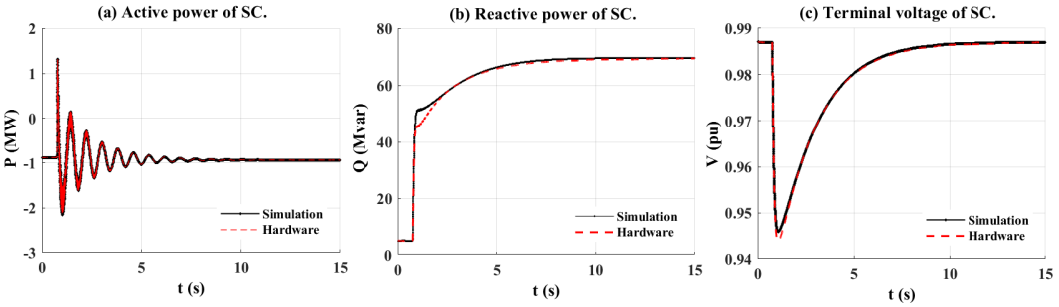

Figure 3.19: Overexcitation responses of SC. (a) Active power of SC. (b) Reactive power of SC. (c) Terminal voltage of SC.

Note that the AVR hardware control responds slightly slower than that of the simulation, which causes the terminal voltage of SC to continue to increase slightly further 1.03 pu instead of 1.028 pu than that of the simulation before achieving the same new steady-state operating point after the disturbance.

Overexcitation condition test

A similar pattern is observed in Fig. 3.19 with the overexcitation condition when the grid voltage decreases 0.1 pu. In this scenario, the AVR systems of the SCs manage to increase the setpoint to supply more reactive power in the vicinity of 65 Mvar from approximately 5 Mvar to nearly 70 Mvar for both SCs, and the hardware is slightly slower during the transient period that causes a lower voltage drop, as shown in Fig 3.19(c). It is noteworthy that the active power responses of the AVR hardware and simulation are almost similar because the AVR controller seems insensitive to the active power.

Load increase

To verify the performance of SiL simulation for parameter optimization of the AVR model in low inertia systems, a test using the future DK1 power system is investigated in this part to compare the behavior of the AVR hardware with that of the AVR simulation model. A 150-MW load increases at t = 0.75 s, as shown in Fig. 3.20. From the comparative results for the simulation and hardware of AVR, the reactive power responses are similar for both cases. They quickly increase to counteract the voltage decrease and return the terminal voltage to the pre-disturbance point, by increasing

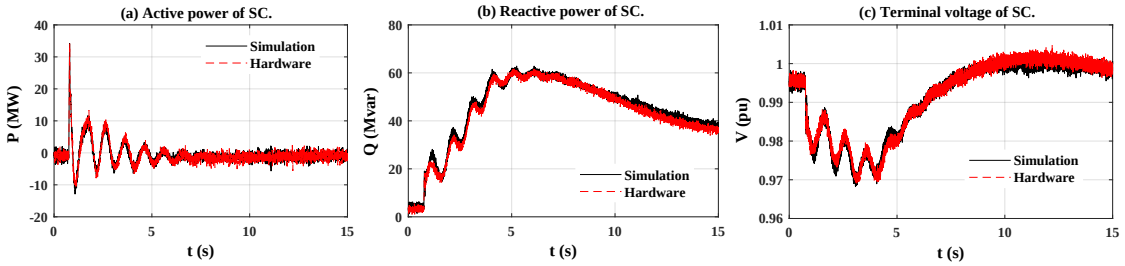

Figure 3.20: SC responses during a load increase. (a) Active power of SC. (b) Reactive power of SC. (c) Terminal voltage of SC.

from approximately 4 Mvar to 61 Mvar and settling down at approximately 38 Mvar after nearly 10 s.

The active power responses are almost similar in terms of magnitude and settling time for the two approaches. The results conclude that parameter optimization based on SiL offers a parameter set for AVR simulation to obtain a characteristic that is similar to the AVR hardware.

3.2.6 Conclusion

The chapter presents HiL testing for the AVR and limiters of SC before deployment in the field. Different tests, such as voltage setpoint changes, under-excitation, and overexcitation conditions, are implemented for AVR in hardware, which demonstrates the possible applications of HiL testing to validate and verify the control function of the equipment in steady-state and dynamic conditions before final construction implementation with low cost, high efficiency, and more flexibility.

Furthermore, a SiL simulation for parameter optimization of the AVR simulation model based on a nonlinear optimization tool is proposed to offer a near-optimal or optimal solution for the control parameter set, which can save control designers a considerable amount of time. This SiL simulation can be applied for any parameter optimization tool by modifying the objective function to satisfy the control purposes and solve similar issues of power systems.

CHAPTER 4

Frequency stability enhancement

In this chapter, different frequency stability enhancement approaches using synchronous condensers and synthetic inertia from WPPs are proposed. First, a frequency stability support from SCs is examined with different wind power levels. Second, a synthetic inertia coordinated with an activation scheme is designed for a WPP to improve the system frequency stability. Last, a combination of SC and SI is investigated to enhance the frequency stability in terms of the rate of change of frequency and frequency deviation.

4.1 Frequency stability support from SC

SCs have a long history of dynamic reactive power support for power systems, which is viewed as a synchronous generator without a prime mover or a synchronous motor without a load. A small pony motor that is attached to the shaft of the SC is only used to accelerate the SC to the synchronous speed. Once the SC is synchronized with power systems, the pony motor is de-energized. A photo of the SC is shown in Fig. 4.1 [123].

An equivalent circuit and a phasor diagram of the synchronous generator (SG) are shown in Fig. 4.2(a) and (b) as the voltage source E behind the reactance X. When the SG operates at a small torque angle δ and large field excitation, it is considered to be an SC. The field excitation increase causes E to increase; therefore, the machine current increases according to the following formula:

$$E = V + jIX \tag{4.1}$$

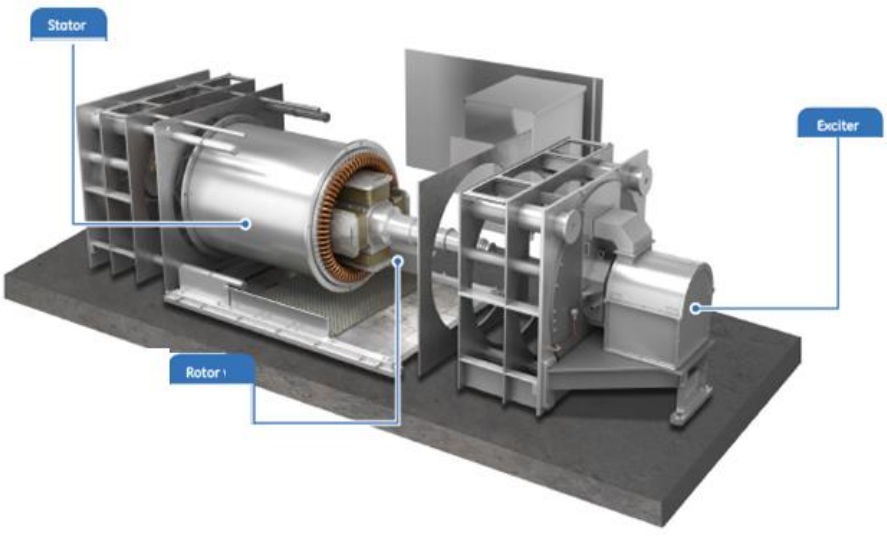

Figure 4.1: Synchronous condenser.

where E, V, I, and X are the internal voltage, terminal voltage, current, and reactance of SG, respectively.

The machine current I increases but the power factor is almost zero, and therefore, I leads to V. In theory, no active power is transferred, but a high and controllable level of reactive power exists. This mode of machine operation is referred to as a synchronous condenser, as shown in Fig. 4.2(c). In this mode, the reactive power is expressed as follows:

$$Q = \sqrt{|V|^2 |I|^2 - P^2} \approx |V|\,|I| \tag{4.2}$$

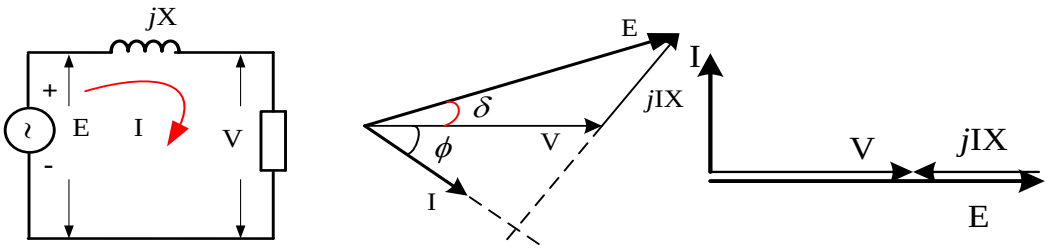

(a) Equivalent circuit of SG (b) Phasor diagram of SG (c) Phasor diagram of SC

Figure 4.2: The equivalent circuit and phase diagram of synchronous machine

When the SC is considered as a generator without a prime mover, it can supply reactive power to power systems by a simple adjustment of its field current with a continuously variable range of reactive power from 50% or more lagging to full leading. At this point, SC is a reactive power generator but is not capable of generating active power.

Some prefer the SC to act as a motor without a load, where SC consumes only a small amount of active power from the grid to compensate for its losses. Like any synchronous motor, the SC can supply reactive power in an overexcited condition and can absorb reactive power when its field current is underexcited.

Regardless of which viewpoint is preferred, the control of the machine field is a critical element that affects the dynamic performance of SC to power systems. The field current is controlled by an automatic voltage regulator (AVR) to keep the voltage or power factor constant at a given point on the system. Increasing the field current causes an increase in the reactive power output. Thus, an SC is considered as a continuous variable sink/source of reactive power.

Since SC is a rotating machine, it can provide an inherently inertial response due to the electromagnetic coupling with the grid. The kinetic energy stored in its rotating mass can naturally counteract the frequency change during disturbances. In addition, an SC can also support the short-circuit power to the network that can improve system interconnections, facilitate system protection, and enhance the operation of modern power electronics installations.

The main objective of this part is to demonstrate different governor gains that affect the frequency stability and impact of large-scale wind farm integration on the Western Danish power system and investigate how SC can enhance the frequency stability of the system under disturbance conditions.

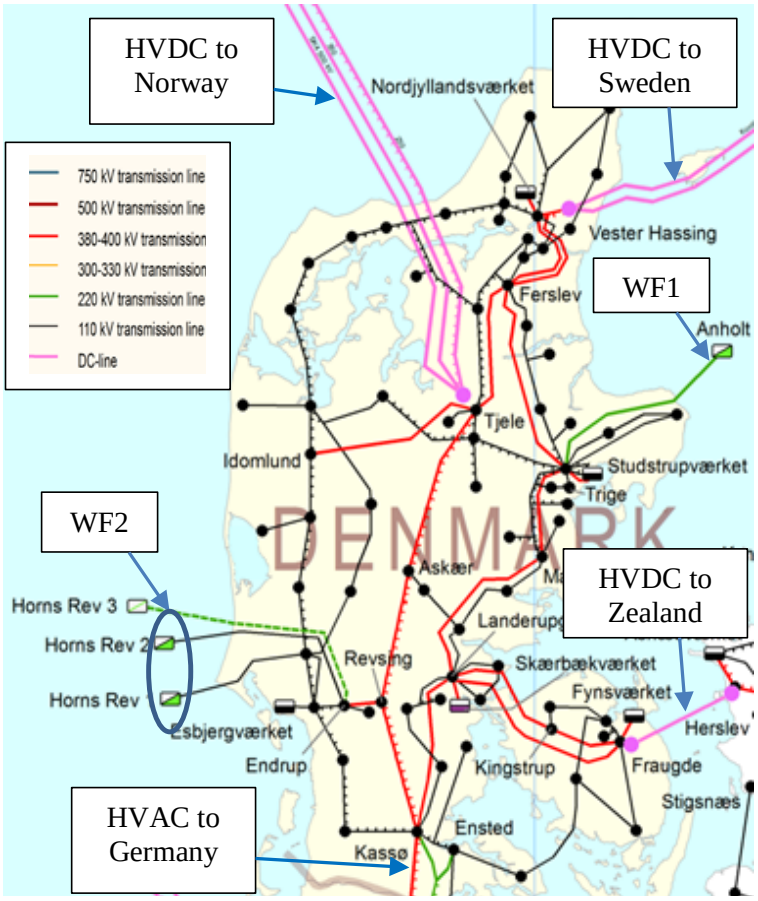

Figure 4.3: Geographical map of current Western Danish power system connected to the neighboring areas: Norway, Sweden, and Germany.

4.1.1 System description

The geographical diagram and sing-line diagram of the Western Danish power grid, where the system connects to the neighboring areas of Norway, Sweden, and Germany, are shown in Fig. 4.3 and Fig. 4.4, respectively. The detail system description is presented in chapter 2.

As mentioned above, the German grid is expected to integrate more renewable energy sources in the coming years, which weaken the system inertia. Therefore, the frequency support from the German HVAC interconnection is poorly modeled by a large synchronous generator with 6 s inertia constant, and its governor gain is 12 instead of 17 in the validation case in chapter 2.

The generation of the system consists of five local synchronous generators in operation and three offshore wind farms (AHA, HRA, and HRB, C) that are connected to the grid via transmission lines. Three synchronous condensers are installed at three HVDC terminals (VHA, FGD, and TJE) for reactive power compensation and short-circuit power support.

The system frequency characteristic is investigated in different operating scenarios with and without the synchronous condensers in service. Various operational conditions of the governor responsibility of synchronous generators and wind penetration levels are examined to verify the performance of synchronous condensers in the frequency stability enhancement.

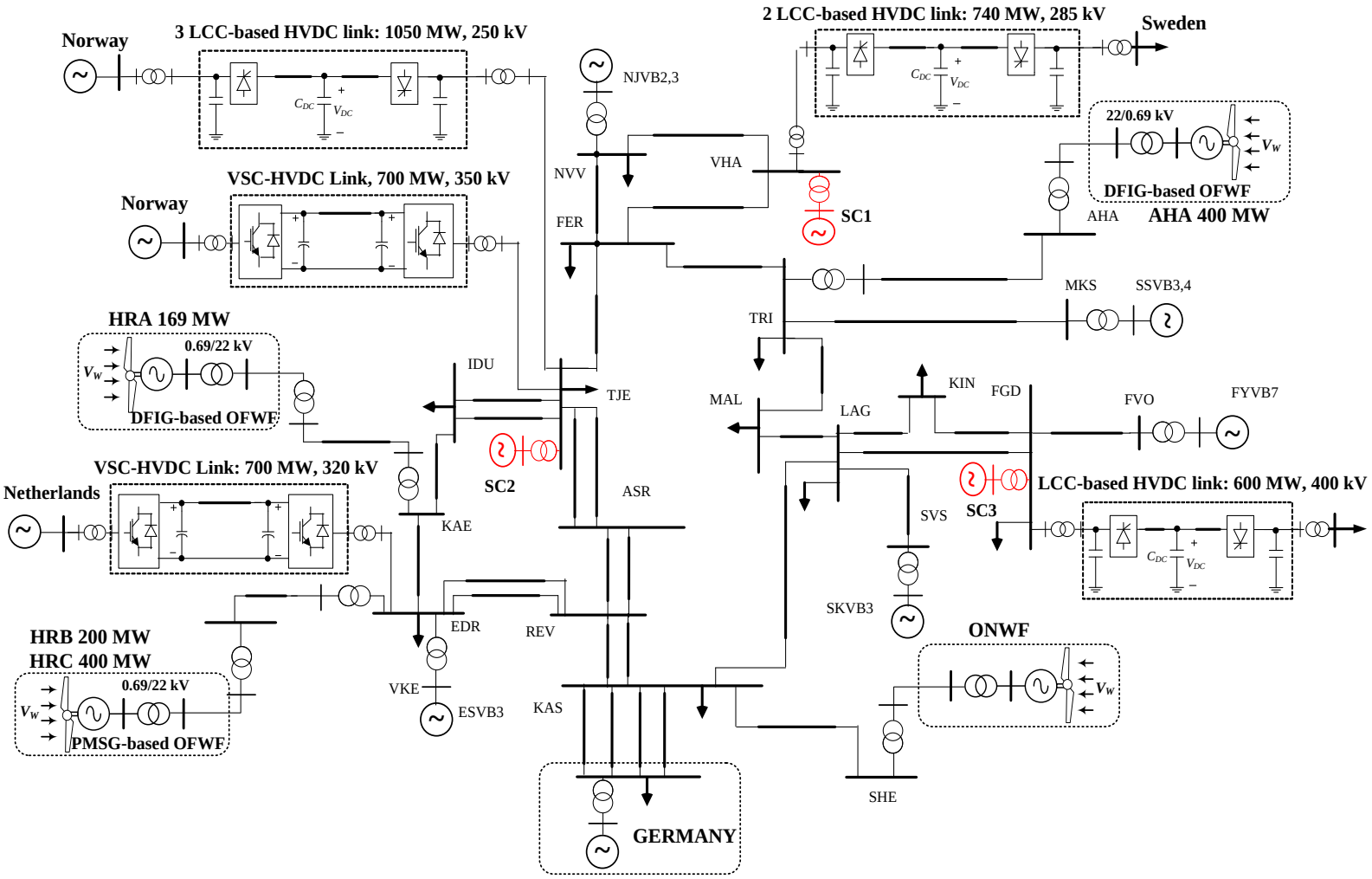

Figure 4.4: Single-line diagram of reduced 400 kV Western Danish power system.

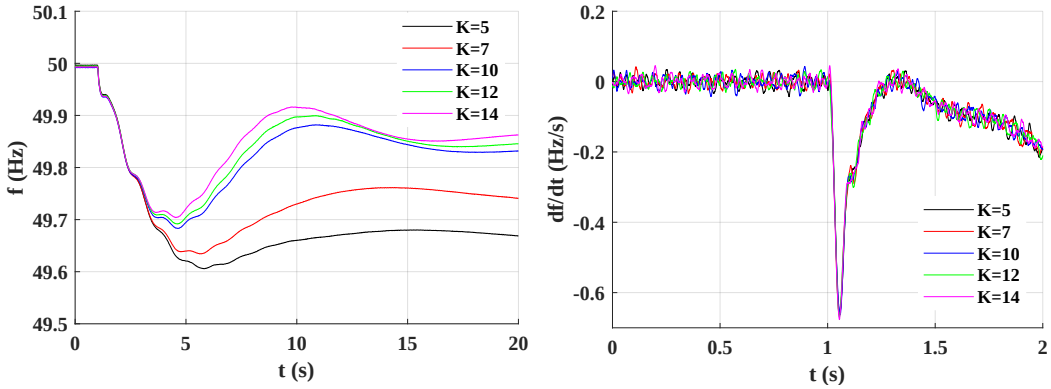

Figure 4.5: System response with different governor gains.

4.1.2 Case study for the DK1 power system

In this section, different scenarios are examined to verify the benefit of SC during different disturbances. First, variable governor gains K (or droop control R) of the generators are investigated to experience how primary control of generators impacts on the system frequency and how SC can contribute to frequency control. Second, an equivalent system inertia with different wind farm levels are calculated to determine how different wind energy penetrations impact on the system inertia. Finally, a replacement of SGs by WPPs is investigated to determine how high-level wind power penetration influences the frequency stability during disturbances.

Different governor gains

Fig. 4.5 describes the frequency response of the system when 5 SGs are in operation subject to 200 MW load increase with different governor gains K. When the governor gain K varies from 14 to 5, which corresponds to R changes from approximately 7% to 20%, respectively, the primary frequency support from synchronous generators will change. The higher is the governor gain, the higher is the primary control contribution. How droop control works (governor reaction of SG) during frequency events is explained in the primary control section of chapter 2.

As shown in the first subplot of Fig. 4.5, different governor gains impact the frequency nadir and the steady-state frequency. The higher is the governor gain, the higher is the frequency nadir and the higher is the steady-state frequency, while ROCOF does not change with K variation.

It can be explained that when K declines, the primary frequency control response from synchronous generators decreases, which causes the frequency to continually decrease and yields a larger steady-state frequency deviation. Conversely, the total inertial responses of SGs do not change, which keeps ROCOF constant when K varies.

Fig. 4.6 shows a comparison of the system response with the governor gain K=12 case. As can be observed,the ROCOF of the system is significantly improved with SCs, where the lowest ROCOF is 0.46 Hz/s compared with an ROCOF of 0.67 Hz/s without SCs. The frequency nadir is slightly lower with SCs due to their losses; however, attaining 49.68 Hz WSC and 49.69 Hz WOSC, respectively, is not significant. A significant enhancement of the ROCOF is due to rapid support from SCs at approximately 24 MW at the first onset of the disturbance, as shown in Fig. 4.6(c). With SCs in operation, the system is stronger, as observed from the active power response of the generator in

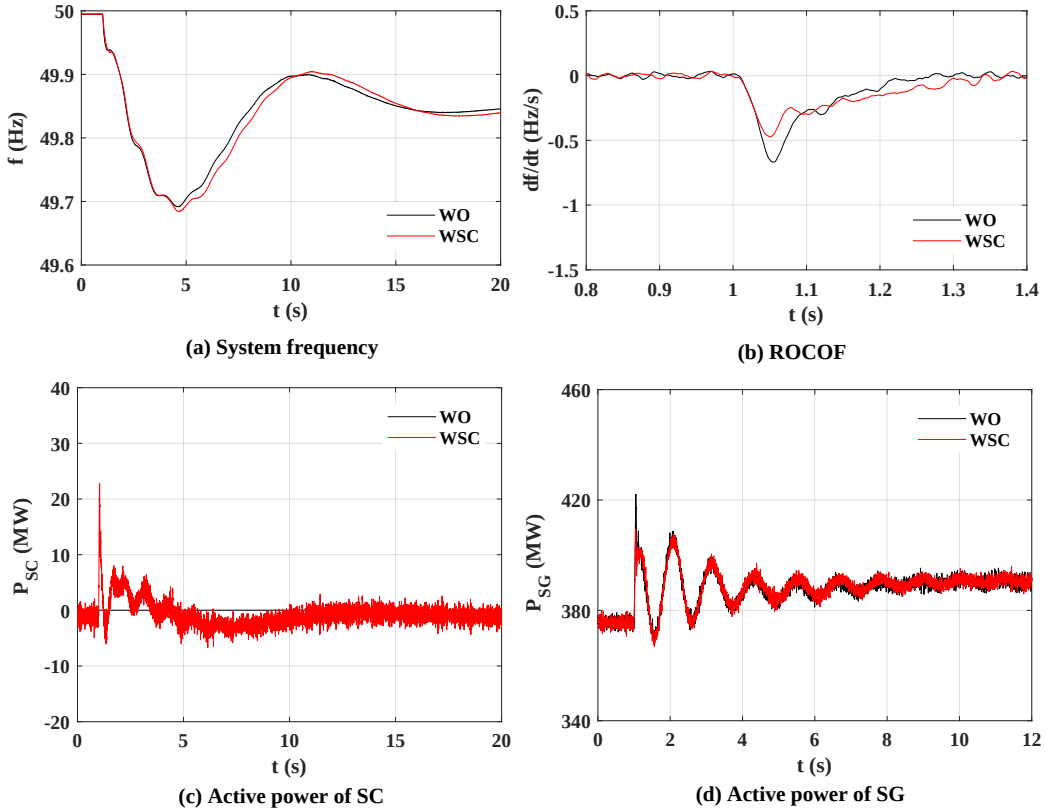

Figure 4.6: System response with and without SC.

Fig. 4.6(d). It can be concluded that SC not only significantly enhances the ROCOF of the system but also makes the system stronger during the disturbance, which is an important feature for renewable-based systems.

Different wind penetration levels

In this scenario, different wind power penetrations are investigated to see the impact of the energy transition from conventional fuel to renewable source on the system inertia, hence making frequency control more challenging.

There are three scenarios investigated in the section. Firstly, when 5 SGs are in operation (5SG), 3 offshore wind farms (OFWF) are out of service. Then when the OFWF located at AHA is in operation with its MW rating, 2 SGs (SSVB3 and FYVB7) are retired, thus 3 SGs are online (3SG). Finally, three OFWFs are in service at their full capacity, only NJVB3 is online (1SG). These three scenarios are investigated during a load increase disturbance to see how differently the system responds. Furthermore, a comparison with and without SCs in 1SG in operation case is examined to verify the performance of SCs in terms of ROCOF enhancement and help system stronger during the disturbance. A negative correlation is observed between the system inertia and wind power penetration as shown in Fig. 4.7. The higher wind power penetration, the lower system inertia has [124].

As can be seen clearly in Fig. 4.8, the high penetration of WPP makes system inertia drastically reduced and primary control decreased which cause a higher ROCOF and a larger frequency

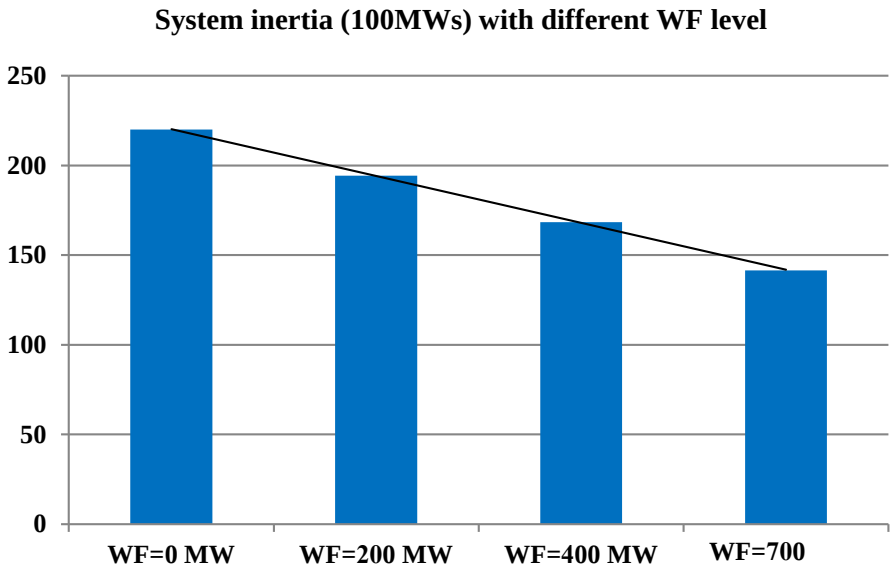

Figure 4.7: Equivalent system inertia with different wind power penetrations.

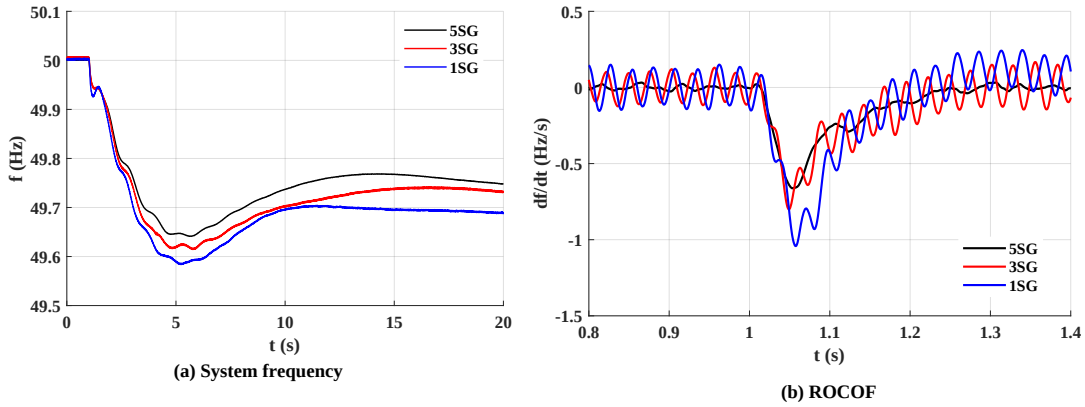

Figure 4.8: System response with different wind power penetrations.

deviation, as well as a lower frequency recovery. Firstly, when SGs are phased out, a certain amount of rotating energy support for inertial response is removed which reduces inertial support for the system at the first few second of disturbances. As a result, the ROCOF is rapidly increased and the system response is weaker as seen in Fig. 4.8(b). In addition, a primary control is missing with WPP replacement, hence causing a larger frequency deviation and a bigger steady-state frequency error after the disturbance. It is worth to note that the higher wind power penetration the more vulnerable the frequency during the disturbance as seen more oscillation in ROCOF responses.

As expected, when SCs are in service, the system frequency is much stronger and significantly improved, ROCOF is around 0.7 Hz/s instead of 1.05 Hz/s without SCs case and the ROCOF curve is much smoother than that of WO case as shown in Fig. 4.9(b).

Since wind plant progressively displaces conventional generation and their inertia, a substantial reduction in power system inertia occurs, and a faster frequency dynamics resulted as its certain consequence. Added inertia contribution from synchronous condenser to improve the frequency

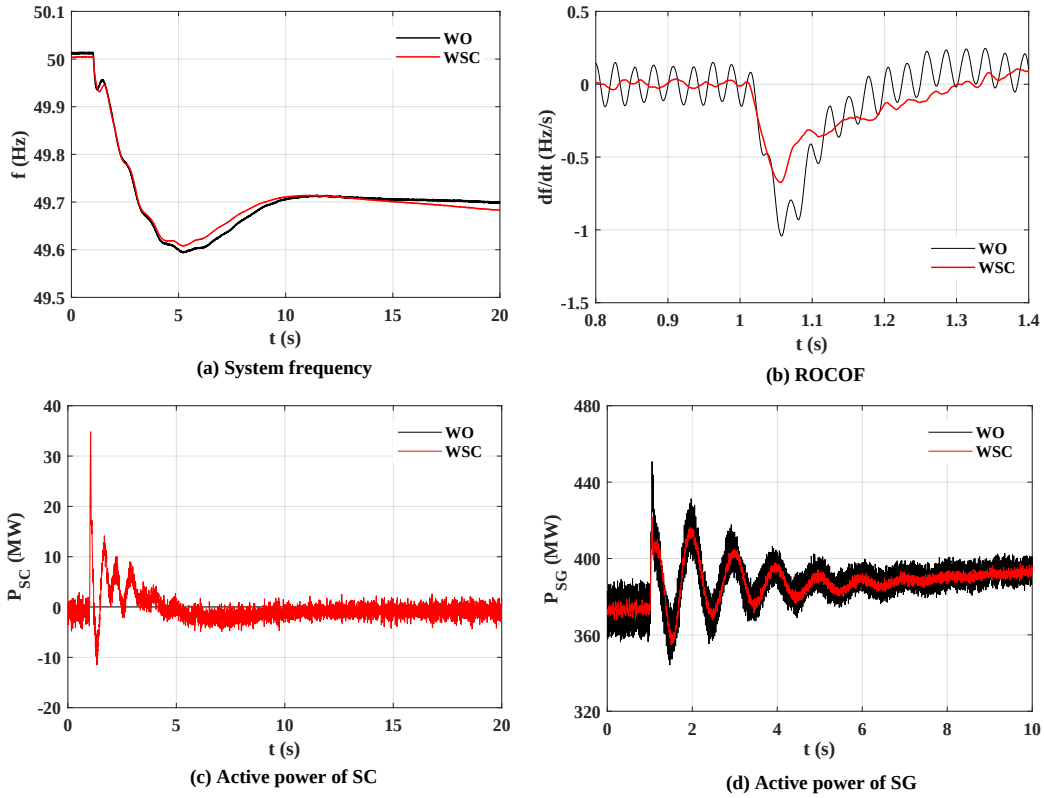

Figure 4.9: System response with high wind power penetration with and without SC.

response performance is extremely necessary which can help ROCOF significantly enhanced and system much stronger during disturbances.

4.1.3 Case study for the California power system

California power system uses a large amount of renewable energy reaching around 70% during the peak time of solar radiation [125]. Solar generation is the highest supply with nearly 68% of the entire amount of renewable sources as shown in Fig. 4.10. Solar plant is an "inertialess" generator which contributes no inertia for the system during incidents. Therefore, the lack of inertia and short-circuit power support is more serious and makes frequency stability jeopardized for the system during the peak time of solar production.

Awareness of the importance of inertia and short-circuit power support of the future renewable-based system, the local operator has been installing seven synchronous condensers commissioned by Siemens company in the California system for voltage regulation, inertia, and short-circuit power support.

This part validates the synchronous condenser performance at Talega substation in Southern California where first two units equipped with a modern and advanced control technology were commissioned. Two different incidents are investigated to verify the performance of SCs in terms of voltage regulation, inertia, and short-circuit power support during disturbances. The data is provided by the local operator which was collected from the phase measurement units (PMU).

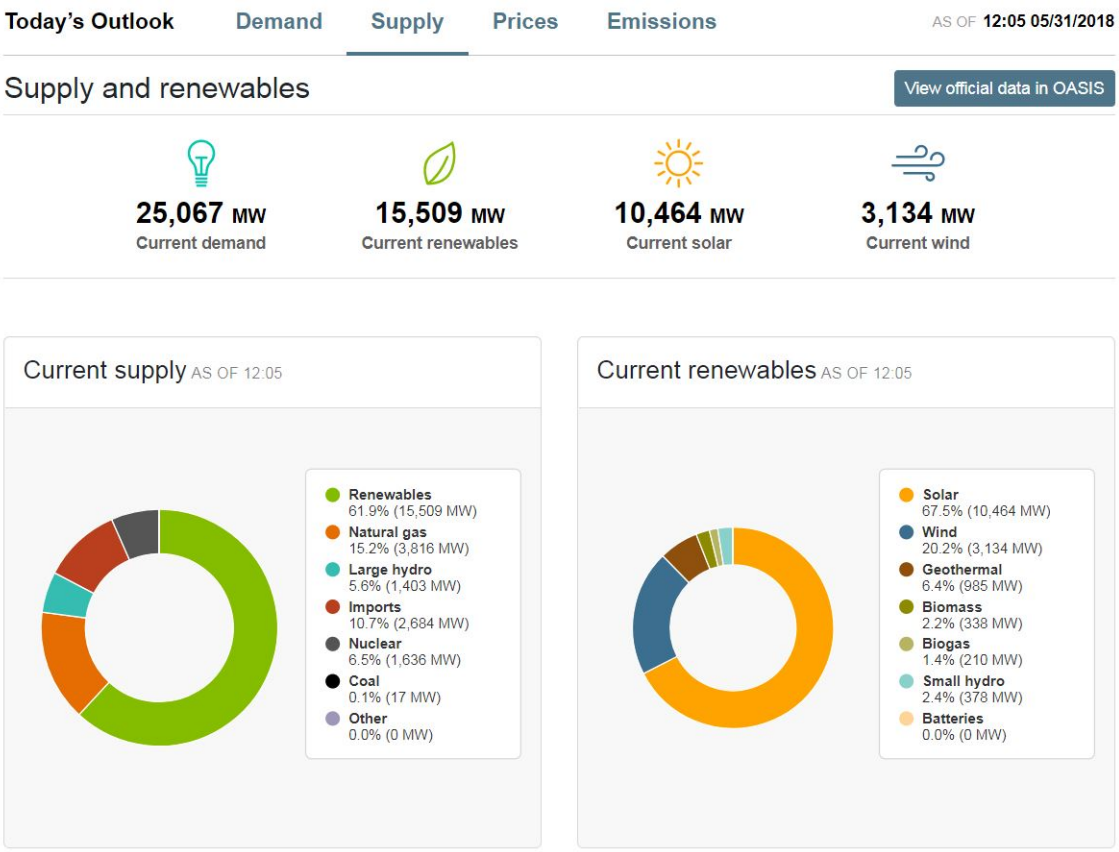

Figure 4.10: California supply outlook. (Collected on May 31, 2018)

A PV plant disconnection

A solar photovoltaic (PV) system (1200-MW) in the Southern California system was disconnected by an under-frequency-based protection which is due to a transient distorted frequency waveform less than its threshold perceived by a PLL measurement. Fig. 4.11 presents the system frequency, ROCOF, and SC responses during the fault. When the incident occurs, SCs immediately release their kinetic energy nearly 20 MW for inertial response to counteract the frequency change as shown in Fig. 4.11(d).

As expected, the reactive power of SCs immediately increases from approximately 9 Mvar to around 51 Mvar to halt the voltage drop during the incident. Consequently, the terminal voltage of SCs rapidly recovers after the fault.

A transmission line trip

In order to verify the plus point of SCs at Talega substation, an event with transmission line connected to a generator trip is examined.

The system frequency and ROCOF responses are shown in Fig. 4.12, while the terminal voltage of 230 kV and SC responses during the incident are shown in Fig. 4.13. The reactive power of SCs rapidly injects around 85 Mvar from -5 Mvar to nearly 80 Mvar to counteract the voltage drop. Additionally, the kinetic energy of SC's rotating mass available as the active power also immediately releases to against the frequency excursion. As a result, the system frequency and

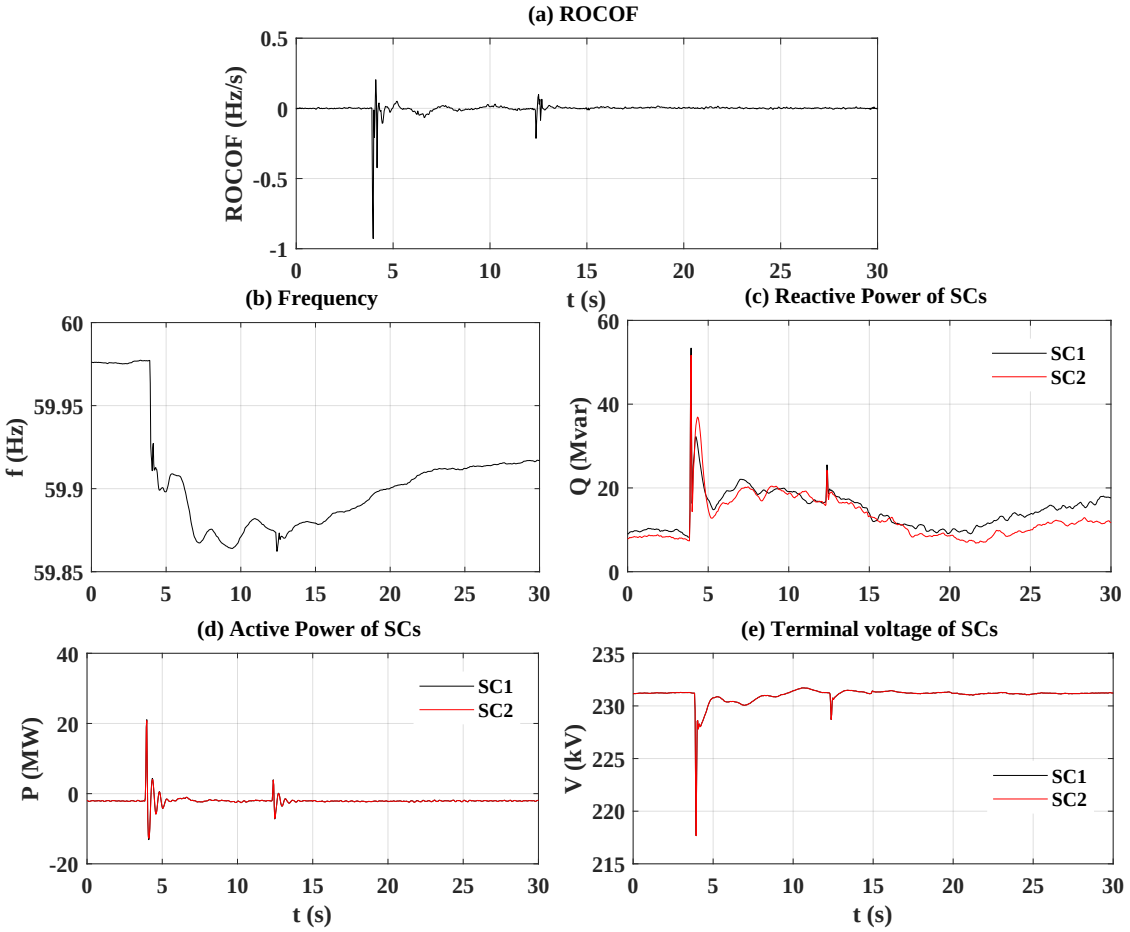

Figure 4.11: A solar generator trip incident: (a) ROCOF. (b) System frequency. (c) Reactive power of SCs. (d) Active power of SCs. (e) Terminal voltage of SCs.

ROCOF are improved, and the terminal voltage of SCs and the busbar quickly recover after the fault as seen obviously in Fig. 4.12 and Fig. 4.13, respectively.

It is worth to mention here is the terminal voltage responses of 230 kV busbar at Talega substation where 2 units installed and that at Otay Mesa which is far away from the SC location. Thanks to the quick support of the reactive power from SCs, the terminal voltage at Talega substation undergoes a small drop around 17 kV from 230 kV to nearly 213 kV instead of 100 kV drop from 230 kV to around 130 kV at Otay Mesa substation which is far from the SC location.

It can be concluded that the fast response of SCs in terms of the inertial response via its rotating power support and the voltage regulation through reactive power supply, the system frequency and terminal voltage at the substation are enhanced significantly during incidents, respectively.

4.1.4 Conclusion

With a high-level penetration of converter-interfaced generation (WF, HVDC, and PV), the system inertia is significantly declined, which results in a faster frequency dynamic with a higher ROCOF and a larger frequency deviation, as well as makes frequency more vulnerable. From the simulation results of the DK1 system and the PMU measurement of different incidents of the California

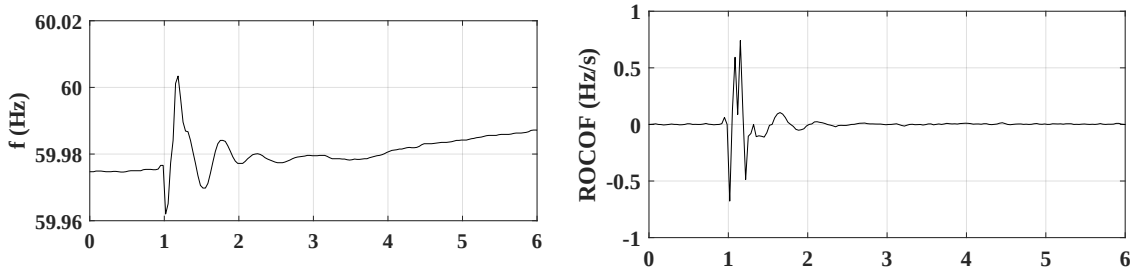

(a) Frequency response

(b) ROCOF

Figure 4.12: A transmission line trip incident: (a) System frequency. (b) ROCOF.

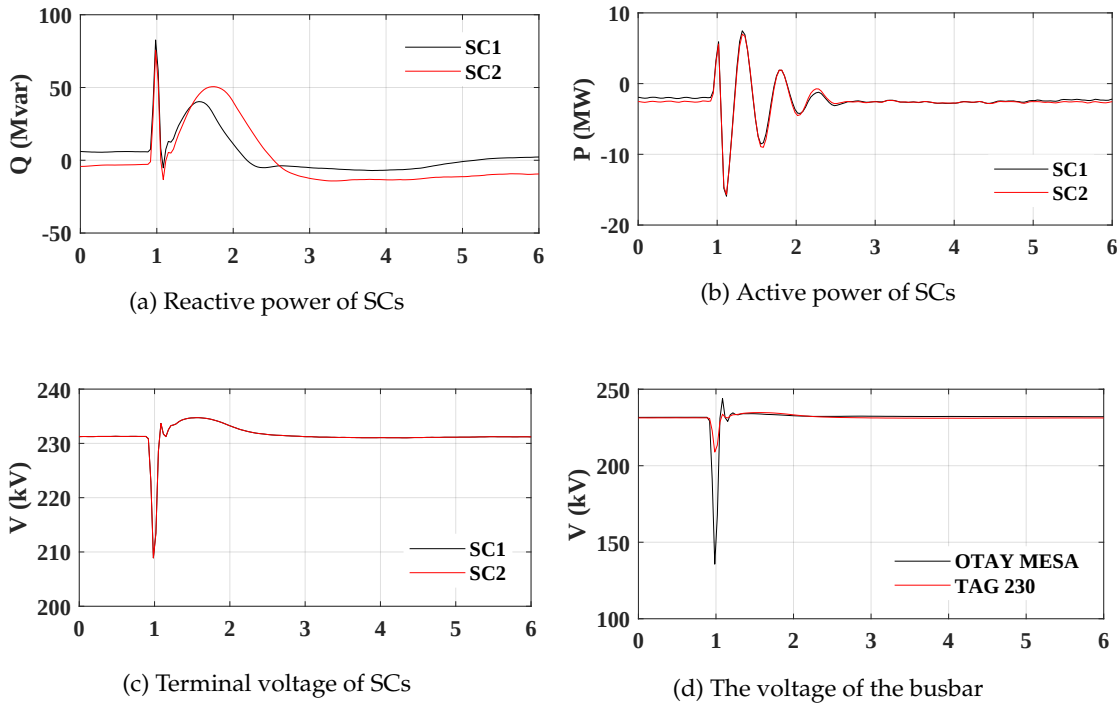

(a) Reactive power of SCs

(b) Active power of SCs

(c) Terminal voltage of SCs

(d) The voltage of the busbar

Figure 4.13: A transmission line trip incident: (a) Reactive power of SCs. (b) Active power of SCs. (c) Terminal voltage of SCs. (d) The voltage of the busbar.

power system, it can be concluded that SC is a critical solution that not only provides short circuit power and reactive power for keeping voltage stability and makes the system stronger, but also participates in the inertial response for the system against the frequency excursion and therefore enhancing significantly ROCOF during perturbations.

4.2 Frequency stability support from SI of WPPs

As mentioned earlier, unlike synchronous generators that can naturally inject or absorb kinetic energy stored in their rotating mass during disturbances, WPPs do not have that ability even they have rotating masses. Hence, a proper controller needs to be implemented to take advantage of the rotating masses.

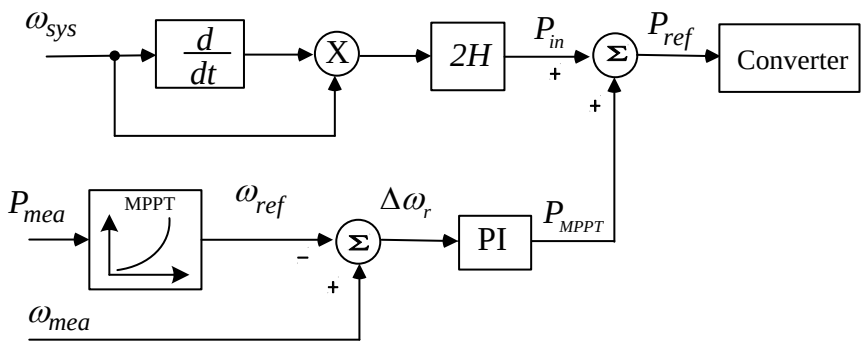

Figure 4.14: Inertial emulation for WPP.

The variable-speed wind power system consists of a variable-frequency VSC system (machine side converter (MSC)) and a controlled DC-voltage power port (grid side converter (GSC)). SI is implemented in the MSC which is in charge of controlling the machine voltage and frequency such that the flux is regulated at its nominal value and the torque is controlled. The torque control in turn, allows regulation of the machine active power. The control inputs of MSC are the torque command T_{ref} and the reference flux λ_{ref}. These two parameters are controlled by i_{rq} and i_{rd} of MSC, respectively [126]. T_{ref} is forced to change proportional to the square of the machine rotor speed to maximize the output power. SI is implemented to change T_{ref} or P_{ref} during frequency disturbances.

In the literature, there are 3 main techniques to implement frequency support using variable speed wind power plants without any energy storage systems namely inertial response control, droop control, and de-loading control. These three controls are explained in the following sections.

4.2.1 Inertial response control

Inertia emulation is implemented to extract the kinetic energy stored in rotating blades of the wind turbine which is used to terminate the frequency change during power imbalances. Fig. 4.14 shows inertial emulation control which imitates the inertial response of traditional power plants [127–132].

As can be seen in Fig. 4.14, the reference rotor speed ω_{ref} is determined from the output power of WPPs P_{mea} via maximum power point tracking (MPPT), then compared to the measured rotor speed ω_{mea}, through a PI controller to generate a maximum power P_{MPPT}. In the steady-state operations, no contribution from the inertial emulation P_{in}, the reference power is equal to the maximum power from MPPT P_{MPPT}. Whenever a power imbalance occurs, an extra power P_{in} which is proportional to ROCOF is created to add to the maximum power P_{MPPT}. Consequently, the reference power transferred to the converter with inertial response becomes:

$$P_{ref} = P_{MPPT} + P_{in} \tag{4.3}$$

The extra power from the inertial response control is expressed as follows:

$$P_{in} = 2H \frac{d\omega_{sys}}{dt} \tag{4.4}$$

This control method is investigated in the case study to compare with other control approaches.

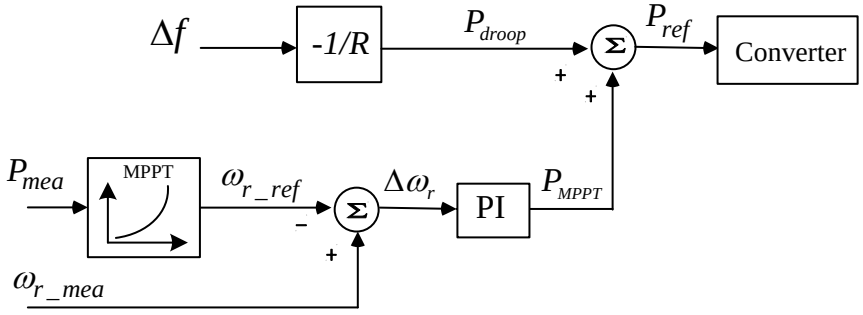

Figure 4.15: Droop control for WPP.

4.2.2 Droop control

Fig. 4.15 shows a droop control implemented for WPPs which is proportional to frequency deviation [133–137]. Whenever a certain frequency deviation exists, the extra power is generated to add to the maximum power to terminate frequency excursions. This control method mainly improves the frequency deviation during disturbances. The active power is controlled based on a linear characteristic as follows:

$$P_{droop} = -\left(f_{nom} - f_{mea}\right)/R \tag{4.5}$$

where R is the droop gain, f_{nom} and f_{mea} are the nominal and measurement frequency, respectively.

The linear characteristic between frequency and the active power of the wind turbine is exactly as the droop control of synchronous generator as illustrated in Fig. 2.3. When the system frequency drops from f_{nom} to f_{mea}, the wind turbine power increases from P_1 and P_2 to offset the frequency deviation.

The extra energy of WPPs releases to the system during disturbances can obtain from either the kinetic energy of the rotating masses of WPPs or the available wind power from blades' pitch control during high wind speed conditions. When the wind speed is below the rated speed, by decelerating the rotor speed, WPPs can supply more active power via the kinetic energy, then they will reduce the electrical power output to recover the pre-disturbance operation point [138]. The power reduction from WPPs during the recovery period is compensated by the primary control reserves of the system. The boost and recovery time constants of WPPs depend on the control strategy. Normally, a fast boost and a slow recovery are implemented for the controller, in [139], WPPs deliver a boosting power of 10% of rated power within 10 s and recover the rotating energy within 20 s.

4.2.3 De-loading control

De-loading control is the technique forced the wind turbine operating at sub-optimal power point tracking curve to ensure a reserve margin for WPPs participating in frequency control.

From the aerodynamic behavior of a wind turbine, the mechanical power extracted by the turbine is expressed as follows:

$$P_m = \frac{1}{2}\rho A C_p\left(\lambda, \beta\right) v^3 \tag{4.6}$$

where ρ is the air density, v is the wind speed, A is the rotor sweep area, β is the pitch angle, C_p is the power coefficient, and λ is the tip speed ratio which is expressed by

$$\lambda = \frac{\omega_r R}{v} \tag{4.7}$$

From equation 4.6, the output power of the wind turbine depends on the tip speed ratio λ and pitch angle β, hence deloading control can be implemented by speed control [140, 141] or pitch angle control [142–145]. However, this method is not optimal regarding the economic point of view, it is not investigated in this work.

4.2.4 The proposed synthetic inertia control

The idea of the proposed control method is changing the torque reference which in turn changes the power command of WPP during frequency excursions. Fig. 4.16 shows the proposed synthetic inertia controller that includes two control loops, the first one takes df/dt as the input to create an additional signal T_1 works as inertial response of synchronous generator, the second one generates an extra signal T_2 from frequency deviation input, reacting like the droop control or fast frequency response. Whenever system frequency changes from the nominal value, the torque command will be changed by the contribution of the SI controller.

As can be seen in Fig. 4.16, the system frequency is firstly measured and filtered by a low pass filter to eliminate the measurement noise. Then, a dead band ($\pm$ 0.015 Hz) is deployed to avoid the participation of the synthetic inertia control on a small frequency variation which may result in heavy power pulsations in the drive-train of the wind turbine in the normal operating condition. The first loop is in charge of additionally providing an offset signal T_1 that is proportional to $\frac{df}{dt}$. The second loop is responsible for supplying an additional torque signal T_2, which is proportional to the frequency deviation from its nominal value [146].

A high pass filter (HPF) is applied to guarantee that the Δf control loop does not contribute and the turbine can recover the operating speed when the system frequency reaches a new steady-state operating point. T_{W2} of HPF is selected to decide how long the second loop output can contribute to frequency control during disturbances. In [139], 10% of rated power boosting for frequency control within 10 s is implemented.

In order to avoid competing for control effect, the proposed method switches the reference from T_{ref} of MPPT control to T_{SI} of the proposed scheme during the inertial response. The output of SI can be expressed as follows:

$$T_{SI} = K_{in}\frac{df}{dt} - K_{droop}\Delta f + T_{refp} \tag{4.8}$$

where T_{refp} is the reference from MPPT corresponding to pre-disturbance rotor speed that is stored on the system data.

It is important to select properly the values of K_{in} and K_{droop}. Otherwise, it may cause a poor performance for the controller. K_{in} is proportional to df/dt control loop, a high K_{in} value may result in over-ramp up a limit of turbine speed that can destroy the mechanical part of the turbine. K_{droop} is the gain of Δf control loop, a high K_{droop} selection may lead to a large turbine speed drop that makes the turbine cannot recover a secure operating point after disturbances. K_{droop} is selected based on the droop characteristics of SG (from 2%-12%) [39]. An optimal combination

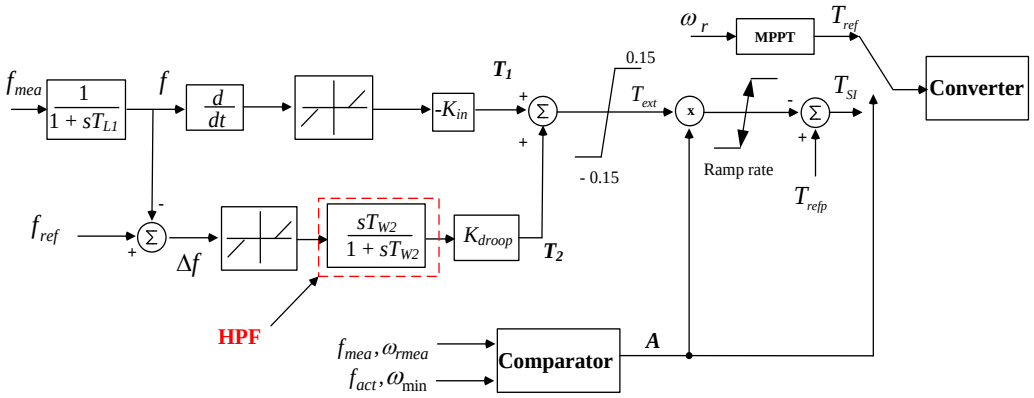

Figure 4.16: Synthetic inertia controller of WPP.

of the two gains can achieve a good performance for SI on the frequency stability improvement. A ramp rate limit ($\pm$ 0.5 pu/s) is added to prevent the immediate on/off activated signal in case reaching the minimum allowable rotor speed limit. A proper value of the ramp rate limit makes the transfer period smoother and less mechanical stress on the turbine and rotor.

An activation scheme combined with a minimum allowable rotor speed check is implemented on this control strategy to guarantee that the rotor does not operate below its the minimum allowable speed that may stall the turbine. The activation scheme can be described by

$$\begin{aligned} if & \begin{cases} f_{\min} \leq f_{mea} \leq f_{\max} & : set\, A = 0 \\ \omega_{rmea} \leq \omega_{\min} \end{cases} \\ else & : set\, A = 1 \end{aligned} \tag{4.9}$$

The SI controller will not be activated when the system frequency is within the allowable operating range and the rotor speed is equal or less than its minimum allowable speed.

4.2.5 Case study

To verify the proposed control method, the SI controller is applied to the Western Danish renewable-based system which uses a majority of converter-interfaced generation like wind power and HVDC interconnections as shown in Fig. 4.4. The SI controller is implemented on an aggregated model of a 400 MW offshore wind farm located at Alholt (AHA). The whole system is modeled and run in 6 continuous racks of RTDS platform. Firstly, three different control strategies the inertial response, the droop control, and the proposed control without HPF are compared and analyzed with the same disturbance to experience how each method can improve the frequency stability in terms of frequency deviation and ROCOF. Then, a comparison of the proposed control with and without HPF is investigated to validate the time constant T_{W2} for having a good performance for the SI controller.

Two different wind conditions studies are discussed to demonstrate the performance of the SI controller during a load increase disturbance. These two different wind speeds with 12 m/s and 11 m/s are simulated in this section to guarantee that the pitch angle controller is not activated. The system responses and the dynamic responses of WPP with different control strategies are investigated and compared.

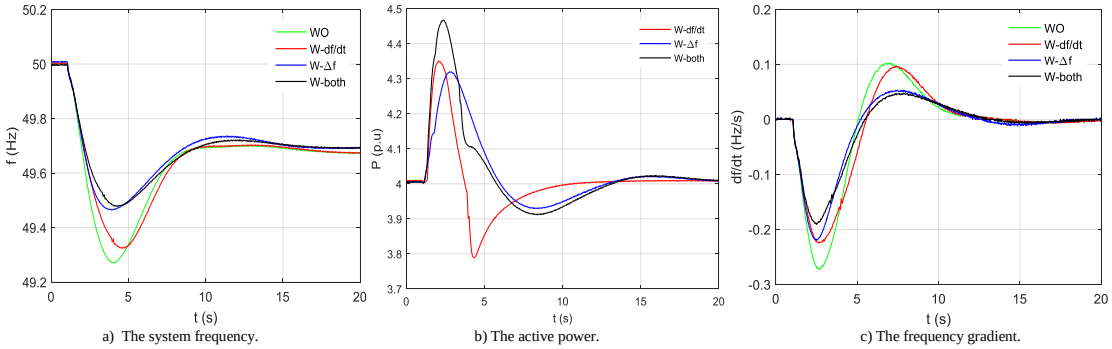

a) The system frequency. b) The active power. c) The frequency gradient.

Figure 4.17: The dynamic responses of system frequency, active power of WPP, and frequency gradient (ROCOF) during 200 MW load increase.

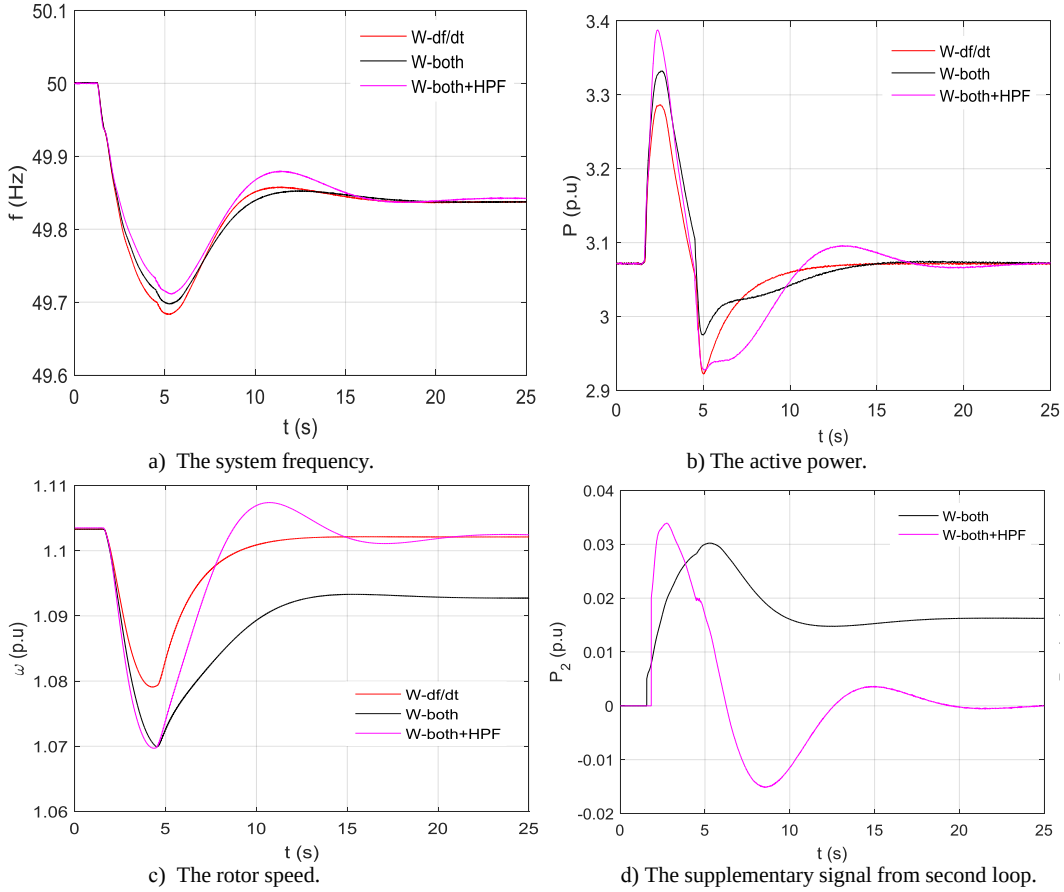

a) The system frequency. b) The active power.

c) The rotor speed. d) The supplementary signal from second loop.

Figure 4.18: The dynamic responses of system frequency and WPP during a 100 MW load increase.

Fig. 4.17 shows the dynamic responses of the system frequency and the active power of WPP at the rated wind speed (12 m/s) during a 200 MW load increase in Germany at t = 1.25 s. The green lines and black lines represent the responses of the power system without the SI controller and with both two control loops, whereas the red lines and blue lines symbolize the values of the system with the first control loop ($\frac{df}{dt}$) and with the second control loop (Δf), respectively. It can be seen from Fig. 4.17 that the system frequency is improved when the SI controller is in service. With the first control loop (red line), there is an enhancement in ROCOF from 0.27 Hz/s to 0.21 Hz/s, but the frequency nadir is slightly lifted around 0.03 Hz compared to that of WO case. The much larger enhancement in the frequency nadir is obtained by the second control loop and both two control loops, which increases from approximately 49.26 Hz to around 49.5 Hz. In addition, considering the active power responses of three SI strategies, it can be observed that the $\frac{df}{dt}$ loop can release with a higher active power and recover in a shorter time compared to the second loop during the frequency drop. However, this may result in higher mechanical stress for the wind turbine.

The coordination of two control loops presents a better performance which combines an inertial response and a fast frequency control as shown in Fig. 4.17b). As expected, with both two control loops, the frequency deviation is remarkably enhanced around 0.34 Hz and the frequency gradient is also improved compared to without the SI controller case as shown in Fig. 4.17.

However, the supplementary signal of the second loop still lasts until the system frequency reaches its nominal value. To deal with this issue, the high-pass filter is added to prevent the participation of T_2 on the primary frequency control. It can be observed in the second case study that investigates the SI implementation on the same testing system to compare the SI controller with and without high-pass filter during a sudden 100 MW load increase. With the lower wind speed (11 m/s), the power output of WPP does not reach its rated power (400 MW).

As can be seen clearly in Fig. 4.18, the SI strategy with HPF results in better performance with a bit higher frequency nadir and a lower the frequency gradient. The extra active power output of WPP is higher compared to without HPF, it means more kinetic energy is extracted from the rotor, while the rotational speed deviation is almost the same. Without HPF, the output signal T_2 of the second loop still exists which is proportional to the frequency deviation. This value keeps adding to change the torque reference, hence changing the rotor speed reference. As a result, the rotor speed cannot recover its pre-disturbance point when the system frequency reaches a new steady-state operating point as shown in Fig. 4.18 c). On contrast, with HPF, T_2 equals to zero when the system gets stable, so the rotor speed can reach the pre-disturbance value after the disturbance as shown in Fig. 4.18 d).

Another thing should be mentioned here is that after WPPs supply kinetic energy for the system during the disturbance, it will reduce the electrical power output to recover its pre-disturbance condition as shown clearly in Figs. 4.17 and 4.18.

From the simulation results, it can be concluded that the proposed SI controller combined with an activation scheme performs a better frequency stability improvement during the disturbance, especially frequency deviation. It should be considered to implement for the low inertia systems that use a majority of renewable power plants.

4.2.6 Conclusion

With the dominance of wind power in the power system, the grid code requirements on frequency control for integration of large wind farms are necessary for secure operation of the network.

Because of the decoupled control between the rotor speed and the system frequency, the inertial response of wind power plants for the frequency support is almost unavailable. However, the SI controller can be implemented for WPPs participating in the frequency support, and the capacity for the SI response depends on the pre-disturbance operating condition of wind turbine that can be controlled through two gains and time constants to satisfy the steady-state operating limits. The simulation results show that the proposed SI strategy and the activation scheme can extract more kinetic energy from wind generators for a better frequency stability enhancement compared to the others.

4.3 Combination of SC and SI for frequency stability improvement

The previous parts have analyzed and investigated the contribution of SC and SI of WPPs to frequency control. SC can improve significantly ROCOF based on its inherently inertial response due to the electromagnetic coupling with the grid. The kinetic energy stored in its rotating mass can naturally counteract with the rate of change of frequency during frequency excursions. SI of WPPs can enhance drastically frequency deviation with a proper parameter set during disturbances. How fast and how large SI of WPPs can react is depending on the control approaches, however, it takes time for measurement and control reaction. Reference [147] shows that synchronous inertial response is much faster than synthetic inertial response as shown in Fig. 4.19.

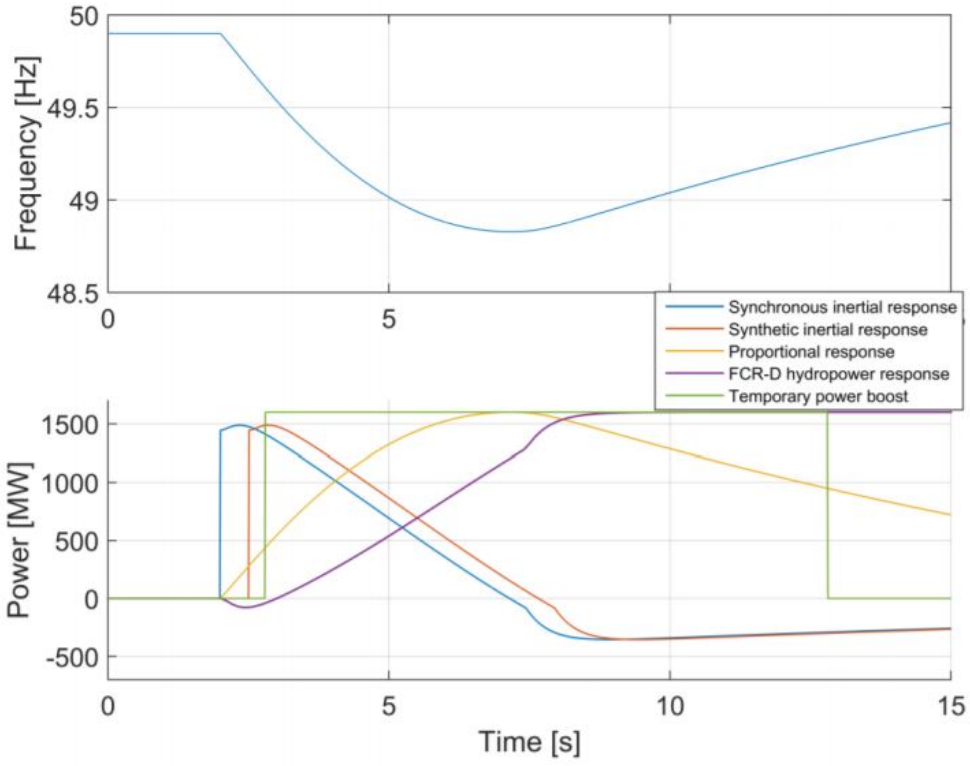

Figure 4.19: Responses of different products during frequency drop.

A combination of SC and SI of WPPs offers a perfect performance for the frequency stability enhancement. While SC can quickly respond to frequency change based on ROCOF due to its electromagnetic connection at the onset of the disturbance, SI of WPPs will support afterwards for counteracting the frequency deviation and compensating kinetic power recovery for SC which SC

needs to return its pre-disturbance speed after participating in frequency control. SI contribution can be controlled to have fast contribution when the disturbance occurs and recover a bit slower to give time for primary control react. As a result, a combination of SC and SI can not only help system frequency improve ROCOF and the frequency deviation, but also make system frequency much stronger during frequency excursions.

4.3.1 System configuration

Fig. 2.8 shows the DK1 system in 2020 that is using a majority of renewable energy and interconnecting to the neighboring countries through HVDC links. This system is based on the current DK1 system adding more 400 MW offshore wind farm (HRC or HR3) and 700 MW VSC-HVDC interconnection to the Netherlands (COBRA cable) that are operating in 2018 and in 2019, respectively. The German grid is modeled by a large synchronous generator and a load. The frequency control support of the German grid is adjusted proportionally to the power exchange. There are three synchronous condensers (the marked red in Fig. 2.8) connected at three LCC-HVDC terminals with the detail parameters in Table 4.1. The AVR of synchronous condenser located at bus FGD uses a real control system to evaluate how it performs during disturbances. There are three aggregate offshore wind farms (OFWFs), and one aggregate onshore wind farm (ONWF) as shown in Fig. 2.8.

Table 4.1: Synchronous condenser parameters.

SCs	Location	S_{rated} (MVA)	V_{rated} (kV)	Q_{min} (Mvar)	Q_{max} (Mvar)
SC1	VHA	200	12	-100	150
SC2	TJE	250	13	-120	200
SC3	FGD	270	15.75	-144	242

4.3.2 Case studies

Different scenarios and wind speed conditions based on the data provided by the local transmission operator are studied in order to examine the proposed method under various disturbances/faults. SI is implemented for 2 OFWFs which are located at AHA and HRB, C.

Base case

The case is based on the DK1 system data in 2020, all 5 local SGs (873 MW central production) are operating with the power flows as shown in Fig. 4.20(a).

To verify the contribution of SC to the frequency stability improvement, the system response during 200 MW load located at MAL increases at t = 1 s is investigated in this case with SCs in red and without SCs in black as shown in Fig. 4.21. With SC in operation, the system frequency response is much smoother and stronger. Additionally, ROCOF is significantly improved nearly 0.29 Hz/s compared to around 0.233 Hz/s without SC case, that are quite accurate with the Matlab calculation based on (2.4) as shown in Table 4.2. It is noteworthy that when the disturbance occurs SC immediately releases the electric energy to counteract the frequency drop with nearly 420 MW/s active power gradient as shown in the last sub-plot of Fig. 4.21.

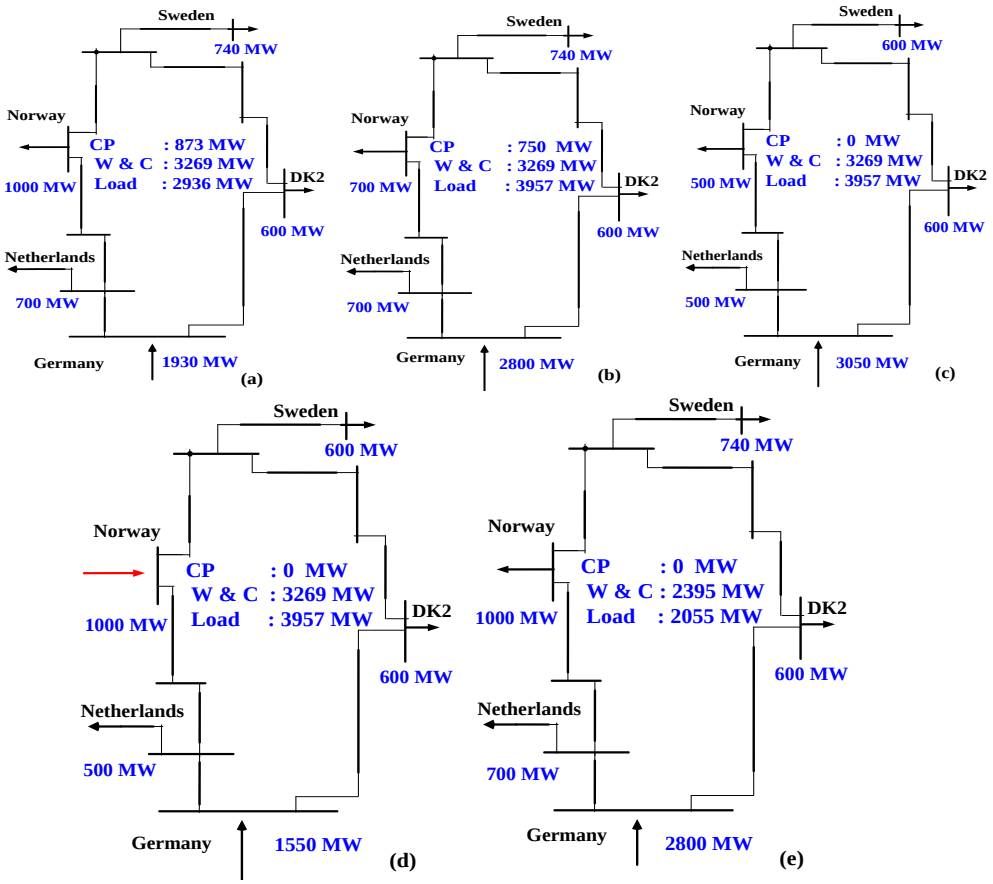

Figure 4.20: Case-study scenarios (CP: central production, W & C: wind and coastal production). (a) Base case. (b) HLHW with 3 SGs. (c) HLHW no SGs, exporting to Norway. (d) HLHW no SGs, importing from Norway. (e) LWLL.

With AVR hardware, based on the updated voltage and current values of SC in RTDS during the disturbance, AVR hardware will calculate AVR SP and send back to SC in RTDS to control the terminal voltage during the disturbance. In this situation, AVR hardware will increase the set point to inject more reactive power for voltage regulation. It can be seen obviously that SC can improve significantly ROCOF of the system thanks to the rapidly rotating energy support during the inertial response.

Table 4.2: System inertia and ROCOF in Matlab calculation.

-	Cases	(a)	(b)	(c)	(e)
H (s)	WOSC	6.53	5.42	4.54	8.76
	WSCs	7.46	6.1	5.52	10.63
ROCOF (Hz/s)	WOSC	-0.26	-0.45	-0.56	-0.43
	WSCs	-0.23	-0.41	-0.45	-0.36

High wind and high load (HWHL)

1. *High wind and high load with 3 online SGs:*

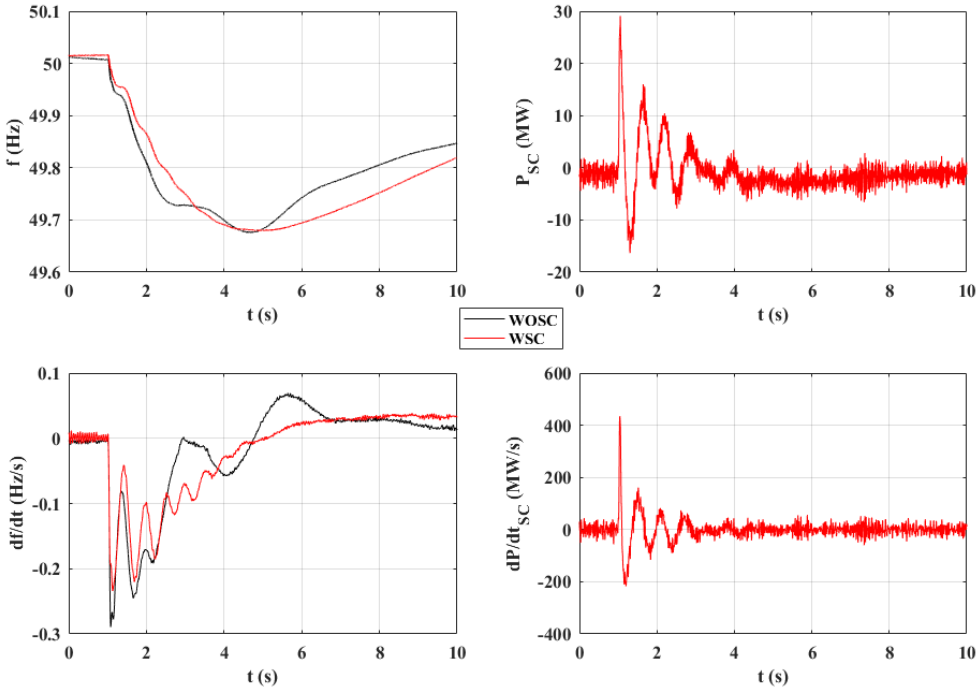

Figure 4.21: System frequency, ROCOF, and SC responses during a disturbance of base case.

Another scenario is investigated in this case where the load is assumed to use in 2050 estimated 1% increase per year based on the base-case load and the wind speed reaches the rated speed at 12 m/s so that WPPs are operating at their rated power output. There is three committed SGs in operation with the power flow as shown in Fig. 4.20(b).

A 10% load increase incident at bus MAL occurs at t = 2 s. The system response during the incident is illustrated in Fig. 4.22 with the black for without any inertia support, the red for with SI controller, and the blue for with SC combined SI. It can be seen clearly that SI can improve significantly frequency nadir from 49.45 Hz to 49.55 Hz, whereas SCs combined SI can enhance both frequency deviation and ROCOF.

By comparing ROCOF response, without any inertia support the system frequency is much more vulnerable, ROCOF reaches a maximum value twice at around 2.1 s and nearly 3.1 s as zoomed in Fig. 4.22(b). It can be explained that at the first onset of the incident, the three online synchronous generators and the German generator rapidly release their kinetic energy to against frequency change that helps ROCOF increasing after experiencing a first maximum value around 0.5 Hz/s. However, this kinetic energy is not sufficient to help ROCOF recover completely, a second maximum ROCOF is at around 3.1 s as its consequence for a low inertial response of the system as seen obviously in Fig. 4.22(b) with the black curve.

This issue is dealt with SC and SI in operation case where ROCOF is quickly settled down instead of undergoing a large oscillation of the WO case. The inertia support of an SC and SI combination can be described as follows: at first few seconds following the disturbance, SC's rotating energy is released in order to support the inertial response that helps ROCOF improved, SI responds afterwards to increase temporarily WPP power output for counteracting the frequency drop as well as compensating for SC's rotating energy recovery. It can be seen much more clearly about the response time that shows how fast they react from the active power gradient (dP/dt) plots

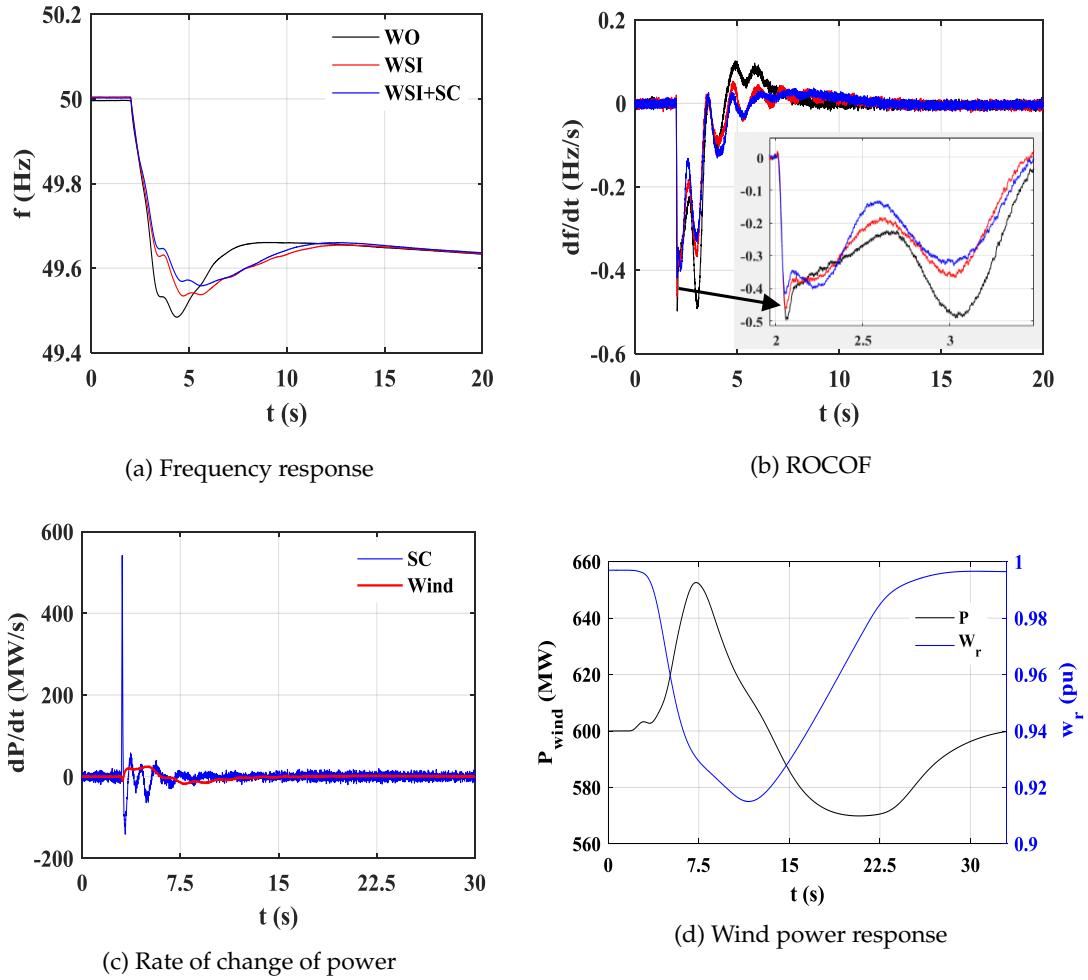

(a) Frequency response

(b) ROCOF

(c) Rate of change of power

(d) Wind power response

Figure 4.22: System responses during 10% load increase disturbance of HWHL 3 SGs in operation.

of SC and WPP in Fig. 4.22(c). Consequently, the combination of SI and SC results in an efficient enhancement of the frequency stability in term of frequency nadir and ROCOF. As expected, WPP can recover the pre-disturbance operating speed when the system frequency reaches a new equilibrium as shown in Fig. 4.22(d). The equivalent system inertia and ROCOF are calculated by Matlab as shown in the fourth column of Table 4.2.

2. *High wind and high load without online SGs*

A scenario with all synchronous generators are phased out (no central production) is studied in this case with the power flow as shown in Fig. 4.20(c).

In order to support the inertial response, three more SCs are installed in the system at KAS, TRI, and EDR buses that have the same specification with SC3 as shown in Fig. 4.25. The locations of SC installation are based on the reactive power support demand through power flow calculation. In this situation, the system operates in a very low inertia constant and relies mainly on the German interconnection. The frequency is measured at three locations KAS, LAG, and FER to witness the frequency synchronization when the system operates in a low inertia condition.

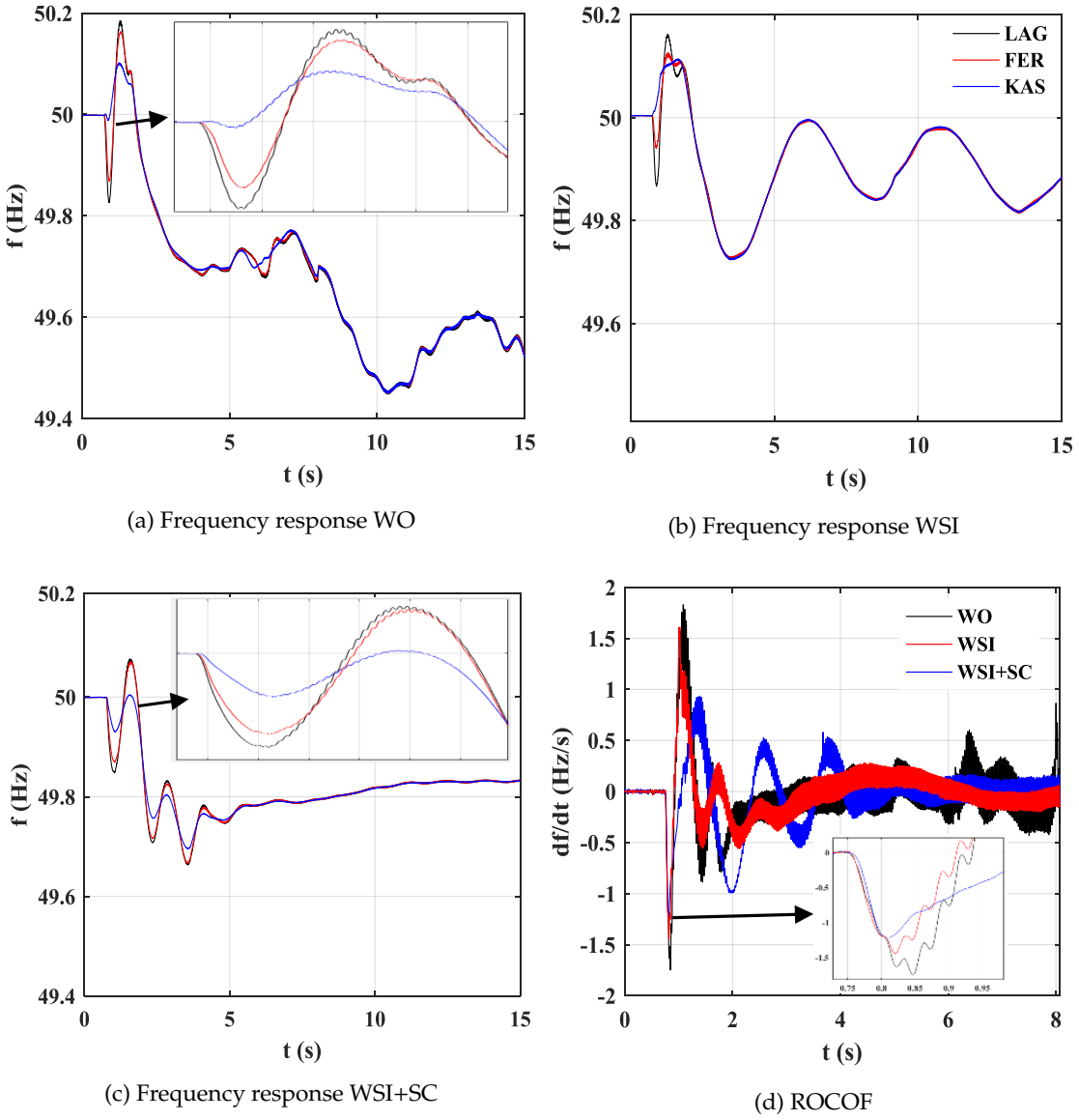

(a) Frequency response WO

(b) Frequency response WSI

(c) Frequency response WSI+SC

(d) ROCOF

Figure 4.23: System responses during 10% load increase disturbance of HWHL no local SGs in operation WO, WSI, and WSI+SC.

Load increase disturbance: The same 10% load increase disturbance size occurs. As can be seen clearly from Fig. 4.23, the system frequency without SCSI (WO) undergoes a huge oscillation and gets unstable after around 5 s because only the German side provided inertial support is not sufficient for the frequency recovery in this operating condition.

It is worth to be mentioned here is the frequency behavior in different locations of the system. A reverse oscillation occurs with the frequency at KAS compared to that of FER and LAG. With the combination of SC and SI in service, the system stays in synchronism and becomes stable after approximately 5 s as seen in Fig. 4.23(c). It can be explained that at the onset of the incident, the inertial response from the German side and SCs tries to restrain the frequency change, after that the inertia support from SI of WPPs and primary control help the system frequency recovery and stable. Only SI in operation is not fast enough for the frequency support in this low inertia

condition, which leads to an asynchronism of frequencies at different parts and a large oscillation before getting stable on the system frequency, as shown in Fig. 4.23(b).

It should be paid attention here is that there are oscillations in the frequency responses which does not exist in the previous case with 3SGs in operation. This might be concluded that the oscillations are caused by a poor frequency control support with a low inertial response and primary control. These oscillation needs further investigation about their frequency range and sources which is discussed more detail in the next chapter.

A three-phase short circuit: A three-phase short-circuit fault occurs for 100 ms at t = 1.6 s and cleared at t = 1.7 s at the bus TRI, and after that, the circuit breaker of TRI load (250 MW) is activated to disconnect the load.

The comparative results show that with SCSI not only the frequency stability is improved significantly, but also the system is much more synchronized (Fig. 4.24). Without any inertia supports of SC and SI, the frequency experiences a huge deviation and ROCOF reaches around 3.5 Hz/s.

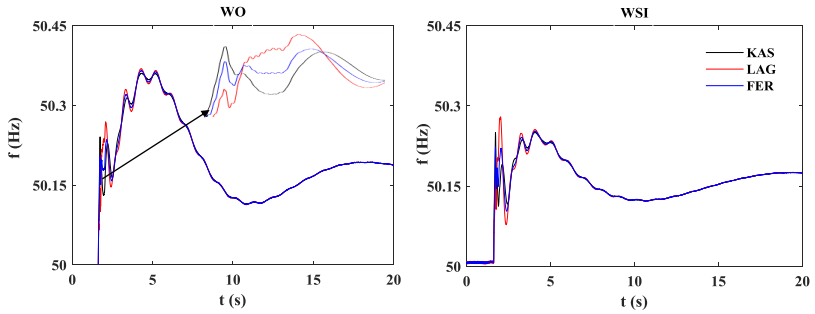

(a) Frequency responses with WO and WSI

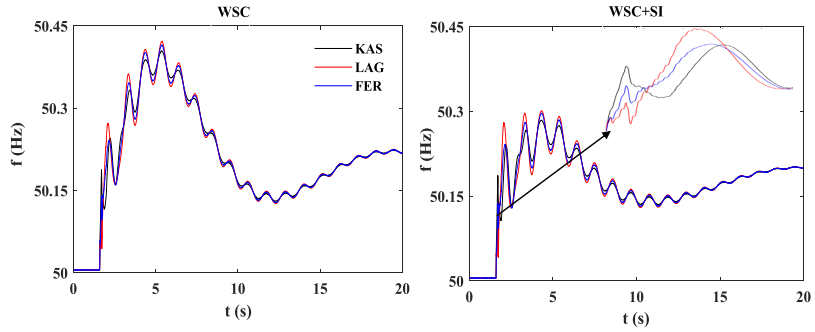

(b) Frequency responses with WSC and WSI+SC

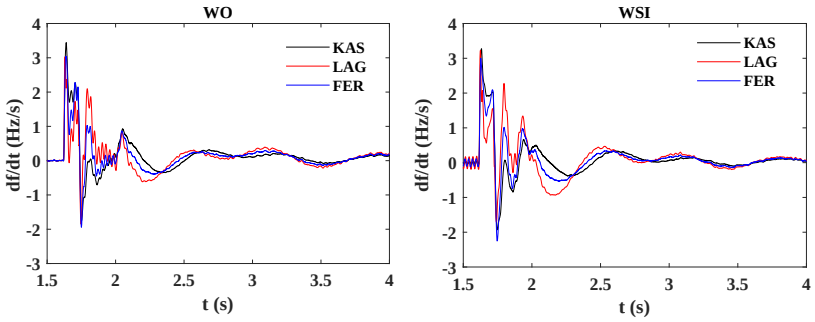

(c) ROCOFs with WO and WSI

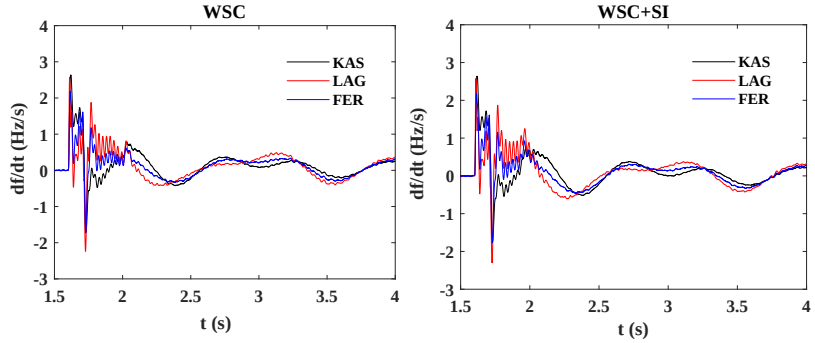

(d) ROCOFs with WSC and WSI+SC

Figure 4.24: System frequency and ROCOF during a three-phase short-circuit fault with WO, WSI, WSC, and WSC+SI (Exporting to Norway).

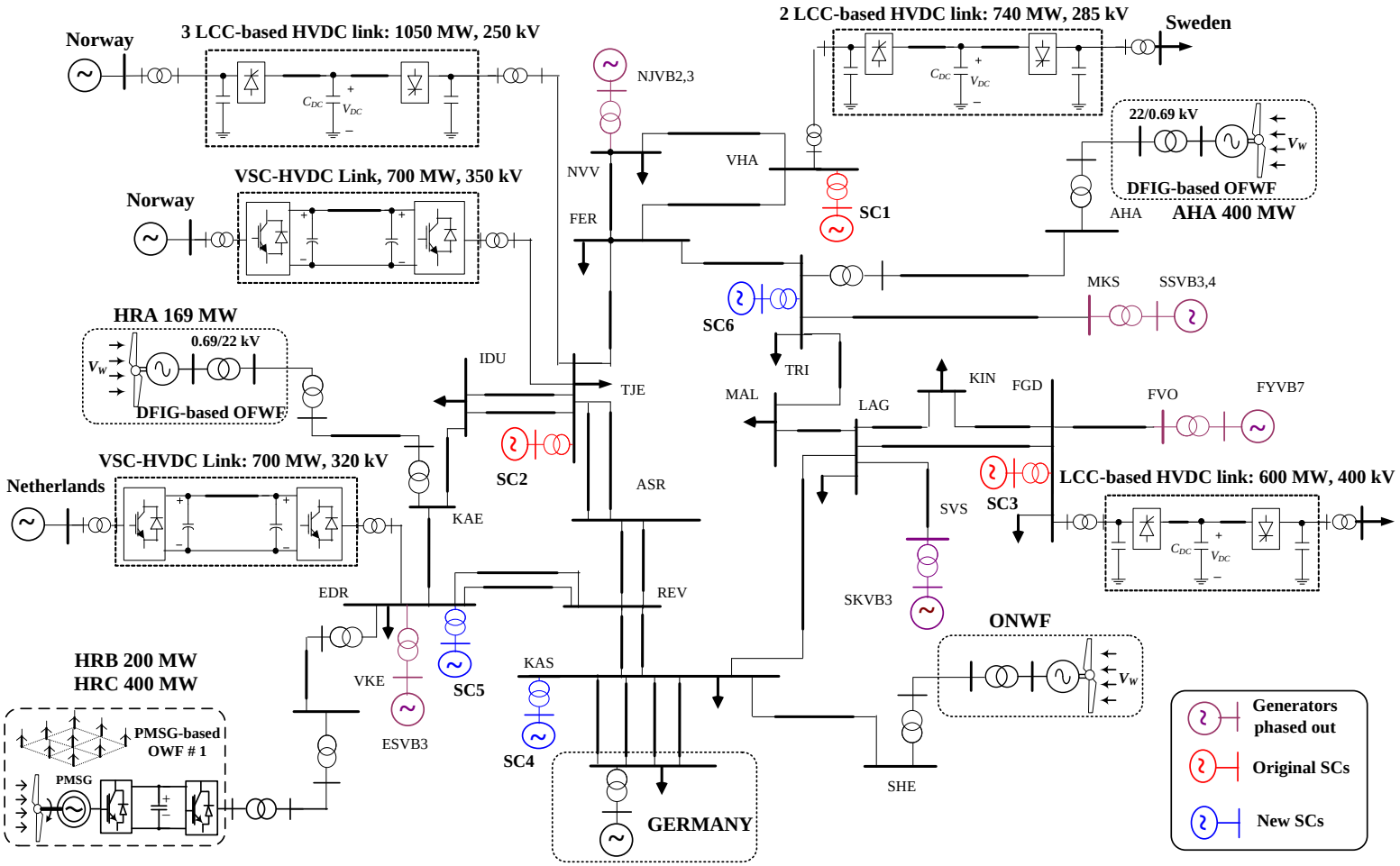

Figure 4.25: Single-line diagram of 400 kV Western Danish renewable-based system with new SCs in 2020.

A remarkable improvement in the frequency deviation is observed when SIs are in service, the maximum frequency is reduced considerably and rapidly settles down without further increase. On the other hand, a huge enhancement is observed in ROCOF with SC in operation. However, a quite large frequency deviation is witnessed with SC case after the TRI load disconnection. This can be explained that at the first few seconds following the fault, the German side and all of SCs inherently contribute inertial response to the grid by absorbing the power to against the frequency increase that can be observed in a significantly ROCOF improvement. After supporting inertial response, SCs release the energy to the grid to recover their speed which makes the frequency deviation larger compared to the WO case as shown in Fig. 4.24. This issue is addressed with the combination of SC and SI in operation. ROCOF is drastically enhanced from nearly 3.5 Hz/s (WO) to 2.5 Hz/s that satisfies the acceptable range of the Continental European grid code ($\pm$ 2.5 Hz/s) [148].

Another scenario of HWHL without any online SGs is switching the power transfer direction of HVDC links to Norway. The current power flow of the system is listed in detail in Fig. 4.20(d). The 1000 MW power is imported from Norway to DK1 through HVDC links, which leads to a reduction in importing power and the frequency control support from the German grid. Consequently, the system frequency dynamics is faster, the frequency deviation and ROCOF are much larger than the exporting HVDC links from Norway case with the same incident sequence at bus TRI as shown in Fig. 4.26. Especially, ROCOF that is measured at bus KAS even reaches approximately 8.5 Hz/s instead of 3.7 Hz/s in the previous one. With SC and SI are in operation, this value is significantly enhanced only around 4.3 Hz/s. However, this value is out of the acceptable range of the grid code ($\pm$ 2.5 Hz/s), a limit of the power output of importing HVDC link, or system inertia minimum requirement, or more synchronous condenser installations should be implemented in low inertia systems.

Low wind and low load (LWLL)

A low wind speed condition (V_W = 9.5 m/s) is investigated in this case to verify the coordination of SI control and the activation scheme when the rotor speed hit its minimum allowable speed during a disturbance. The system operates with 70% of the base-case load and no synchronous generator in operation with the detail data as shown in Fig. 4.20(e). In this situation, the DK1 system operates like a corridor to transfer the power from Germany to Norway, Sweden, and the Netherlands.

As expected, the ROCOF experiences a 0.2 Hz/s improvement from -0.6 Hz/s to -0.4 Hz/s when SCs are in service during 15% current load increase disturbance as shown in Fig. 5.3. Meanwhile, the frequency nadir and settling time experience a significant enhancement with the SI controller. It is noteworthy that (2.4) is not precise in low inertia systems as shown in Table 4.2.

An interesting point which should be of concern here is the rotor speed hits the minimum speed limit that is set at 0.75 pu during the disturbance. This causes an unsmooth response in the recovery section of the active power and the rotor speed. It is worth to mention that a proper ramp rate limit and coordination of the control with its activation scheme help the rotor speed response smoother and reduce the mechanical stress.

A comparative load behavior of frequency dependent load (FDL) and voltage & frequency dependent load (V&FDL) of FER load is shown in Fig. 5.3(d). It can be seen clearly that the load changes immediately after the onset of the disturbance and is mainly caused by the voltage dependence.

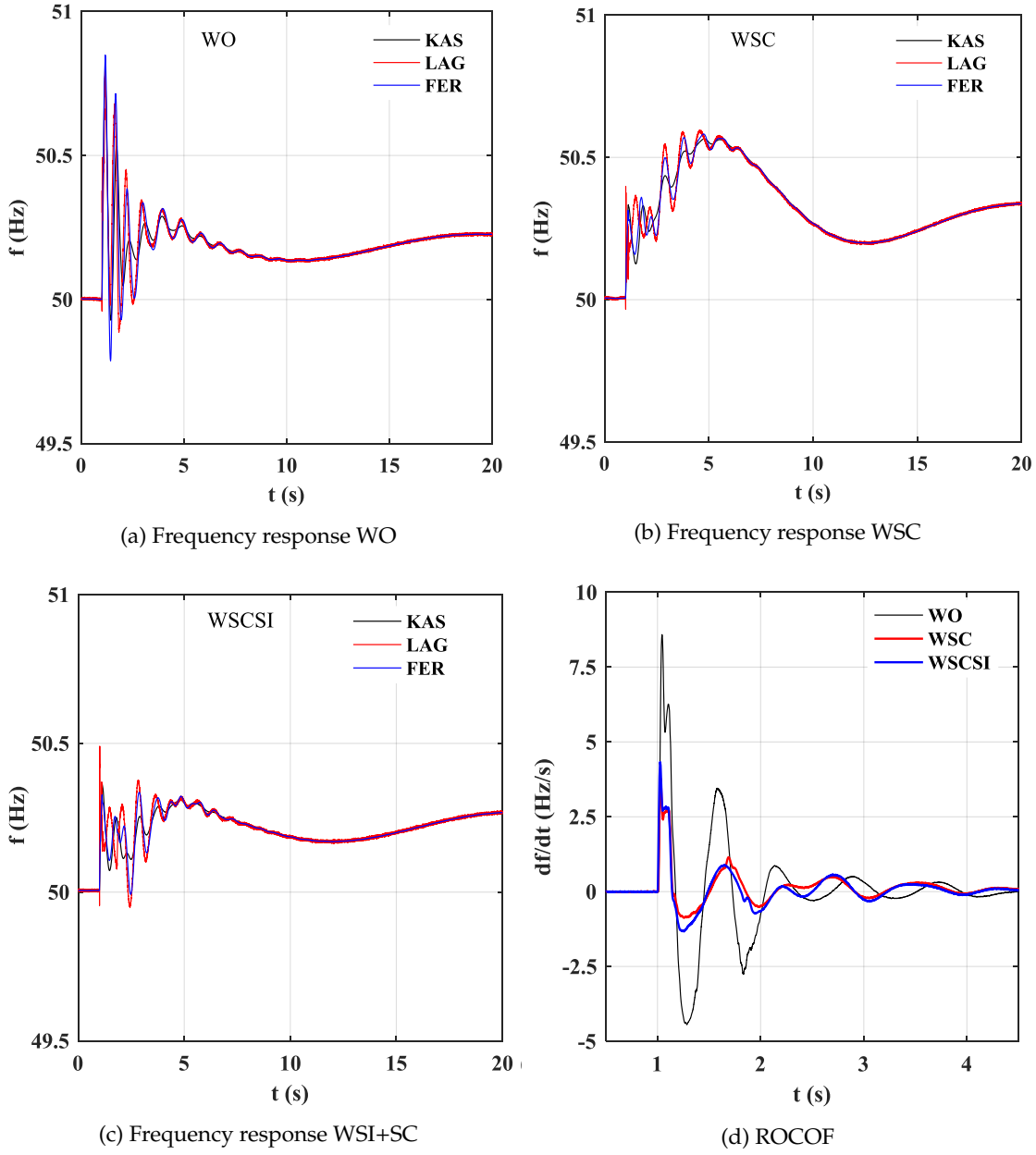

(a) Frequency response WO

(b) Frequency response WSC

(c) Frequency response WSI+SC

(d) ROCOF

Figure 4.26: System frequency and ROCOF during a three-phase short-circuit fault with WO, WSC, and WSC+SI (Importing from Norway).

4.3.3 Conclusion

With a rapid increase of converter-based generation in power system, there is a significant reduction on the system inertia and the primary frequency control. That may cause faster frequency dynamics and a larger frequency deviation during disturbances. Furthermore, the system inertia constant becomes time-variant because of the variability of power dispatch and demand scenarios.

The combination of SC and SI may pronounce the inertial response and a fast frequency control of a synchronous generator during power imbalances. The inertial response from SC remarkably improves ROCOF, afterwards a frequency control support with fast time response from SI of WPPs

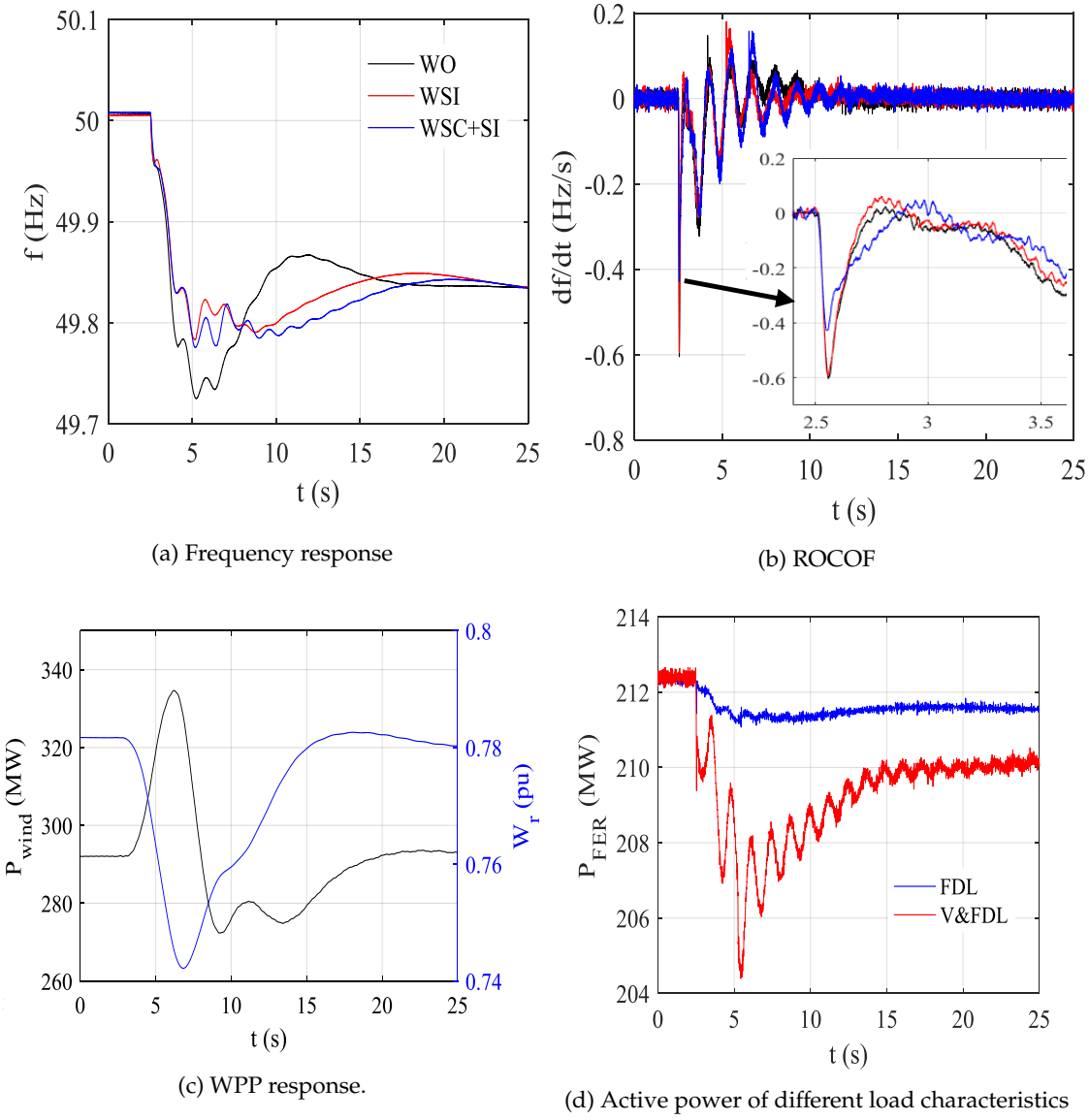

(a) Frequency response

(b) ROCOF

(c) WPP response.

(d) Active power of different load characteristics

Figure 4.27: System responses during a disturbance of LWLL.

takes over and significantly enhances frequency deviation. This work is based on the simulation to show how to tune K_{in} and K_{droop} to adjust the output of WPP to support frequency stability and compensate the kinetic energy recovery of SC after its inertial response to help the system quickly settle down. K_{in} is tuned to get a proper power at the beginning of the SI response based on df/dt whereas K_{droop} and T_2 are tuned based on frequency deviation to adjust how large and fast the output of SI is. As a result, a combination of SC and SI provides a better performance that not only enhances frequency deviation and ROCOF but also helps the low inertia system more synchronized during different disturbances. In addition, TSOs may impose requirements on the minimum system inertia and examine the impact of HVDC in low inertia operating conditions.

CHAPTER 5

Power oscillation damping for low inertia systems

In this chapter, a POD controller incorporating SCs that adapts to the modern system characteristics is proposed for low inertia systems to damp power oscillation and enhance frequency stability. Furthermore, a parameter optimization that is based on SiL linking RTDS and Matlab through OPC communication is implemented. Prony technique is applied to extract the frequency and damping ratio of the dominant oscillation mode from the system frequency measurement. The near-optimal or optimal parameter set of the POD controller is determined by a GA objective function to maximize the damping ratio of the dominant mode. The future Western Danish power system supplied by renewable energy sources and HVDC interconnections with the neighboring countries is used as a typical low inertia system in this study.

5.1 Power oscillation in low inertia systems

The rapid penetration of converter-interfaced generation into power systems renders the system inertia significantly reduced. Low inertia systems with a limit of short-circuit power support from converter-interfaced generation may cause poor dynamic performance and make the system frequency more vulnerable compared to conventional grids. A poor frequency control support in low inertia systems may cause an oscillation (around 0.8 Hz - 1.3 Hz) in frequency responses during a small disturbance as shown in Fig. 5.1 [85, 149].

To avoid confusion with the oscillatory stability issue in traditional systems, the difference of power oscillation in synchronous-machine-based systems and converter-based systems is clarified. There are two types of power oscillations in traditional systems which are related to rotating power generators. The first is a single generator oscillating against the system which is called local oscillation, while the second involves many generators in one area of the system acting against other generators in other areas of the system, namely inter-area oscillation [150, 151]. The local or inter-area oscillations usually occur when the system subjects to small disturbances such as a small load step or voltage step, which is defined small-signal stability. The oscillation is usually a periodic curve with an amplitude as an exponential function as shown in Fig. 5.2 [152]. In converter-based systems which are free of conventional power plants, power oscillation does not completely involve any power exchange between generators. This oscillation results from a poor inertial response which makes the system suffers from low-frequency oscillation before recovering completely when subjecting to disturbances. This oscillation does not make the system unstable but leads the system quality worse after disturbances. As can be seen from Fig. 5.1 and Fig. 5.2, these type of oscillations of the two power systems have different characteristics.

To address the oscillatory stability issue of traditional power systems, a supplementary controller called PSS is implemented to existing power plants that is used as an auxiliary excitation control

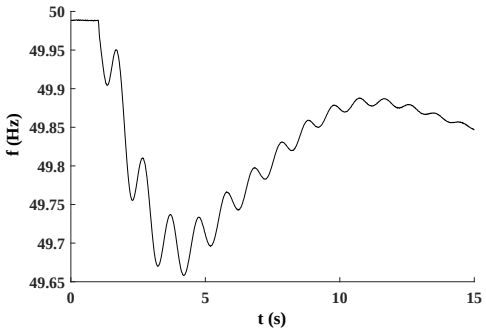

(a) A load increase disturbance [149].

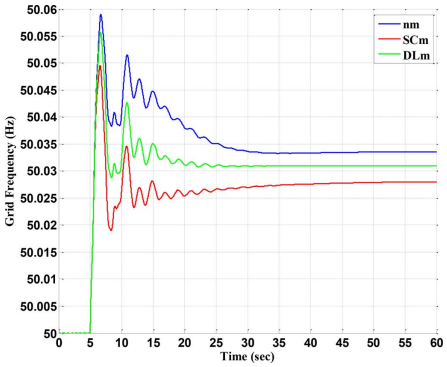

(b) A load decrease disturbance [85].

Figure 5.1: Frequency responses in low inertia systems.

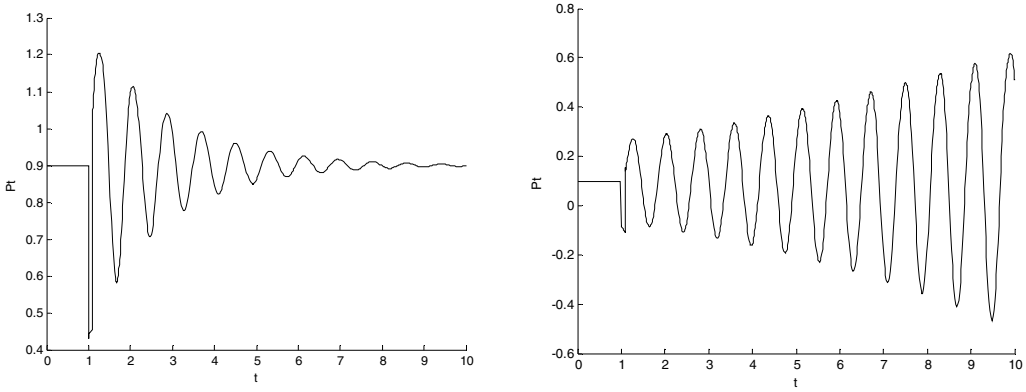

(a) (b)

Figure 5.2: Power oscillations in traditional systems.

to damp generator oscillations [66, 71, 72]. The basic principle of PSS is introducing an electrical torque in phase with the rotor speed variations of power plants to damp the rotor oscillation [13]. This issue is usually solved with small-signal analysis using a linear system model to find the dominant oscillation mode. However, with the dominance of converter-based generators in the modern power systems, new stability issues and requirements for the controls are introduced due to the different physical characteristics and interaction with the grid of converter-interfaced components, traditional PSSs may not work well in the renewable-based systems.

To illustrate the contributions of different components to the oscillation, two scenarios: one applied with/without one major wind power plant and one applied with a synchronous condenser are investigated as shown in Fig. 5.3. It can be seen that without a major wind power plant, the post contingency oscillation is highly reduced, while the effect without a synchronous condenser is only a phase delay. It can be envisaged that by having more power converters replacing synchronous machines in the power system, the converters will become the main oscillation source. Due to the complexity of the inertia characteristics of a low inertia system, the mode of oscillation may shift over time, depending on the types of generators online and the design of the converter controls. This requires innovative solutions for oscillation damping controller which adapt to

the modern system characteristics to guarantee a secure operation. In this chapter, a power oscillation damping controller incorporating SCs is proposed for low inertia systems which uses a local frequency and a tie line power measurement to control the reactive power of SCs during disturbances. By controlling the terminal voltage through the reactive power of SCs, the active powers of transmission lines, HVDC links, and loads are influenced to damp the oscillation and enhance significantly the frequency stability in terms of frequency nadir and settling time.

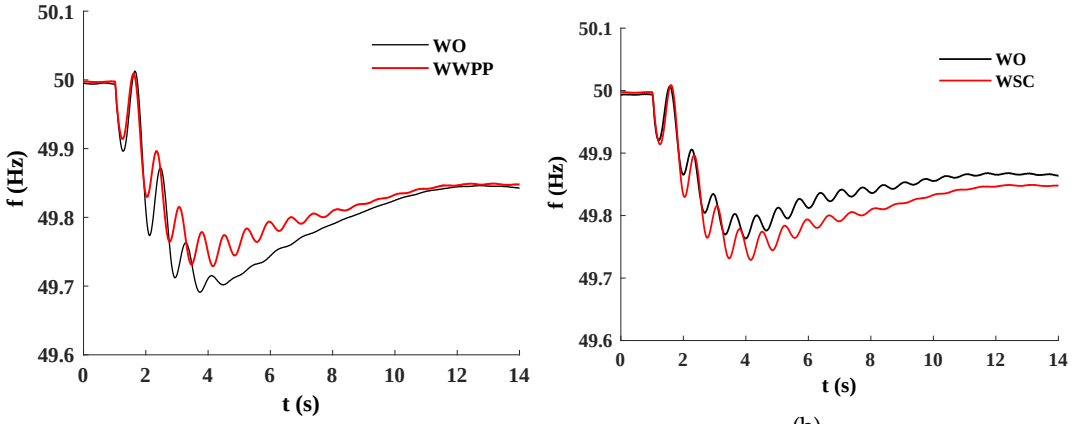

Figure 5.3: Sensitivities of different components of oscillation in the prospective Western Danish power system. (a) Frequency oscillation without (WO) and with a major wind power plant (WWPP). (b) Frequency oscillation without (WO) and with a synchronous condenser (WSC).

5.2 Power oscillation damping control design

In this section, a theoretical background of power oscillation damping control design is presented, which illustrates the control of the active power flow through reactive power modulation of the SC. Then, the POD controller is proposed based on the background to damp the low-frequency oscillation and enhance frequency stability.

5.2.1 Theoretical background

The idea of the control is based on using reactive power to modulate the system voltages, while the change in the voltages will, in turn, affect the active power flow, such as the transmission lines, loads, and HVDC links.

The mathematical formula of the transferred active power on a simplified transmission line as shown in Fig. 5.4, can be expressed as:

$$P = \frac{V_1 V_2}{X} \sin \delta \tag{5.1}$$

where V_1 and V_2 are the line-to-line voltages of the two end sides of the transmission line; δ is the angle of V_1 with respect to V_2; and X is the reactance of the transmission line.

The active power of a load expressed in a voltage and frequency dependent load (V&FDL) model [153–155] is as follows:

$$P_{Load} = P_0(1 + k_{Pf}\Delta f)(p_p + p_c \frac{V}{V_0} + p_z(\frac{V}{V_0})^2) \tag{5.2}$$

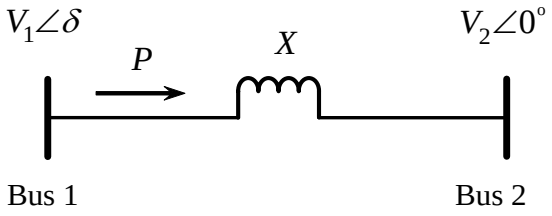

Figure 5.4: Active power transferred on a transmission line.

where P_0 is the rated active power of the load; V_0 and V are the nominal and actual voltage magnitude at the load bus, respectively; f_0 and Δf are the nominal frequency and frequency deviation, respectively; k_{Pf} is the frequency characteristic coefficient; and p_p, p_c, and p_z are the portions of total load proportional to constant active power load, constant current load, and constant impedance load, respectively.

The active power of LCC-HVDC link at the rectifier is expressed as follows:

$$P_{HVDC} = 1.654 V_m I_d \cos\alpha \tag{5.3}$$

where V_m is the peak line-to-line voltage of the AC terminal; I_d is the DC current of the HVDC; and α is the firing angle of the rectifier.

The basic control principle of the LCC-HVDC link is that the rectifier controls the DC current and the α limit, whereas the inverter is responsible for a constant extinction angle control to keep the transferred power tracking to the set point.

According to (5.1)-(5.3), the active power on the transmission lines, LCC-HVDC links, and loads can be manipulated by the AC terminal voltage through the reactive power channel. This concept will work under low inertia grids, where the voltage can be affected by the SCs instead of the grid.

5.2.2 Power oscillation damping controller

To achieve a smooth transition to the renewable energy system, a POD control design incorporating SCs adapting to the modern system characteristics is designed in this paper. By regulating the terminal voltage through the reactive power modulation, the POD controls the active power transferred on the transmission lines, HVDC links, and loads to damp the power oscillation and improve the frequency stability.

The lead-lag control structure is still preferred due to a better tradeoff between the static accuracy, system stability and insensibility to disturbances in the frequency domain [156]. Low-frequency oscillation can be efficiently damped by the proper selection of lead-lag block parameters.

The input of the POD controller is always a point of debate. In the literature, many valuable signals are suggested, including the rotor speed deviation, the frequency, the electrical power or the acceleration power [13, 157]. It is worth noting that the frequency behavior represents the active power oscillation or imbalance; therefore, it is selected as an input to damp the power oscillation. Furthermore, due to the locality of the frequency in a low inertia system, it is essential to select a signal from a central path of the oscillation as one of the inputs, where in this case, a measured tie line flow between the Danish and German system is selected. In implementation, this

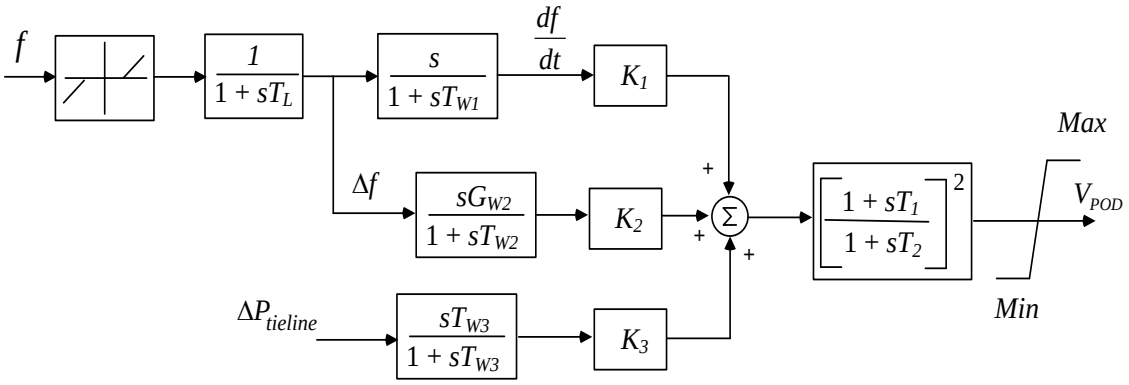

Figure 5.5: Proposed POD control diagram.

measurement is best taken by synchrophasor measurement units to maintain time synchronization with the local measurements.

The control diagram of the proposed POD controller is shown in Fig. 5.5. The local frequency measurement and the active power on a tie line are selected as the input signals of POD to create an output which is added to the AVR of the SC. This output regulates the excitation field current to control the terminal voltage, which therefore changes the active power on the tie line, HVDC links and voltage-dependent loads to enhance the power oscillation and frequency deviation during disturbances. With the frequency input, a deadband is applied to eliminate small frequency changes that may result in an unexpected contribution of POD during steady state conditions. A following low-pass filter ($\frac{1}{1+sT_L}$) filters the measurement noise that can make the control function poor. There are 2 control signals created by the frequency measurement. The first one, with a small time constant (T_{W1}), works similar to a differentiation to capture the frequency derivation during frequency excursions. The second, with a larger time constant (T_{W2}), catches the frequency deviation to generate a signal with a longer response time. The second input (active power on a tie line) first moves through a washout, which allows the desired frequency oscillation mode (inter-area oscillation around 0.1 Hz to 1.5 Hz) to pass and optimizes the compensation at low-frequency range (normally less than 0.5 Hz). Washout time constants (T_{W2} and T_{W3}) are typically adjusted in the range of 2 s - 15 s [158].

A limiter is a crucial part of each controller that hedges the control participation in conditions of uncertainty. This limiter is more critical when the SC connected to the same bus with voltage-sensitive components, such as PV sources or wind power plants which have strict fault ride-through requirements and voltage-based protection settings. These limitation values may change from site to site depending on grid codes.

The magnitude and phase shift of the output are adjusted through control gains (K_1, K_2, and K_3) and the lead/lag time constants (T_1 and T_2) to compensate the system oscillation. They are optimized by the objective function of genetic algorithms. The GA objective is to maximize the damping ratio of the dominant oscillation mode of the system frequency measurement.

5.3 POD parameter optimization through software-in-the-loop simulation

Traditionally, to design the PSS or POD control parameters in traditional systems, a linear system model is computed to find the eigenvalues of the system, therefore the dominant oscillation mode

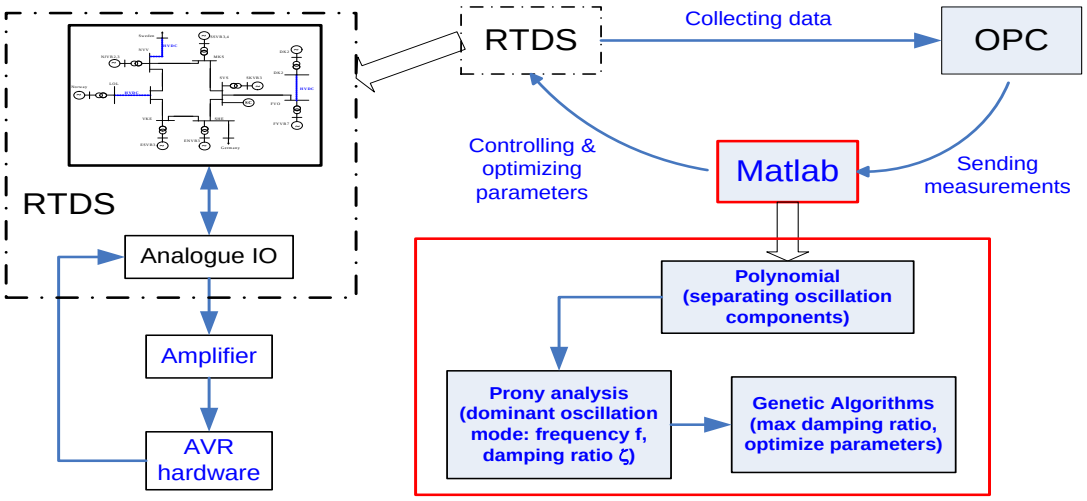

Figure 5.6: System arrangement of HiL and SiL simulations.

is determined. The control parameters are designed based on that dominant mode by increasing its real part, hence moving the mode to the left side of the complex plane [159–161].

However, in the converter-interfaced systems which are complex and consist of thousands of variables. It is extremely hard to achieve their linear models. As a result, the state-space model may not suit well to these systems. To overcome the issue, Prony technique has been extensively applied based on the measurement data to directly extract the eigenvalues, oscillation frequency, and damping ratio, etc. [81, 82]. A nonlinear optimization called GA that is completely independent of the complexity of systems [83, 84, 86] may suit well for parameter optimization of controllers in the modern power systems. With the GA optimization, the issue of parameterization is transformed into a simple optimization problem by setting specific objectives. In this study, a parameter optimization for POD using SiL simulation in real time based on a closed-loop interface among RTDS, Matlab, and OPC is proposed and implemented as shown in Fig. 5.6. The POD optimal parameter set is determined by the GA objective function that maximizes the damping ratio of the dominant oscillation mode.

5.3.1 System setup

The prospective future Western Danish power system run in the RTDS platform is driven by a MATLAB script for system startup and disturbance simulations. The data of the system are collected by an OPC server and sent directly to the MATLAB workspace. In MATLAB, the signal is first processed to remove the fundamental frequency component. The oscillation component is then analyzed by the Prony technique for extracting the frequency and damping ratio of the dominant oscillation mode. The damping ratio is maximized by a GA objective function to determine the better parameters of the POD. After that, these parameters are updated on the RTDS model for further verification. These steps are iterative by a closed-loop and run in real time with the RTDS, OPC, and MATLAB communications as shown in Fig. 5.6. The loop will continue until the objective function satisfies the damping ratio maximization of the dominant mode constraint to determine the optimal values of POD parameters. The entire setup among RTDS, Matlab, and OPC is similar to that of the AVR parameter optimization mentioned in chapter 4.

5.3.2 Prony analysis

A Prony analysis is a least-square approximation technique of fitting a linear sum of exponential terms to a measured signal. A brief overview of this technique is given in [162]. The important feature of this technique is that it directly determines the frequency, damping ratio, energy, and relative phase of the modal components present in a given measurement signal by an extended Fourier analysis [163]. The ability to extract such information from transient signal simulations would overcome the computing burden of the linear model for large-scale systems, which consists of thousands of variables.

Consider a generally continuous signal $\hat{y}(n)$ that is to be modeled by

$$\hat{y}(n) = \sum_{i=1}^{p} (b_i z_i^n) = \sum_{i=1}^{p} A_i e^{j\theta_i} e^{(\alpha_i + j2\pi f_i)n\Delta t} \tag{5.4}$$

with

$$\begin{cases} b_i = A_i e^{j\theta_i} \\ z_i = e^{(\alpha_i + j2\pi f_i)n\Delta t} \end{cases}$$

where $n = 0, 1, 2, ..., N-1$, N is the sampling number; Δt is the time interval of sampling; p is the order of the Prony mode; A_i and θ_i are the amplitude and inception phase angle of the ith oscillation mode, respectively; and f_i and α_i are the frequency and damping ratio of the ith oscillation mode, respectively.

Overall, the Prony analysis can be summarized into three steps:

1. Constructing a linear prediction model from the measured data and solving it.

2. Computing the discrete-time poles of the characteristic polynomial equation generated by the linear model which in turn results in the eigenvalues.

3. From these eigenvalues, the damping ratios and oscillation frequencies and related parameters can be extracted.

A polynomial fitting is implemented to find the fundamental frequency component. This step separates the oscillatory component for Prony analysis conduction. The Prony analysis obtains many oscillation modes which include the dominant mode and disturbance modes. This results from the mixing noise and trend in the measurement which cannot be eliminated completely in the signal processing step.

The dominant mode is recognized by the energy analysis approach, which evaluates the contribution of each oscillation mode and is expressed as follows:

$$E_i = \sum_{n=0}^{N-1} (R_i z_i^n)^2 \tag{5.5}$$

where E_i, R_i, and z_i are the energy, the amplitude, and the pole of the ith oscillation mode, respectively; $i = 1, 2, ..., p$.

The entire oscillation energy is defined as follows:

$$E_{tot} = \sum_{n=0}^{N-1} [\hat{y}(n)]^2 \tag{5.6}$$

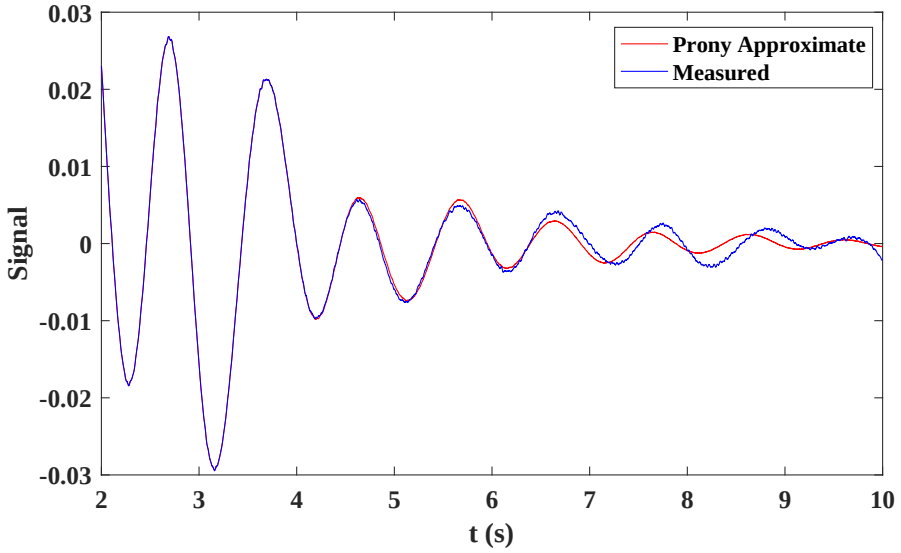

Figure 5.7: The comparison of Prony analysis and the measured signal.

Then the contribution of the i-th oscillation mode can be expressed as

$$\eta_i = \frac{E_i}{E_{tot}} \tag{5.7}$$

The dominant mode is determined by the largest energy contribution to the oscillation. A comparison of Prony approximate and measurement is shown in Fig. 5.7 which presents how accurately the Prony analysis works in this study.

5.3.3 Genetic algorithm

GA is used as the optimization algorithm for the parameterization of the POD which is described in detail in chapter 4. The objective function is to maximize the damping ratio of the dominant oscillation mode as follows:

$$f(x) = max\left\{\xi = -\frac{\alpha}{\sqrt{\alpha^2+\beta^2}}\right\} \tag{5.8}$$

subject to

$$T_{imin} \leq T_i \leq T_{imax}\ (i = 1, 2) \tag{5.9}$$

$$K_{jmin} \leq K_j \leq K_{jmax}\ (j = 1, 2, 3) \tag{5.10}$$

where α and β are real and imaginary parts of the dominant mode, respectively which is extracted by Prony analysis. It means that GA determines the variables x (T_1, T_2, K_1, K_2, and K_3) based on boundary settings to maximize the damping ratio ξ of the oscillation mode. The boundary settings of POD parameters are listed in the Appendix. The GA may be terminated after a certain number of generations when the objective value does not enhance after a certain generation. The whole procedure of parameterization for POD base on a SiL is shown in Fig. 5.8.

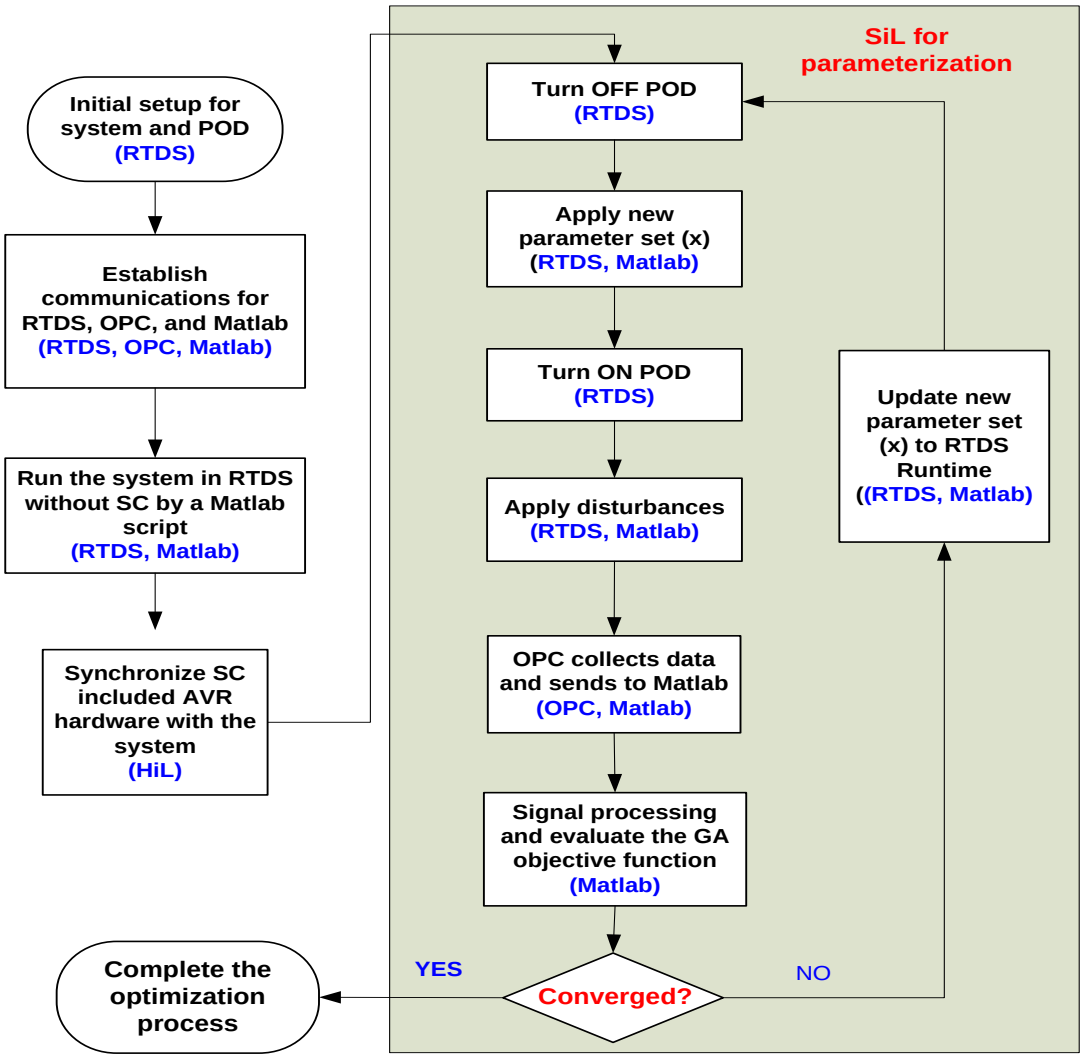

Figure 5.8: The flowchart of parameterization process of POD.

5.4 Case study

To verify the performance of the proposed method on the damping and frequency stability, a load increase disturbance and a three-phase short-circuit fault are investigated in this section. To determine how the PSS performs in low inertia systems, a comparison of system responses with PSS, with GA-based POD and without either is investigated in the first scenario. It is worth noting that the modeled future Danish power system is a typical low inertia system due to a high installation of RE, HVDC links, and a weaker German grid.

The single-line diagram of 400 kV DK1 renewable-based system in 2020 is shown in Fig. 4.21. All synchronous generators are phased out to give way to WPPs and importing HVDC interconnection. There are six synchronous condensers installed in the system, while the SCs at FGD and KAS (SC3 and SC4) are equipped with the proposed POD controller.

5.4.1 Load increase disturbance

A comparison of the system responses with PSS (PSS), with GA-based POD (GA-POD), and without either (WO) during a load increase disturbance is intuitively shown in this scenario. Fig. **??** shows

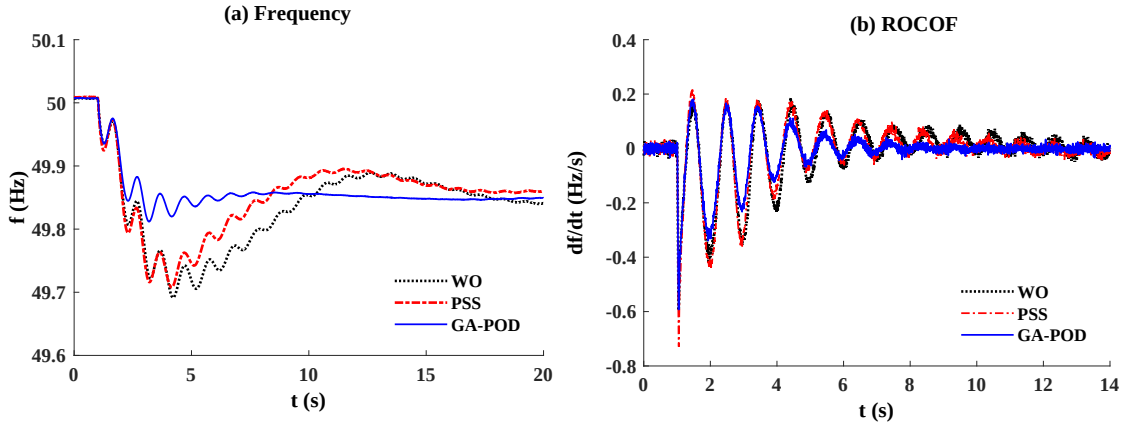

Figure 5.9: Load increase scenario: (a) System frequency. (b) ROCOF.

the comparative results of the system frequency, ROCOF, active power on transmission line KAS to LAG, LCC-HVDC, VSC-HVDC links, load, and the SC responses. The responses are without in the dotted black lines, with the PSS in the dash and dotted red lines, and with the GA-based POD in the solid blue lines, respectively. From the comparative results, it can clearly be seen that with the POD controller, the system response is significantly enhanced in terms of the damping

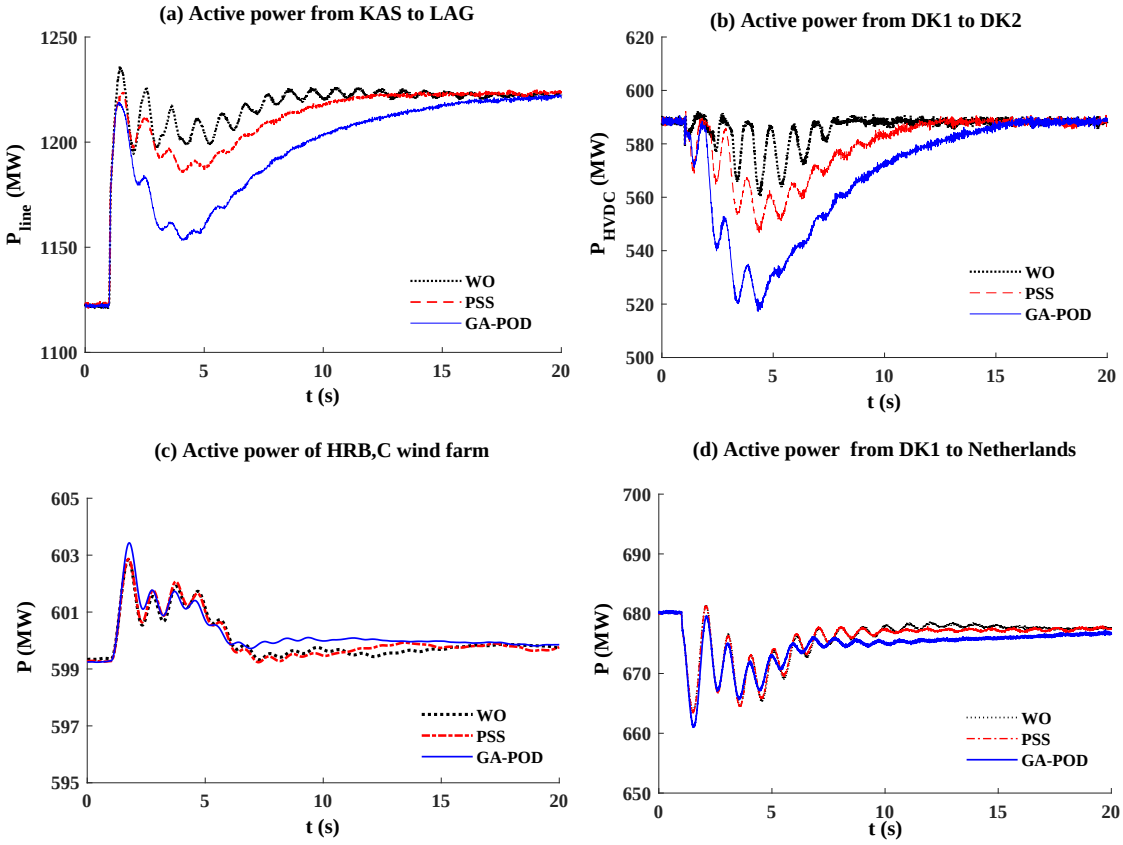

Figure 5.10: Load increase scenario: (a) Active power from KAS to LAG. (d) Active power of LCC-HVDC link from DK1 to DK2. (c) Active power of HRB,C wind farm. (d) Active power of VSC-HVDC from DK1 to Netherlands.

Table 5.1: Without, with PSS, and with GA-based POD comparison of dominant mode.

Cases	Domi. mode	Freq. (Hz)	Damp. ratio	Freq. nadir (Hz)	Set. time (s)
WO	-0.525 $\pm$ j6.585	1.048	0.079	49.7	$\sim$ 17
WPSS	-0.635 $\pm$ j6.870	1.093	0.092	49.71	$\sim$ 16
WPOD	-1.933 $\pm$ j6.379	1.015	0.29	49.82	$\sim$ 8

ratio and frequency stability. By comparing the system frequency in Fig. **??**(a), without the POD it experiences a large and long oscillation (the dominant mode has a 0.079 damping ratio) as well as a significant frequency deviation (0.3 Hz) before obtaining a new equilibrium. In contrast, with the GA-based POD these parameters are remarkably improved by a damping ratio of 0.29 and a frequency deviation of 0.18 Hz. The frequency rapidly reaches the steady-state condition. Taking a look at the ROCOF, faster damping and quicker settling down are obviously seen in Fig. **??**(b) with the POD controller.

A comparison of the system responses with PSS (PSS), with GA-based POD (GA-POD), and without either (WO) during a load increase disturbance is intuitively shown in this scenario. The comparative results of system frequency, ROCOF, active power on transmission line KAS to LAG, wind farm, and HVDC links are shown in Figs. 5.9 and 5.10, while SC responses and the active powers of loads are presented in Fig. 5.11 and Fig. 5.12, respectively. From the comparative results, it can clearly be seen that with the POD controller, the system response is significantly enhanced in terms of the damping ratio, settling time, and frequency nadir. By comparing the system frequency in Fig. 5.9(a), without the POD it experiences a large and long oscillation (the dominant mode has a 0.079 damping ratio) as well as a significant frequency deviation (0.3 Hz) before obtaining a new equilibrium. In contrast, with the GA-based POD these parameters are remarkably improved by a damping ratio of 0.29 and a frequency deviation of 0.18 Hz. The frequency rapidly reaches the steady-state condition. Taking a look at the ROCOF, faster damping and quicker settling down are obviously seen in Fig. 5.9(b) with the POD controller.

The active powers on the transmission line from KAS to LAG, HVDC links, and load are controlled during the disturbance to reduce the power imbalance and damp the oscillation. As a result, the system frequency with the GA-based POD is improved in terms of the oscillation damping, frequency nadir, and settling time, as shown in Figs. 5.9, 5.10, 5.11, 5.12.

An opposite trend is observed from the reactive power response of the SC during the disturbance without and with the POD controller. Instead of rapidly increasing the reactive power from 31 Mvar to approximately 83 Mvar to keep the voltage constant at the nominal value as in the WO case, the POD decreases the terminal voltage by absorbing approximately 58 Mvar reactive power (from 31 Mvar to approximately -27 Mvar) to control the power flow. Consequently, a large decrease and less oscillation are seen from the active powers on the transmission lines, HVDC links, and load with the POD controller as shown in Figs. 5.10, 5.11, 5.12.

As expected, the active power of the SC rapidly releases kinetic energy for the inertial response and quickly settles down, while the rotor speed significantly improves both the deviation and the damping with the POD controller, as seen in Fig. 5.11(a) and (c). As a result, the power oscillation and frequency stability are improved during the disturbance with the POD controller. The comparison of the dominant mode information with and without the POD is listed in Table 5.1,

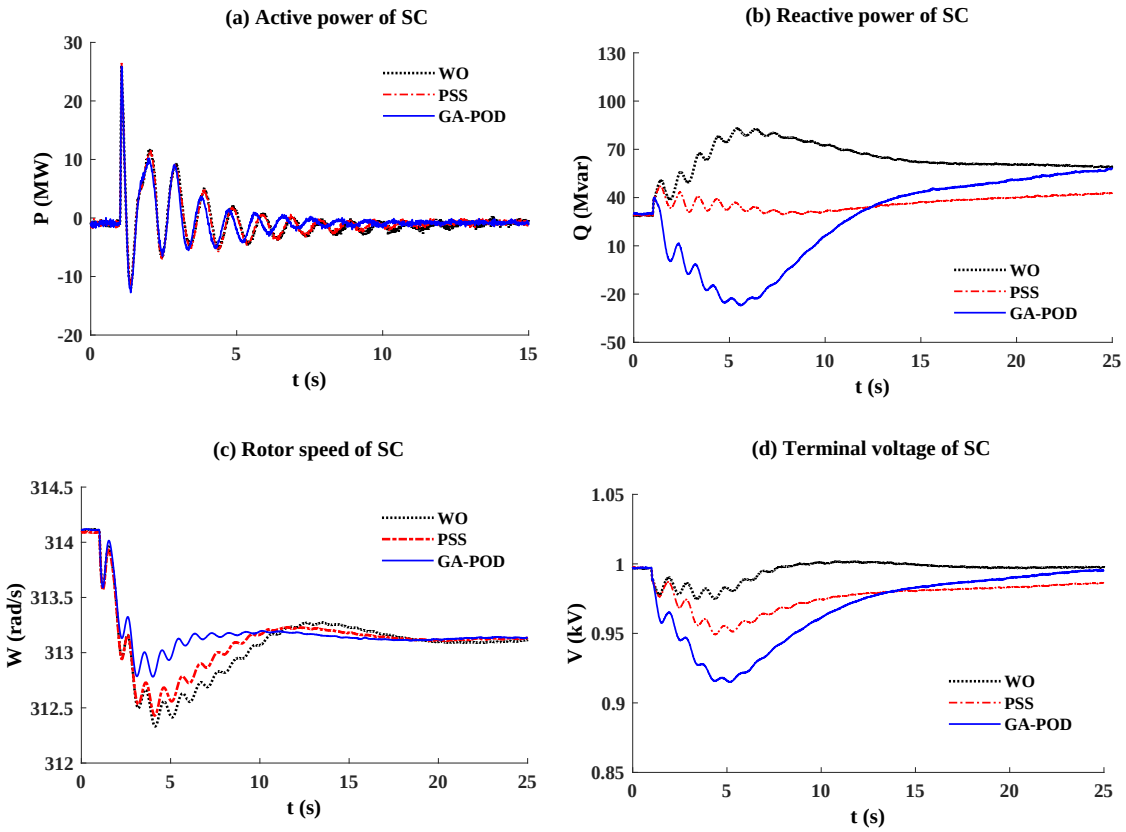

Figure 5.11: Load increase scenario: (a) Active power of SC. (b) Reactive power of SC. (c) Rotor speed of SC. (d) Terminal voltage of SC.

which shows a significant enhancement in terms of the frequency stability and power damping with the POD controller. The settling time and frequency nadir are improved significantly from 17 s and 49.7 Hz to 8 s and 49.82 Hz without and with GA-based POD, respectively.

To clarify the active power decrease of the LCC-HVDC link, the rectifier is set to maintain the DC current at its setpoint by controlling the firing angle. When the busbar voltage decreases, the DC current is less than its order, and the rectifier tends to reduce the firing angle, hence increasing the DC current. However, the firing angle reduction hits the minimum firing angle limit (typical 5^o). This results in the DC current decreasing, thereby reducing the HVDC active power during the disturbance.

By comparison, the PSS does not handle well in the converter-based system, while the GA-based POD can further improve the frequency stability and damping ratio by absorbing more reactive power to allow for a lower voltage but still satisfy the grid code.

5.4.2 Three-phase short-circuit fault

To verify the performance of the proposed controller, a three-phase short-circuit fault with 0.1 s duration and a load trip occurring afterwards are investigated. At t = 1 s, a three-phase short-circuit fault is applied on one of the feeders of the TRI bus and cleared at t = 1.1 s, and then the circuit breaker of the feeder suddenly disconnects the load (250 MW). Figs. **??** and **??** show the system responses without and with the proposed controller. A similar pattern is plotted in this scenario.

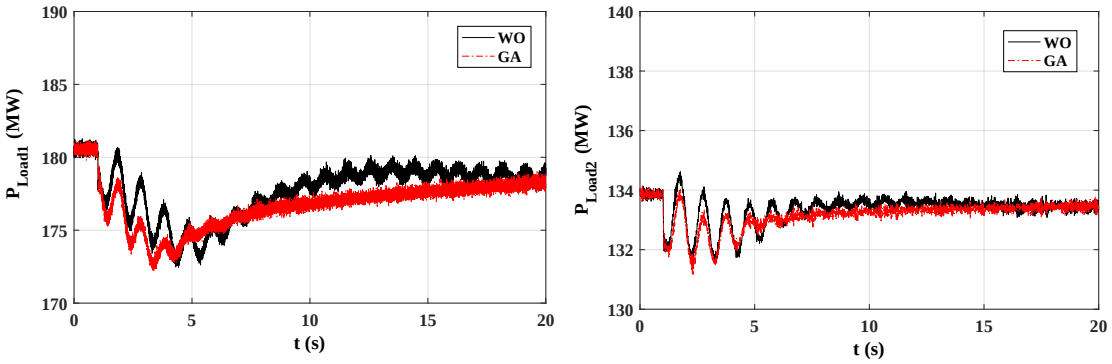

Figure 5.12: Load increase scenario: Active powers of load at KAS and FER buses.

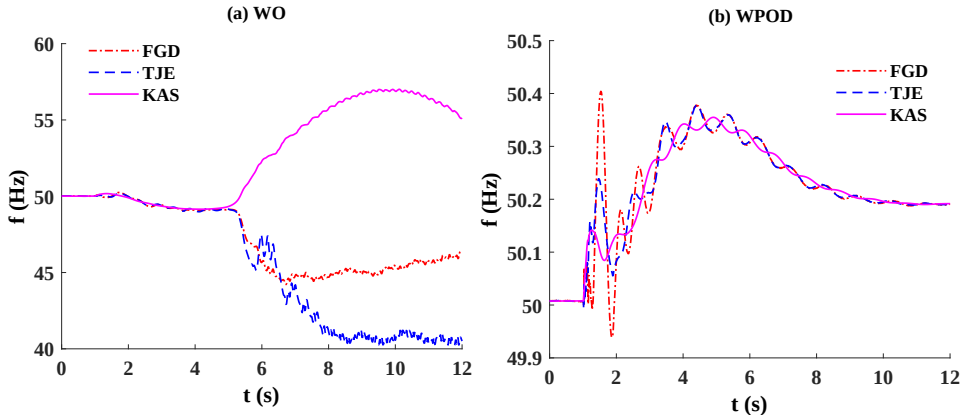

Figure 5.13: Frequency responses at different substations during a three-phase short-circuit fault: (a) WO. (b) WPOD.

While the uncontrolled system exhibits a severe oscillation and system collapse after around 4 s, the system with the POD controller performs a better damping and becomes stable after the fault.

As shown in Fig. 5.13, for this scenario without the POD (WO), after the fault the frequencies at different substations tend to oscillate against each other, which leads to a system collapse, while they quickly become stable with the GA-based POD (GA). Because of the asynchronism issue, the active power could not transfer from Germany to the DK2 system through the transmission line KAS to LAG, HVDC link, and load as shown in Figs. 5.14 and 5.15.

By comparing the reactive power, instead of decreasing the reactive power to prevent the voltage surge, the POD allows terminal voltage increase within the limit range. Therefore, the transmission line, HVDC link, and load can absorb more active power to offset the power imbalance during the load trip, as can be intuitively seen in Fig. 5.14 and Fig. 5.15. This phenomenon helps the system maintaining stability after the fault.

In this scenario, the active power of the HVDC link does not significantly contribute to the power oscillation control during the disturbance with the GA-based POD. It can be explained that the busbar voltage increases, making the DC current higher than the current set-point. With the ability of firing angle control to transiently reach 90^o in order to quickly reduce the DC current, the active power can be kept constant during the voltage increase. In contrast, the load tends to absorb more active power to counteract the power imbalance and damp the oscillation, as seen in Fig. 5.14(c).

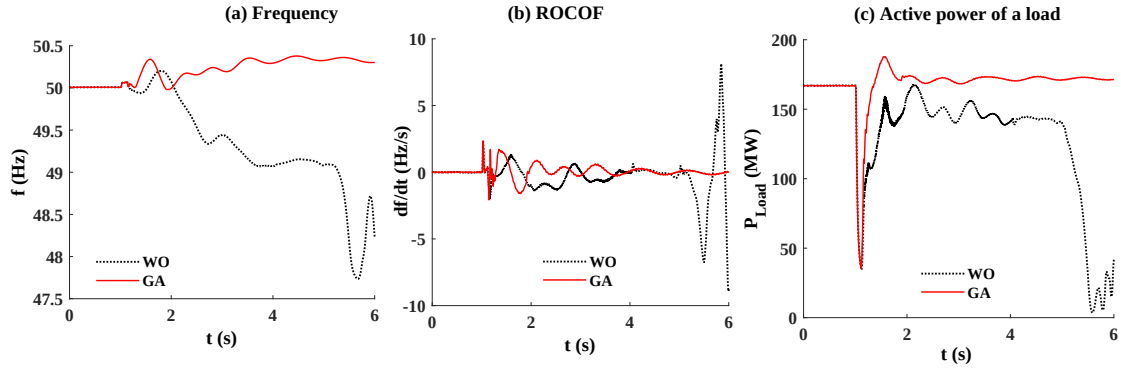

Figure 5.14: Three-phase short-circuit fault scenario: (a) System frequency. (b) ROCOF. (c) Active power of FER load.

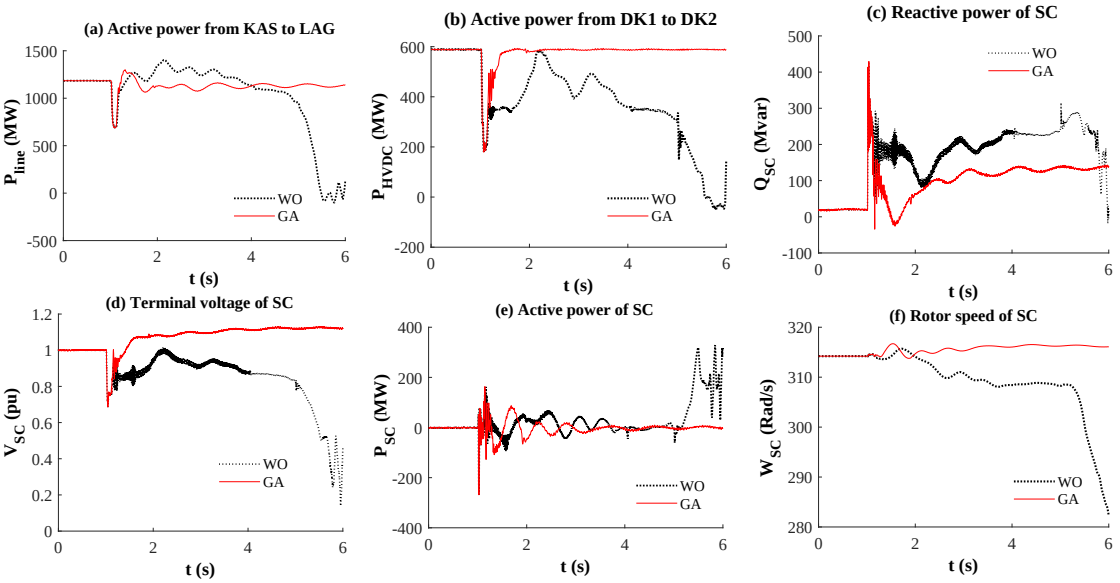

Figure 5.15: Three-phase short-circuit fault scenario: (a) Active power from KAS to LAG. (b) Active power from DK1 to DK2 through HVDC connection. (c) Reactive power of SC. (d) Terminal voltage of SC. (e) Active power of SC. (f) Rotor speed of SC.

5.5 Conclusion

In order to address the oscillatory stability issue for converter-based systems that introduce new stability issues and requirements for the controls, a POD controller incorporating SCs is proposed. The POD controls the terminal voltage through the reactive power regulation to damp the power oscillations for low inertia systems. A Prony technique is applied to extract the system oscillation characteristics from the data measurement, which benefits large-scale systems with thousands of variables. A parameter optimization for the POD based on a GA objective which maximizes the damping ratio of the dominant mode is implemented by SiL simulation. Comparative results show that by controlling the terminal voltage, the oscillation damping and frequency stability can be significantly improved with the POD controller. In addition, the parameter optimization algorithm can help control designers, thereby saving time while still offering near-optimal or optimal solutions for the control parameter set compared to the empirical tuning method.

To properly apply the POD controller to a specific grid, some important conclusions should be drawn as follows:

1. Controlling the terminal voltage of the SC to change the active power should take the limitation of the transmission lines, HVDC links, and loads into consideration to set the limit values for the POD output.

2. The limits of the terminal voltage of the connected busbar may impact the components connected to the same bus of the SC (PV system, wind generator) which are sensitive to the low-voltage ride-through threshold, voltage-based protection, etc.

3. The active power of the transmission line selected as the control input should represent the power oscillation where the dominant power exchange takes place.

CHAPTER 6

Conclusion and future work

6.1 Conclusion

The dominance of converter-based generation in modern power systems causes system inertia significantly reduced, which may create more challenges for system frequency stability and control. Additionally, new stability issues and requirements for the controls are introduced due to the different physical characteristics and interaction with the grid of converter-interfaced components. Consequently, faster frequency dynamics with a higher rate of change of frequency and a larger frequency deviation during disturbances resulted as its certain consequences. Furthermore, the system inertia constant becomes time-variant due to the variability of power dispatch and demand scenarios. A poor frequency response may cause oscillatory issues in frequency responses during disturbances, which worsens the system situation.

This thesis has investigated frequency characteristics and control of converter-based systems, which are low inertia systems due to the inherent inertia characteristics of converter-based generation. The impact of high renewable-energy penetration on frequency characteristics has been analyzed, and different approaches have been proposed for frequency stability improvement, damping of the oscillatory issues, and parameter optimization.

6.1.1 Frequency stability enhancement

The study clarifies the benefit of SCs and SI on frequency stability enhancement. Due to their rotating machine nature, SCs can naturally provide inertial response during frequency excursions. As a result, SCs can enhance frequency stability in terms of the ROCOF and help a system become more synchronized during disturbances. Despite decoupling to the system by power electronics converters, with a proper controller implementation, WPPs can participate in frequency control. A control algorithm for WPPs coordinated with an activation scheme that considers the wind turbine minimum allowable speed achieves excellent performance for frequency stability enhancement.

The combination of SCs and SI may pronounce the inertial response and fast frequency control of a synchronous generator during power imbalances. The inertial response from SCs remarkably improves the ROCOF, and afterwards, a frequency control support with a fast time response from the SI of WPPs takes over and significantly enhances the frequency deviation. This work is based on the simulation to show how to tune K_{in} and K_{droop} to adjust the output of WPPs to support frequency stability and compensate the kinetic energy recovery of SCs after its inertial response to help the system quickly settle down. As a result, a combination of SCs and SI of WPPs provides better performance that not only enhances the frequency deviation and ROCOF but also helps the low inertia system become more synchronized during different disturbances.

From these above conclusions, TSOs should consider implementing an SI on existing or planned large-scale wind farms to extract the inertial response of WPPs, and combine with existing

or placement SCs to enhance the frequency stability, short-circuit power support, and voltage regulation to achieve a smooth transition to renewable-based systems. The combination of SCs and SI with properly tuning the gains of the controller can achieve better performance for the frequency stability of low inertia systems. In addition, TSOs may impose requirements on the minimum system inertia and maximum importing power via HVDCs in low inertia operating conditions.

6.1.2 Hardware-in-the-loop test

A HiL test has been implemented for an AVR system to validate and verify the control functions in steady-state and dynamic conditions with different scenarios. Furthermore, different limiters of an excitation system, such as UEL, OEL, SCL, and VHz limiters, have been implemented in hardware. Different tests, such as the startup procedure of the system, voltage setpoint changes, overexcitation, under-excitation, and AVR setpoint loss, were explored to evaluate the AVR hardware response and compare the performance of an SC with the AVR hardware and that of simulation. The comparative results show that the HiL test is an effective approach for testing devices in both healthy and faulty conditions before deployment and is able to parameterize the controller with lower cost, higher efficiency, and more flexibility.

6.1.3 Power oscillation damping

To deal with the oscillatory stability issue for converter-based systems where new stability issues and requirements for the controls are introduced, the ability of SCs for providing a power oscillation damping with a proper control approach named POD has been proposed. The control uses the local frequency measurement and the active power on a tie line to control the reactive power of SC. Consequently, the voltage at the SC-connected busbar is controlled, which in turn manipulates the active power flow on transmission lines, load, and HVDC links to damp power oscillation. The parameter is optimized based on a SiL simulation using Prony analysis from the simulation results and a nonlinear optimization tool that is suitable for large-scale power systems with thousands of state variables.

Application of this controller is simple for existing SCs on the grid to provide the supplementary control service for frequency control and oscillation damping. To properly apply the POD controller to a specific grid, the following important discussion is presented:

1. Controlling the terminal voltage of SC to change the active power should consider the limitation of the transmission lines, HVDC links, and loads to establish the limit values for the POD output.

2. The limits of the terminal voltage of the connected busbar may impact the components connected to the same bus of the SC (PV system, wind generator), which are sensitive to the low-voltage ride-through threshold and voltage-based protection.

3. The line flow selected as the control input should represent the power oscillation where the dominant power exchange occurs.

6.1.4 Parameter optimization via a SiL simulation

A SiL simulation using Matlab and RTDS via OPC for parameterization of the POD and AVR simulation model has been performed. Depending on the optimization purpose to implement the objective based on a nonlinear algorithm, the near-optimal or optimal parameter set is determined. The simulation can be applied to parameter optimization of any controller in power systems, which is more efficient than the empirical tuning approach. This SiL simulation can also solve different issues in power systems, where the RTDS is replaced by the real system, OPC represents the data acquisition system, and Matlab acts as the control center.

6.2 Future work

Some solutions have been proposed to deal with the challenges of converter-based systems in frequency characteristics and control. Further research on frequency stability and control for modern power systems is needed. Future work is suggested as follows:

6.2.1 Synchronous condenser

The implementation of the POD in hardware is necessary. Different tests should be investigated to validate the control in steady-state and dynamic conditions. Additionally, verifying the performance of the POD in low inertia systems under different disturbances for damping power oscillations is necessary.

Comparing SCs with FACTS devices is needed to address the drawbacks of SC by implementing supplementary controls. For instance, the response time of FACTS devices for the reactive power compensation is faster than that of SC. The problem can be solved by improving the response time of the excitation system of SC using static excitation. As a result, SC may take over the tasks of FACTS devices to provide supplementary control for modern power systems.

6.2.2 Frequency control support

The proposed SI controller should be coordinated with a pitch control to optimize the frequency control during over-frequency disturbances. During over-frequency disturbances, the pitch control will adjust the blade angle to reduce the aerodynamic force from wind, therefore decreasing the power output of WPPs. Consequently, the power imbalance reduces, which improves the frequency stability. Additional research is needed on the performance of SI of WPPs combined with energy storage devices to supply both the inertial response and primary control for frequency control during frequency excursions.

Researching the capability of HVDC for providing inertial response and implementing control service to extract frequency control support from HVDC interconnections is necessary for low inertia systems. During power imbalances, HVDC should participate in frequency control by increasing/decreasing the power transferred by changing the power setpoint to reduce the power imbalances. As a result, HVDC interconnections can provide frequency control support for power systems.

Researching and implementing supplementary control for frequency control on the demand side during frequency events is needed. Demand-side control is a method for managing the demand from the consumer's side to support frequency control during disturbances. The technique usually reduces the demand to compensate for power imbalances, such as loss of generation, which is considered in Great Britain [164]. Demand-side control requires consumer participation and data management, which is considered to be a potential solution for frequency control in low inertia systems. However, this approach has not been fully developed, and further research is required.

Monitoring and forecasting system inertia to ensure stable system operation for low inertia systems. Being aware of the system inertia and kinetic energy, TSOs can actively schedule power reserves and understand good insight into the upcoming operation conditions. An online inertia estimation tool through the SCADA system has been implemented in the Nordic power system based on the breaker status of synchronous generators and their apparent power and inertia constant. However,

more research in this area is necessary to propose a complete and accurate approach for low inertia systems.

Researching simulation-based approaches for determining the oscillatory characteristics in low inertia systems, which include many different components and are large-scale systems, is necessary. In the literature, the oscillatory characteristics of power systems are extracted based on small-signal analysis using the linear system model. This method has benefits for studying sensitivity problems and drawing general conclusions. However, the method places limits on the system model, which requires some simplifications, especially simplified control systems. As a result, the method may be inaccurate for some characteristics that have a crucial effect on the system performance during disturbances. Conversely, simulation-based approaches are less limited by the system modeling, which enables quantitative conclusions to be obtained for each particular scenario but hinders the formation of general conclusions. Therefore, more research for determining the oscillation characteristics of simulation-based approaches will help to obtain general and accurate conclusions for this simulation-based approach.

Bibliography

[1] IEA, "Medium term renewable energy market report 2015," Energinet, Tech. Rep., 2015. [Online]. Available: http://www.iea.org/bookshop/708-Medium-Term-Renewable-Energy-Market-Report-2015

[2] Energinet, "Annual report 2015," Energinet, Denmark, Tech. Rep., 2015.

[3] B. Parsons, M. Milligan, B. Zavadil, D. Brooks, K. D. B. Kirby, and J. Caldwell, "Grid impacts of wind power: A summary of recent studies in the United States," *Wind Energy*, vol. 7, no. 2, May 2004.

[4] J. C. Smith, M. R. Milligan, E. A. DeMeo, and B. Parsons, "Utility wind integration and operating impact state of the art," *IEEE Transactions on Power Systems*, vol. 22, no. 3, pp. 900–908, Aug 2007.

[5] B. Heard, B. Brook, T. Wigley, and C. Bradshaw, "Burden of proof: A comprehensive review of the feasibility of 100% renewable-electricity systems," *Renewable and Sustainable Energy Reviews*, vol. 76, pp. 1122 – 1133, 2017. [Online]. Available: http://www.sciencedirect.com/science/article/pii/S1364032117304495

[6] AEMO, "Black system South Australia 28 september 2016," AEMO, Tech. Rep., 2017.

[7] Nordic TSOs, "Challenges and opportunities for the Nordic power system," Energinet, Tech. Rep., 2016.

[8] NERC, "1200 MW fault induced solar photovoltaic resource interruption disturbance," NERC, Tech. Rep., 2017.

[9] ENTSO-E, "Frequency stability evaluation criteria for the synchronous zone of continental europe," ENTSO-E, Tech. Rep., 2016.

[10] The Danish Ministry of Climate and Energy, "Energy strategy 2050 from coal, oil and gas to green energy," Energinet, Copenhagen, Denmark, Tech. Rep., 2011.

[11] Energinet, "System plan 2016," Energinet, Denmark, Tech. Rep., 2016.

[12] SCAPP, "Synchronous condenser application in low inertia systems." [Online]. Available: http://www.scapp.dk/

[13] P. Kundur, *Power System Stability and Control*. New York: McGraw-Hill, 1994.

[14] W. Winter, K. Elkington, G. Bareux, and J. Kostevc, "Pushing the limits: Europe's new grid: Innovative tools to combat transmission bottlenecks and reduced inertia," *IEEE Power and Energy Magazine*, vol. 13, no. 1, pp. 60–74, Jan 2015.

[15] B. Kroposki, B. Johnson, Y. Zhang, V. Gevorgian, P. Denholm, B. M. Hodge, and B. Hannegan, "Achieving a 100% renewable grid: Operating electric power systems with extremely high levels of variable renewable energy," *IEEE Power and Energy Magazine*, vol. 15, no. 2, pp. 61–73, Mar 2017.

[16] M.-S. Debry, G. Denis, T. Prevost, F. Xavier, and A. Menze, "Maximizing the penetration of inverter-based generation on large transmission systems," in *6th Solar Integration Workshop*, 2017, pp. 1–6.

[17] P. Tielens and D. V. Hertem, "The relevance of inertia in power systems," *Renewable and Sustainable Energy Reviews*, vol. 55, no. 2, pp. 999–1009, Mar 2016.

[18] A. Ulbig, T. S. Borsche, and G. Andersson, "Impact of low inertia on power system stability and operation," in *IFAC World Congress 2014*, Dec 2014, pp. 265–275.

[19] F. Milano, F. Dörfler, G. Hug, D. J. Hill, and G. Verbic, "Foundations and challenges of low-inertia systems," in *20th Power Systems Computation Conference (PSCC)*, Dublin, Ireland, Jul 2018, pp. 1–25.

[20] J. A. Oliver, B. J. Ware, and R. C. Carruth, "345 MVA fully water-cooled synchronous condenser for Dumont station Part I. Application considerations," *IEEE Transactions on Power Apparatus and Systems*, vol. PAS-90, no. 6, pp. 2758–2764, Nov 1971.

[21] S. Nakamura, T. Yamada, T. Nomura, M. Iwamoto, Y. Shindo, S. Nose, A. Ishihara, and H. Fujino, "30 MVA superconducting synchronous condenser: Design and it's performance test results," *IEEE Transactions on Magnetics*, vol. 21, no. 2, pp. 783–790, Mar 1985.

[22] S. Kalsi, D. Madura, and M. Ross, "Performance of superconductor dynamic synchronous condenser on an electric grid," in *2005 IEEE/PES Transmission Distribution Conference Exposition: Asia and Pacific*, Dec 2005, pp. 1–5.

[23] Siemens, "The stable way synchronous condenser solutions," Energinet, Tech. Rep., 2014.

[24] H. Abildgaard and N. Qin, "Synchronous Condensers for reliable HVDC operation and bulk power transfer," in *2015 IEEE Power Energy Society General Meeting*, Denver, CO, Jul 2015, pp. 1–9.

[25] T. V. Cutsem and R. Mailhot, "Validation of a fast voltage stability analysis method on the hydro-quebec system," *IEEE Transactions on Power Systems*, vol. 12, no. 1, pp. 282–292, Feb 1997.

[26] I. Kamwa, J. Beland, G. Trudel, R. Grondin, C. Lafond, and D. McNabb, "Wide-area monitoring and control at hydro-quebec: past, present and future," in *2006 IEEE Power Engineering Society General Meeting*, Montreal, Que., Canada, Jun 2006, pp. 1–12.

[27] P. E. Marken, J. P. Skliutas, P. Y. Sung, K. S. Kim, H. M. Kim, L. H. Sailer, and R. R. Young, "New synchronous condensers for jeju island," in *2012 IEEE Power and Energy Society General Meeting*, San Diego, CA, USA, July 2012, pp. 1–6.

[28] J. woo Park, Y. ho Park, and S. il Moon, "Instantaneous wind power penetration in jeju island," in *2008 IEEE Power and Energy Society General Meeting - Conversion and Delivery of Electrical Energy in the 21st Century*, Pittsburgh, PA, USA, Jul 2008, pp. 1–7.

[29] P. E. Marken, M. Henderson, D. LaForest, J. Skliutas, J. Roedel, and T. Campbell, "Selection of synchronous condenser technology for the granite substation," in *IEEE PES T&D 2010*, New Orleans, LA, USA, April 2010, pp. 1–6.

[30] J. Skliutas, D. LaForest, R. D'Aquila, D. Derr, and E. Kronbeck, "Next-generation synchronous condenser installation at the VELCO granite substation," in *2009 IEEE Power Energy Society General Meeting*, Calgary, AB, Canada, Jul 2009, pp. 1–8.

[31] J. P. Skliutas, R. D. Aquila, J. M. Fogarty, R. Konopinski, P. Marken, C. Schartner, and G. Zhi, "Planning the future grid with synchronous condensers," in *CIGRE US National Committee 2013 Grid of the Future Symposium*, 2013.

[32] M. Nedd, C. Booth, and K. Bell, "Potential solutions to the challenges of low inertia power systems with a case study concerning synchronous condensers," in *2017 52nd International Universities Power Engineering Conference (UPEC)*, Heraklion, Greece, Aug 2017, pp. 1–6.

[33] H. Zhang, J. P. Hasler, N. Johansson, L. Angquist, and H. P. Nee, "Frequency response improvement with synchronous condenser and power electronics converters," in *2017 IEEE 3rd International Future Energy Electronics Conference and ECCE Asia (IFEEC 2017 - ECCE Asia)*, Kaohsiung, Taiwan, Jun 2017, pp. 1002–1007.

[34] N. A. Masood, R. Yan, T. K. Saha, and N. Modi, "Frequency response and its enhancement using synchronous condensers in presence of high wind penetration," in *2015 IEEE Power Energy Society General Meeting*, Denver, CO, USA, July 2015, pp. 1–5.

[35] F. Diaz-Gonzalez, M. Hau, A. Sumper, and O. Gomis-Bellmunt, "Participation of wind power plants in system frequency control: Review of grid code requirements and control methods," *Renew. Sustain. Energy Rev.*, vol. 34, pp. 551–564, Jun 2014.

[36] ENTSO-E, "Network code for requirements for grid connection applicable to all generators," ENTSO-E, Brussels, Belgium, Tech. Rep., Mar 2013.

[37] M. Kayikci and J. V. Milanovic, "Dynamic contribution of DFIG-based wind plants to system frequency disturbances," *IEEE Transactions on Power Systems*, vol. 24, no. 2, pp. 859–867, May 2009.

[38] J. Hu, L. Sun, X. Yuan, S. Wang, and Y. Chi, "Modeling of type 3 wind turbines with df/dt inertia control for system frequency response study," *IEEE Transactions on Power Systems*, vol. 32, no. 4, pp. 2799–2809, July 2017.

[39] J. V. D. Vyver, J. D. M. D. Kooning, B. Meersman, L. Vandevelde, and T. L. Vandoorn, "Droop control as an alternative inertial response strategy for the synthetic inertia on wind turbines," *IEEE Transactions on Power Systems*, vol. 31, no. 2, pp. 1129–1138, Mar 2016.

[40] M. Wang-Hansen, R. Josefsson, and H. Mehmedovic, "Frequency controlling wind power modeling of control strategies," *IEEE Transactions on Sustainable Energy*, vol. 4, no. 4, pp. 954–959, Oct 2013.

[41] J. M. Mauricio, A. Marano, A. Gomez-Exposito, and J. L. M. Ramos, "Frequency regulation contribution through variable-speed wind energy conversion systems," *IEEE Transactions on Power Systems*, vol. 24, no. 1, pp. 173–180, Feb 2009.

[42] K. Das, M. Altin, H. A. Daniela, P. E. Sørensen, D. Flynn, and H. Abildgaard, "Wind power support during overfrequency emergency events," *CIGRE Science & Engineering*, vol. 9, pp. 73–83, 2018.

[43] Z. S. Zhang, Y. Z. Sun, J. Lin, and G. J. Li, "Coordinated frequency regulation by doubly fed induction generator-based wind power plants," *IET Renewable Power Generation*, vol. 6, no. 1, pp. 38–47, Jan 2012.

[44] L. R. Chang-Chien and Y. C. Yin, "Strategies for operating wind power in a similar manner of conventional power plant," *IEEE Transactions on Energy Conversion*, vol. 24, no. 4, pp. 926–934, Dec 2009.

[45] Z. Zhang, Y. Wang, H. Li, and X. Su, "Comparison of inertia control methods for DFIG-based wind turbines," in *2013 IEEE ECCE Asia Downunder*, Melbourne, VIC, Australia, June 2013, pp. 960–964.

[46] L. R. Chang-Chien, W. T. Lin, and Y. C. Yin, "Enhancing frequency response control by DFIGs in the high wind penetrated power systems," *IEEE Transactions on Power Systems*, vol. 26, no. 2, pp. 710–718, May 2011.

[47] M. Kang, K. Kim, E. Muljadi, J. W. Park, and Y. C. Kang, "Frequency control support of a doubly-fed induction generator based on the torque limit," *IEEE Transactions on Power Systems*, vol. 31, no. 6, pp. 4575–4583, Nov 2016.

[48] M. F. M. Arani and E. F. El-Saadany, "Implementing virtual inertia in DFIG-based wind power generation," *IEEE Transactions on Power Systems*, vol. 28, no. 2, pp. 1373–1384, May 2013.

[49] J. Lee, E. Muljadi, P. E. Sørensen, and Y. C. Kang, "Releasable kinetic energy-based inertial control of a DFIG wind power plant," *IEEE Transactions on Sustainable Energy*, vol. 7, no. 1, pp. 279–288, Jan 2016.

[50] H. Lee, M. Hwang, E. Muljadi, P. E. Sørensen, and Y. Kang, "Power-smoothing scheme of a DFIG using the adaptive gain depending on the rotor speed and frequency deviation," *Energies*, vol. 10, no. 4, 2017.

[51] N. W. Miller, K. Clark, M. E. Cardinal, and R. W. Delmerico, "GE wind plant dynamic performance for grid and wind events," in *2009 AEE TECHWINDGRID*, Madrid, Apr. 2009.

[52] G. C. Tarnowski, "Coordinated frequency control of wind turbines in power systems with high wind power penetration," Ph.D. dissertation, Dept. Elec. Eng., Tech. Univ. Denmark, 2011.

[53] F. M. Gonzalez-Longatt, "Activation schemes of synthetic inertia controller on full converter wind turbine (type 4)," in *2015 IEEE Power Energy Society General Meeting*, Denver, CO, USA, July 2015, pp. 1–5.

[54] O. Craciun, A. Florescu, S. Bacha, I. Munteanu, and A. I. Bratcu, "Hardware-in-the-loop testing of PV control systems using RT-Lab simulator," in *14th International Power Electronics and Motion Control Conference EPE-PEMC 2010*, Ohrid, Macedonia, Sept 2010, pp. 1–6.

[55] K. Song, W. Liu, and G. Luo, "Permanent magnet synchronous motor field oriented control and HIL simulation," in *2008 IEEE Vehicle Power and Propulsion Conference*, Harbin, China, Sept 2008, pp. 1–6.

[56] M. S. Almas and L. Vanfretti, "RT-HIL testing of an excitation control system for oscillation damping using external stabilizing signals," in *2015 IEEE Power Energy Society General Meeting*, Denver, CO, USA, July 2015, pp. 1–5.

[57] Y. Dong, L. Pan, D. Qiu, J. Tian, W. Wang, and W. Li, "Hardware-in-the-loop simulation and test of a control and protection system for MMC-based UPFC," in *2016 IEEE Power and Energy Society General Meeting (PESGM)*, Boston, MA, USA, July 2016, pp. 1–5.

[58] M. Rakhshan, N. Vafamand, M. H. Khooban, and F. Blaabjerg, "Maximum power point tracking control of photovoltaic systems: A polynomial fuzzy model-based approach," *IEEE Journal of Emerging and Selected Topics in Power Electronics*, vol. 6, no. 1, pp. 292–299, Mar 2018.

[59] L. Meng, S. Yang, L. Wang, Y. Liu, and F. Peng, "Hardware-in-loop test for automatic voltage regulator based on identification model," in *2012 15th International Power Electronics and Motion Control Conference (EPE/PEMC)*, Novi Sad, Serbia, Sept 2012, pp. 1–6.

[60] F. Alvarez-Gonzalez, A. Griffo, B. Sen, and J. Wang, "Real-time hardware-in-the-loop simulation of permanent-magnet synchronous motor drives under stator faults," *IEEE Transactions on Industrial Electronics*, vol. 64, no. 9, pp. 6960–6969, Sept 2017.

[61] X. H. Mai, S. K. Kwak, J. H. Jung, and K. A. Kim, "Comprehensive electric-thermal photovoltaic modeling for power-hardware-in-the-loop simulation (PHILS) applications," *IEEE Transactions on Industrial Electronics*, vol. 64, no. 8, pp. 6255–6264, Aug 2017.

[62] M. Steurer, C. S. Edrington, M. Sloderbeck, W. Ren, and J. Langston, "A megawatt-scale power hardware-in-the-loop simulation setup for motor drives," *IEEE Transactions on Industrial Electronics*, vol. 57, no. 4, pp. 1254–1260, April 2010.

[63] R. Brandl, M. Calin, and T. Degner, "Power hardware-in-the-loop setup for power system stability analyses," *CIRED - Open Access Proceedings Journal*, vol. 2017, no. 1, pp. 387–390, 2017.

[64] Y. J. Kim and J. Wang, "Power hardware-in-the-loop simulation study on frequency regulation through direct load control of thermal and electrical energy storage resources," *IEEE Transactions on Smart Grid*, vol. 9, no. 4, pp. 2786–2796, July 2018.

[65] G. Gurrala and I. Sen, "Power system stabilizers design for interconnected power systems," *IEEE Transactions on Power Systems*, vol. 25, no. 2, pp. 1042–1051, May 2010.

[66] A. I. Konara and U. D. Annakkage, "Robust power system stabilizer design using eigenstructure assignment," *IEEE Transactions on Power Systems*, vol. 31, no. 3, pp. 1845–1853, May 2016.

[67] U. K. Verma, S. Banerjee, and A. P. Singh, "An approach towards effective power oscillation damping with deployment and tuning of AVR, and PSS," in *2017 International Conference on Innovations in Electrical, Electronics, Instrumentation and Media Technology (ICEEIMT)*, Coimbatore, India, Feb 2017, pp. 265–275.

[68] U. P. Mhaskar and A. M. Kulkarni, "Power oscillation damping using FACTS devices: modal controllability, observability in local signals, and location of transfer function zeros," *IEEE Transactions on Power Systems*, vol. 21, no. 1, pp. 285–294, Feb 2006.

[69] M. Zarghami, M. L. Crow, and S. Jagannathan, "Nonlinear control of FACTS controllers for damping interarea oscillations in power systems," *IEEE Transactions on Power Delivery*, vol. 25, no. 4, pp. 3113–3121, Oct 2010.

[70] W. Yao, L. Jiang, J. Wen, Q. H. Wu, and S. Cheng, "Wide-area damping controller of FACTS devices for inter-area oscillations considering communication time delays," *IEEE Transactions on Power Systems*, vol. 29, no. 1, pp. 318–329, Jan 2014.

[71] Y. Wang, J. Meng, X. Zhang, and L. Xu, "Control of PMSG-based wind turbines for system inertial response and power oscillation damping," *IEEE Transactions on Sustainable Energy*, vol. 6, no. 2, pp. 565–574, April 2015.

[72] Ayesha, B. Khan, K. Zeb, N. Zeb, R. Sajjad, M. Aqib, A. Haider, H. G. Abood, and V. Sreeram, "An adaptive controller scheme implemented on multiple links VSC-HVDC for effective damping of low frequency power oscillations," in *2016 IEEE International Conference on Power System Technology (POWERCON)*, Wollongong, NSW, Australia, Sept 2016, pp. 1–6.

[73] M. Edrah, K. L. Lo, and O. Anaya-Lara, "Reactive power control of DFIG wind turbines for power oscillation damping under a wide range of operating conditions," *IET Generation, Transmission Distribution*, vol. 10, no. 15, pp. 3777–3785, 2016.

[74] L. Zeni, R. Eriksson, S. Goumalatsos, M. Altin, P. Sorensen, A. Hansen, P. Kjaer, and B. Hesselbaek, "Power oscillation damping from VSC-HVDC connected offshore wind power plants," *IEEE Transactions on Power Delivery*, vol. 31, no. 2, pp. 829–838, April 2016.

[75] Y. Pipelzadeh, N. R. Chaudhuri, B. Chaudhuri, and T. C. Green, "Coordinated control of offshore wind farm and onshore HVDC converter for effective power oscillation damping," *IEEE Transactions on Power Systems*, vol. 32, no. 3, pp. 1860–1872, May 2017.

[76] C. D. Barker, R. S. Whitehouse, A. G. Adamczyk, and G. G. Soto, "Low frequency active power oscillation damping using a MMC-VSC HVDC link," in *13th IET International Conference on AC and DC Power Transmission (ACDC 2017)*, Manchester, UK, Feb 2017, pp. 1–6.

[77] L. Zeni, R. Eriksson, S. Goumalatsos, M. Altin, P. E. Sørensen, A. Hansen, P. Kjær, and B. Hesselbæk, "Power oscillation damping from VSC-HVDC connected offshore wind power plants," *IEEE Transactions on Power Delivery*, vol. 31, no. 2, pp. 829–838, April 2016.

[78] N. Kshatriya, U. D. Annakkage, F. M. Hughes, and A. M. Gole, "Optimized partial eigenstructure assignment-based design of a combined PSS and active damping controller for a DFIG," *IEEE Transactions on Power Systems*, vol. 25, no. 2, pp. 866–876, May 2010.

[79] T. Surinkaew and I. Ngamroo, "Hierarchical co-ordinated wide area and local controls of DFIG wind turbine and PSS for robust power oscillation damping," *IEEE Transactions on Sustainable Energy*, vol. 7, no. 3, pp. 943–955, July 2016.

[80] C. Zhang, D. Ke, Y. Sun, C. Y. Chung, J. Xu, and F. Shen, "Coordinated supplementary damping control of DFIG and PSS to suppress inter-area oscillations with optimally controlled

plant dynamics," *IEEE Transactions on Sustainable Energy*, vol. 9, no. 2, pp. 780–791, April 2018.

[81] L. Zacharia, L. Hadjidemetriou, and E. Kyriakides, "Cooperation of wide area control with renewable energy sources for robust power oscillation damping," in *2017 IEEE Manchester PowerTech*, June 2017, pp. 1–6.

[82] T. T. Nguyen and R. Gianto, "Optimisation-based control coordination of PSSs and FACTS devices for optimal oscillations damping in multi-machine power system," *IET Generation, Transmission & Distribution*, vol. 1, no. 4, pp. 564–573, July 2007.

[83] H. Maleki and R. K. Varma, "Coordinated control of PV solar system as STATCOM (PV-STATCOM) and power system stabilizers for power oscillation damping," in *2016 IEEE Power and Energy Society General Meeting (PESGM)*, July 2016, pp. 1–5.

[84] S. Sharma and S. Narayan, "Damping of low frequency oscillations using robust PSS and TCSC controllers," in *2017 8th International Conference on Computing, Communication and Networking Technologies (ICCCNT)*, July 2017, pp. 1–7.

[85] A. Moeini and I. Kamwa, "Analytical concepts for reactive power based primary frequency control in power systems," *IEEE Transactions on Power Systems*, vol. 31, no. 6, pp. 4217–4230, Nov 2016.

[86] F. Dorfler, "Control of low-inertia power systems: Naive & foundational approaches," Swiss Federal Institute of Technology (ETH) Zurich, Switzerland, Tech. Rep., 2017.

[87] A. Safari, H. A. Shayanfar, and A. Kazemi, "Robust PWMSC damping controller tuning on the augmented lagrangian PSO algorithm," *IEEE Transactions on Power Systems*, vol. 28, no. 4, pp. 4665–4673, Nov 2013.

[88] S. Q. Yuan and D. Z. Fang, "Robust PSS parameters design using a trajectory sensitivity approach," *IEEE Transactions on Power Systems*, vol. 24, no. 2, pp. 1011–1018, May 2009.

[89] S. M. Baek and J. W. Park, "Nonlinear parameter optimization of FACTS controller via real-time digital simulator," *IEEE Transactions on Industry Applications*, vol. 49, no. 5, pp. 2271–2278, Sept 2013.

[90] Y. L. Abdel-Magid, M. A. Abido, S. Al-Baiyat, and A. H. Mantawy, "Simultaneous stabilization of multimachine power systems via genetic algorithms," *IEEE Transactions on Power Systems*, vol. 14, no. 4, pp. 1428–1439, Nov 1999.

[91] M. Cloughley, K. M. Muttaqi, and H. Du, "Damping of low-inertia machine oscillations using Takagi-Sugeno fuzzy stabiliser tuned by genetic algorithm optimisation to improve system stability," *IET Generation, Transmission & Distribution*, vol. 8, no. 2, pp. 339–352, Feb 2014.

[92] L. H. Hassan, M. Moghavvemi, H. A. F. Almurib, and K. M. Muttaqi, "A coordinated design of PSSs and UPFC-based stabilizer using genetic algorithm," *IEEE Transactions on Industry Applications*, vol. 50, no. 5, pp. 2957–2966, Sept 2014.

[93] D. Rerkpreedapong, A. Hasanovic, and A. Feliachi, "Robust load frequency control using genetic algorithms and linear matrix inequalities," *IEEE Transactions on Power Systems*, vol. 18, no. 2, pp. 855–861, May 2003.

[94] J. J. Grainger and W. D. Stevenson, *Power system analysis*, 3rd ed. McGraw-Hill, 1994.

[95] T. Ackerman, *Wind power in power system*, 3rd ed. NJ 07030, USA: John Wiley & Sons, 2005.

[96] ENTSO-E, "The load-frequency and reserves network code," ENTSO-E, Tech. Rep., 2013.

[97] ENTSO-E, "The frequency and reserves network code," ENTSO-E, Tech. Rep., Feb. 2013.

[98] ——, "Frequency containment reserves (FCR)," ENTSO-E, Tech. Rep., Nov. 2017.

[99] ——, "Nordic balancing philosophy," ENTSO-E, Tech. Rep., Jun. 2016.

[100] Emissions-EUETS, "Frequency restoration reserve (FRR)," Emissions-EUETS, Tech. Rep., Sep. 2018.

[101] ——, "Replacement reserve (RR)," Emissions-EUETS, Tech. Rep., Apr. 2018.

[102] ENTSO-E, "Network code on load-frequency control and reserves," ENTSO-E, Tech. Rep., 2013.

[103] P. Energy, "Rate of Change of Frequency (ROCOF) Review of TSO and Generator Submissions Final Report," PPA Energy, Tech. Rep., May 2013.

[104] 4Coffshore, "Horns Rev 1 offshore wind farm," Mar 2016. [Online]. Available: https://www.4coffshore.com/windfarms/horns-rev-1-denmark-dk03.html

[105] 4Coffshore, "Horns Rev 2 offshore wind farm," Jun 2017. [Online]. Available: https://www.4coffshore.com/windfarms/horns-rev-2-denmark-dk10.html

[106] 4Coffshore, "Anholt offshore wind farm," Apr 2018. [Online]. Available: https://www.4coffshore.com/windfarms/anholt-denmark-dk13.html

[107] Energinet, "COBRAcable: interconnector to the Netherlands," 2016. [Online]. Available: https://en.energinet.dk/Infrastructure-Projects/Projektliste/COBRAcable

[108] Energinet, "Viking link: interconnector from Denmark to Great Britain," 2016. [Online]. Available: https://en.energinet.dk/Infrastructure-Projects/Projektliste/Viking-Link

[109] 4Coffshore, "Horns Rev 3 offshore wind farm," Jun 2018. [Online]. Available: https://www.4coffshore.com/windfarms/horns-rev-3-denmark-dk19.html

[110] Energinet, "Horns rev 3 offshore wind farm," April 2014. [Online]. Available: https://ens.dk/sites/ens.dk/files/Vindenergi/radio_communication_and_radars_ver3.pdf

[111] T. Weckesser, H. Johannsson, and J. stergaard, "Impact of model detail of synchronous machines on real-time transient stability assessment," in *2013 IREP Symposium Bulk Power System Dynamics and Control - IX Optimization, Security and Control of the Emerging Power Grid*, Aug 2013, pp. 1–9.

[112] IEEE Std 421.5-2005, "IEEE recommended practice for excitation system models for power system stability studies," IEEE, New York, USA, Tech. Rep., 2006.

[113] H. T. Nguyen, G. Y. Yang, A. H. Nielsen, and P. H. Jensen, "Hardware-in-the-loop test for automatic voltage regulator of synchronous condenser," in *20th International Conference on Power Systems and Energy Conversion*, Tokyo, Japan, Mar 2018, pp. 1–6.

[114] RTDS, "RTDS hardware manual," Jan. 2009. [Online]. Available: https://www.rtds.com/

[115] IEEE Task Force on Excitation Limiters, "Underexcitation limiter models for power system stability studies," *IEEE Trans. Energy Conversion*, 1995.

[116] G. K. Girgis and H. D. Vu, "Verification of limiter performance in modern excitation control systems," *IEEE Trans. Energy Conversion*, 1995.

[117] IEEE Task Force on Excitation Limiters, "Recommended models for overexcitation limiting devices," *IEEE Trans. Energy Conversion*, 1995.

[118] A. Murdoch, R. W. Delmerico, S. Venkataraman, R. A. Lawson, J. E. Curran, and W. R. Pearson, "Excitation system protective limiters and their effect on volt/var control-design, computer modeling, and field testing," *IEEE Trans. Energy Conversion*, 2000.

[119] A. S. Q. Wu, S-T. Cha and J. Østergaard, "Communication test for MatrikonOPC Server for SCADA DNP3 with RTDS," Department of Electrical Engineering, Technical University of Denmark, Tech. Rep., 2010.

[120] AEMC, "EMT and RMS model requirements," AEMC, Tech. Rep., 2017.

[121] L. H. Hassan, M. Moghavvemi, H. A. F. Almurib, and K. M. Muttaqi, "A coordinated design of PSSs and UPFC-based stabilizer using genetic algorithm," *IEEE Transactions on Industry Applications*, vol. 50, no. 5, pp. 2957–2966, Sept 2014.

[122] W. M. da Rosa, P. Rossoni, J. C. Teixeira, E. A. Belati, and P. T. L. Asano, "Optimal allocation of capacitor banks using genetic algorithm and sensitivity analysis," *IEEE Latin America Transactions*, vol. 14, no. 8, pp. 3702–3707, Aug 2016.

[123] GE Digital Energy, "Synchronous condenser systems," 2014. [Online]. Available: http://www.gegridsolutions.com/products/brochures/powerd_vtf/Synch_Cond_web.pdf

[124] H. T. Nguyen, G. Y. Yang, A. H. Nielsen, and P. H. Jensen, "Frequency stability improvement of low inertia systems using synchronous condensers," in *2016 IEEE International Conference on Smart Grid Communications (SmartGridComm)*, Sydney, NSW, Australia, Nov 2016, pp. 650–655.

[125] CAISO, "Monthly renewable performance report-Mar 2018," Mar 2018. [Online]. Available: https://www.caiso.com/Documents/MonthlyRenewablesPerformanceReport-Mar2018.html

[126] Y. Amirnaser and I. Reza, *Voltage-Sourced Converters in Power Systems: Modeling, control, and applications*. John Wiley & Sons, Inc., Hoboken, New Jersey, 2010.

[127] F. Gonzalez-Longatt, E. Chikuni, and E. Rashayi, "Effects of the synthetic inertia from wind power on the total system inertia after a frequency disturbance," in *2013 IEEE International Conference on Industrial Technology (ICIT)*, Feb 2013, pp. 826–832.

[128] Y. Z. Sun, Z. S. Zhang, G. J. Li, and J. Lin, "Review on frequency control of power systems with wind power penetration," in *2010 International Conference on Power System Technology*, Oct 2010, pp. 1–8.

[129] J. Ekanayake and N. Jenkins, "Comparison of the response of doubly fed and fixed-speed induction generator wind turbines to changes in network frequency," *IEEE Transactions on Energy Conversion*, vol. 19, no. 4, pp. 800–802, Dec 2004.

[130] G. Ramtharan, J. B. Ekanayake, and N. Jenkins, "Frequency support from doubly fed induction generator wind turbines," *IET Renewable Power Generation*, vol. 1, no. 1, pp. 3–9, March 2007.

[131] J. Morren, S. W. H. Haan, W. L. Kling, and J. A. Ferreira, "Wind turbines emulating inertia and supporting primary frequency control," *IEEE Transactions on Power Systems*, vol. 21, no. 1, pp. 433–434, Feb 2006.

[132] L. Holdsworth, J. Ekanayake, and N. Jenkins, "Power system frequency response from fixed speed and doubly fed induction generator based wind turbines," *Wind Energy*, vol. 7, pp. 21–35, 2004.

[133] S. Mishra, P. P. Zarina, and P. C. Sekhar, "A novel controller for frequency regulation in a hybrid system with high PV penetration," in *2013 IEEE Power Energy Society General Meeting*, July 2013, pp. 1–5.

[134] W. Yao and K. Y. Lee, "A control configuration of wind farm for load-following and frequency support by considering the inertia issue," in *2011 IEEE Power and Energy Society General Meeting*, July 2011, pp. 1–6.

[135] B. H. Chowdhury and H. T. Ma, "Frequency regulation with wind power plants," in *2008 IEEE Power and Energy Society General Meeting - Conversion and Delivery of Electrical Energy in the 21st Century*, July 2008, pp. 1–5.

[136] J. F. Conroy and R. Watson, "Frequency response capability of full converter wind turbine generators in comparison to conventional generation," *IEEE Transactions on Power Systems*, vol. 23, no. 2, pp. 649–656, May 2008.

[137] M. Kayikci and J. V. Milanovic, "Dynamic contribution of DFIG-based wind plants to system frequency disturbances," *IEEE Transactions on Power Systems*, vol. 24, no. 2, pp. 859–867, May 2009.

[138] I. Erlich and M. Wilch, "Primary frequency control by wind turbines," in *IEEE PES General Meeting*, July 2010, pp. 1–8.

[139] E. Quitmann, "Ancillary services from wind turbines and related grid codes," in *5th International Conference in Integration of Renewable and Distributed Energy Resources*, Berlin, Dec 2012, pp. 1–6.

[140] N. A. Janssens, G. Lambin, and N. Bragard, "Active power control strategies of DFIG wind turbines," in *2007 IEEE Lausanne Power Tech*, July 2007, pp. 516–521.

[141] E. Loukarakis, I. Margaris, and P. Moutis, "Frequency control support and participation methods provided by wind generation," in *2009 IEEE Electrical Power Energy Conference (EPEC)*, Oct 2009, pp. 1–6.

[142] P. Moutis, E. Loukarakis, S. Papathanasiou, and N. D. Hatziargyriou, "Primary load-frequency control from pitch-controlled wind turbines," in *2009 IEEE Bucharest PowerTech*, June 2009, pp. 1–7.

[143] R. Sakamoto, T. Senjyu, N. Urasaki, T. Funabashi, H. Fujita, and H. Sekine, "Output power leveling of wind turbine generators using pitch angle control for all operating regions in wind farm," in *Proceedings of the 13th International Conference on, Intelligent Systems Application to Power Systems*, Nov 2005, pp. 1–6.

[144] R. G. de Almeida and J. A. P. Lopes, "Participation of doubly fed induction wind generators in system frequency regulation," *IEEE Transactions on Power Systems*, vol. 22, no. 3, pp. 944–950, Aug 2007.

[145] R. G. de Almeida, E. D. Castronuovo, and J. A. P. Lopes, "Optimum generation control in wind parks when carrying out system operator requests," *IEEE Transactions on Power Systems*, vol. 21, no. 2, pp. 718–725, May 2006.

[146] H. T. Nguyen, G. Y. Yang, A. H. Nielsen, and P. H. Jensen, "Frequency stability enhancement for low inertia systems using synthetic inertia of wind power," in *2017 IEEE Power Energy Society General Meeting*, July 2017, pp. 1–5.

[147] ENTSO-E, "Future system inertia 2," 2015. [Online]. Available: http://www.statnett.no/Global/Dokumenter/Kraftsystemet/Systemansvar/Nordic%20report,%20Future%20System%20Inertia2_Vfinal.pdf

[148] ELFORSK, "Report of vindforsk project V-369," ELFORSK, Tech. Rep., Jan. 2013. [Online]. Available: http://www.elforsk.se/Programomraden/El-Varme/Vindforsk/reports/reports-VFIII

[149] H. T. Nguyen, G. Y. Yang, A. H. Nielsen, and P. H. Jensen, "Combination of synchronous condenser and synthetic inertia for frequency stability enhancement in low inertia systems," *IEEE Transactions on Sustainable Energy*, 2018.

[150] G. Rogers, "Demystifying power system oscillations," *IEEE Computer Applications in Power*, vol. 9, no. 3, pp. 30–35, Jul 1996.

[151] M. Klein, G. J. Rogers, and P. Kundur, "A fundamental study of inter-area oscillations in power systems," *IEEE Transactions on Power Systems*, vol. 6, no. 3, pp. 914–921, Aug 1991.

[152] W. Du, H. F. Wang, and R. Dunn, "Power system small-signal oscillation stability as affected by large-scale pv penetration," in *2009 International Conference on Sustainable Power Generation and Supply*, Nanjing, China, Apr 2009, pp. 1–6.

[153] IEEE Task Force on Load Representation for Dynamic Performance, "Standard load models for power flow and dynamic performance simulation," *IEEE Transactions on Power Systems*, vol. 10, no. 3, pp. 1302–1313, Aug 1995.

[154] A. A. M. Zin, H. M. Hafiz, and W. K. Wong, "Static and dynamic under-frequency load shedding: a comparison," in *2004 International Conference on Power System Technology (PowerCon 2004)*, Singapore, Nov 2004, pp. 941–945.

[155] R. Ramirez-Betancour, V. J. Gutierrez-Martinez, and C. R. Fuerte-Esquivel, "Static simulation of voltage instability considering effects of governor characteristics and voltage and frequency dependence of loads," in *North American Power Symposium 2010*, Arlington, TX, USA, Sept 2010, pp. 1–7.

[156] Y. Chen, "Replacing a PID controller by a lag-lead compensator for a robot - A frequency response approach," *IEEE Trans. Robotics and Automation*, 1989.

[157] A. Murdoch, S. Venkataraman, R. A. Lawson, and W. R. Pearson, "Integral of accelerating power type PSS. Parts I and II," *IEEE Trans. Energy Convers.*, 1999.

[158] I. Kamwa, R. Grondin, and G. Trudel, "IEEE PSS2B versus PSS4B: the limits of performance of modern power system stabilizers," *IEEE Transactions on Power Systems*, vol. 20, no. 2, pp. 903–915, May 2005.

[159] L. Wang, Q. S. Vo, and A. V. Prokhorov, "Stability improvement of a multimachine power system connected with a large-scale hybrid wind-photovoltaic farm using a supercapacitor," *IEEE Transactions on Industry Applications*, vol. 54, no. 1, pp. 50–60, Jan 2018.

[160] Y. Pipelzadeh, N. R. Chaudhuri, B. Chaudhuri, and T. C. Green, "Coordinated control of offshore wind farm and onshore hvdc converter for effective power oscillation damping," *IEEE Transactions on Power Systems*, vol. 32, no. 3, pp. 1860–1872, May 2017.

[161] L. Wang and D. N. Truong, "Stability enhancement of dfig-based offshore wind farm fed to a multi-machine system using a statcom," *IEEE Transactions on Power Systems*, vol. 28, no. 3, pp. 2882–2889, Aug 2013.

[162] L. Scharf, *Statistical Signal Processing: Detection, Estimation, and Time Series Analysis*. New York: Addison-Wesley, 1991.

[163] X. Xia, C. Li, and W. Ni, "Dominant low-frequency oscillation modes tracking and parameter optimisation of electrical power system using modified Prony method," *IET Generation, Transmission Distribution*, vol. 11, no. 17, pp. 4358–4364, Dec 2017.

[164] A. Saffarian and M. Sanaye-Pasand, "Enhancement of power system stability using adaptive combinational load shedding methods," *IEEE Transactions on Power Systems*, vol. 26, no. 3, pp. 1010–1020, Aug 2011.

Appendix

Table 1: Offshore wind farm of the DK1 power system.

Name	Type	Substation	MW rating
Anholt	Type 3	AHA	400
Horns Rev 1	Type 3	HRA	169
Horns Rev 2	Type 4	HRB	200
Horns Rev 3	Type 4	HRC	400

Table 2: HVDC interconnection of the DK1 power system.

Name	Type	Substation	MW rating	DC voltage level (kV)	Interconnection
Konti Skan 1, 2	LCC	VHA	250/300	250/300	Sweden
Skagerrak 1, 2	LCC	TJE	250/250	250/250	Norway
Skagerrak 3	LCC	TJE	440	350	Norway
Skagerrak 4	VSC	TJE	700	400	Norway
Storebœlt	LCC	FGD	600	400	DK2
COBRAcable	VSC	EDR	700	320	The Netherlands

Table 3: Employed system parameters for the DK1 power system.

	ESVB3	FYVB7	NJVB2,3	SKVB3	SSVB3,4
Rated MVA	528	489	524	524	441
Rated kV	19	21	21	21	19

Table 4: The boundary settings of the POD parameters.

$T_{1,2min}$	$T_{1,2max}$	K_{1min}	K_{1max}	K_{2min}	K_{2max}	K_{3min}	K_{3max}	Min/Max
0.01	10	0.5	50	0.5	12	0.05	2	± 0.13

Department of Electrical Engineering
Center for Electric Power and Energy (CEE)
Technical University of Denmark
Elektrovej, Building 325
DK-2800 Kgs. Lyngby
Denmark

www.elektro.dtu.dk/cee
Tel: (+45) 45 25 35 00
Fax: (+45) 45 88 61 11
E-mail: cee@elektro.dtu.dk